A Two-Armed Forward Dynamic Model of a Golf Drive: A Simulation and Optimization Tool for Golf Equipment and Biomechanics

by

Spencer Ferguson

A thesis
presented to the University of Waterloo
in fulfillment of the
thesis requirement for the degree of
Master of Applied Science
in
Systems Design Engineering

Waterloo, Ontario, Canada, 2023

Author's Declaration

This thesis consists of material all of which I authored or co-authored: see Statement of Contributions included in the thesis. This is a true copy of the thesis, including any required final revisions, as accepted by my examiners.

I understand that my thesis may be made electronically available to the public.

Statement of Contributions

Spencer Ferguson was the sole author of the entirety of the contents of this document with the exception of two previously published conference papers which are reproduced in part in this thesis for completeness.

Exceptions to sole authorship of material are as follows:

Chapter 3: S. Ferguson, W. McNally, and J. McPhee, "Predicting the flight of a golf ball: Comparing a physics-based aerodynamic model to a neural network," In: Engineering of Sport 14: Proceedings of the 14th Conference of the International Sports Engineering Association, West Lafayette, USA, 2022 https://doi.org/10.5703/1288284317493.

This research was conducted at the University of Waterloo by Spencer Ferguson under the supervision of Prof. John McPhee with input on developing neural networks from Dr. William McNally. Spencer Ferguson designed the physical experiments, conducted them, analyzed the data, and developed both the physics-based aerodynamic model and neural network from the dataset. The neural network portion of this publication is not mentioned in this thesis as it was not used in this work. Spencer Ferguson drafted the manuscript while Prof. McPhee and Dr. McNally provided their input.

Chapter 5: S. Ferguson, W. McNally, and J. McPhee, "The effect of club length, face bulge radius, and center of gravity depth on optimal golf drives—a simulation study," In: Engineering of Sport 14: Proceedings of the 14th Conference of the International Sports Engineering Association, West Lafayette, USA, 2022 https://doi.org/10.5703/1288284317486.

This research was conducted at the University of Waterloo by Spencer Ferguson under the supervision of Prof. John McPhee with input on the use of the forward dynamic golfer model from Dr. William McNally. Spencer Ferguson designed the simulation experiments, conducted them, and analyzed the data. Spencer Ferguson drafted the manuscript while Prof. McPhee and Dr. McNally provided their input.

Abstract

Golf club manufacturers and golf's governing bodies both have clear interests in understanding how equipment design changes affect the performance of a golfer. Traditionally, to capture this interaction it was necessary to engage in time-consuming and expensive experimental testing. With the comprehensive modeling and computing tools available today, an opportunity exists to develop a forward dynamic model of a golf drive that can perform much of this testing in a virtual environment using predictive dynamic simulations. The experimentally-validated novel forward dynamic model developed in this thesis is a synthesis of four sub-models: a two-armed model of the golfer with 13 individual biomechanical joints, a continuous analytical flexible shaft model based on a Rayleigh beam formulation, an adjusted impulse-momentum clubhead-ball impact model, and a golf ball aerodynamic model. In concert, these sub-models combine to fully simulate a golf drive from biomechanics to ball flight.

Experimental validation of the model was aided by the completion of a motion capture experiment in which the biomechanics, club kinematics, and ball launch conditions of ten elite golfers were quantified using three unique drivers. To validate the shaft model, the grip kinematics of a training dataset of experimental swings were used to drive an isolated model of the club while stiffness properties were tuned to minimimize the difference between simulated and experimental clubhead deflection. The golf ball aerodynamic model was validated using a set-aside training dataset of launch conditions and ball flights, showing excellent agreement and marked improvement over previous spin-rate dependent models.

The biomechanical timings of the full model were optimized subject to a cost function maximizing carry distance while penalizing shots hit sufficiently far offline. Comparing the optimized swing to the biomechanics of the motion capture study participants showed that the model successfully reproduces swing traits of elite golfers. Additionally, the resultant ball speeds of the model closely matched the median of the experimental participants.

Using the validated model, a series of "what-if?" predictive dynamic simulation experiments were performed. Pertinent findings related to golf's distance debate included the positive correlation between both club and tee length and driving distance. The effects of wind on optimal golf drives were studied showing that golfers can benefit from a different combination of ideal launch conditions and ball position depending on the presence of a headwind or tailwind. Finally, with two unique drivers it was shown how club design can have an effect on the dispersion of mis-hits caused by noise in the biomechanical timings of the swing.

Acknowledgements

I would like to thank Prof. John McPhee for his invaluable support and guidance throughout the supervision of this research.

I would like to thank my thesis committee members, Prof. Clark Dickerson and Prof. Katja Mombaur, for their advice in improving this work.

I would like to acknowledge the Natural Sciences and Engineering Research Council of Canada's Canada Graduate Scholarship program, the Canada Research Chairs Program, and the University of Waterloo's Engineering Excellence Master's Fellowship program for their financial support of this research.

I would like to thank all my colleagues from the Motion Research Group for their suggestions and wisdom over the past two years.

Finally, I would like to thank my parents Peter and Cindy Ferguson for their unwavering support of my academic journey, and for encouraging me to pursue my passions with this research.

Table of Contents

List of Figures

List of Tables

Chapter 1

Introduction

Golf is among the most geographically diffused sports in the world, with more than 38,000 courses in 206 countries [1]. Worldwide participation in the sport has been on the upswing of late, with the number of golfers growing by 5.5 million between 2016 and 2020 to a record total of 66.6 million [2]. Much of this increase in participation occurred during the COVID-19 pandemic, when individuals turned to golf as a form of safe recreation. Golf appears poised to continue its upward trajectory, with year-over-year increases in the number of rounds played reported across North America between 2020 and 2021 [3].

With this surge in popularity, there is renewed pressure on golf's equipment manufacturers to continue to innovate and bring yearly performance improvements to their product lines. This is particularly true with the driver, which is often the most expensive club in a golfer's bag. There has been a flurry of innovation surrounding the driver since the 1990s including the introduction of 460 cubic centimeter heads with adjustable weights [4], and composite material construction [5]. These advances and many others have contributed (at least in part) to driving distance increasing at the elite level of the sport, where the average driving distance on the PGA Tour has risen from 262 yards to 296 yards since 1990 [6].

This increase in driving distance is an active area of study for golf's governing bodies: the United States Golf Association (USGA) and Royal and Ancient (R&A), who are concerned that the skill required to play the game is being eroded. Consequently, in 2021 the USGA and R&A introduced a model local rule limiting driver length from 48 to 46 inches for elite competitions [7] and have set out to study several other "areas of interest" that could result in changes to other equipment regulations.

1.1 Problem Description

Both equipment manufacturers and golf's governing bodies spend much of their efforts evaluating the effects of equipment design changes on golfer performance. From the manufacturers' perspective, they seek to maximize the performance of their equipment to deliver the best products to their customers. From the governing bodies' perspective, they seek to ensure that advances in equipment do not unduly take away from the skill required to play the sport, or violate the spirit of the game.

Historically, equipment testing has been completed via trials with prototypes and a human or robotic golfer [8]. While these trials can provide insight into the research question being proposed, they suffer from drawbacks that limit the scope of studies, and the speed at which the work can be completed. A physical prototype of a driver clubhead may take weeks to fabricate, and incur significant financial costs with investments in tooling and labor; studies involving the flight of the ball are subject to atmospheric conditions such as wind, barometric pressure, and humidity; human participants inherently suffer from swing repeatability issues; and swing robots have fixed swing arcs that cannot optimally adjust to changes in equipment design like a human.

These drawbacks with physical equipment testing point to the opportunity for a high-fidelity model of a golf drive. Although stand-alone models of golfer biomechanics, shaft dynamics, clubhead-ball impact, and golf ball aerodynamics exist, these models are only able to provide insights into the isolated subsystem being studied. For example: optimizing the mass distribution within a driver clubhead as a result of a stand-alone impact simulation does not consider how the golfer's swing biomechanics may change as a result of the change in mass distribution. An experimentally-validated full golfer model including biomechanics, the shaft, impact, and ball flight allows for a more holistic approach in model-based design that considers the interplay between the golfer and their club.

As will be discussed in Section 2.2, these full golfer models have been published in the literature. However, there is much room for improvement. Most notably, an experimentally-validated forward dynamic full golfer model including the trailing arm of the golfer along with clubhead-ball impact and ball flight has yet to be published in the literature.

The goal of this thesis is to develop a state of the art, forward dynamic full golfer model with the golfer's trailing arm and pelvis translation, and an updated golf ball aerodynamic model, plus several other improvements.

1.2 Contributions

- A first of its kind experimentally-validated forward dynamic golfer model including the trailing arm and pelvis translation.
- A physics-based golf ball aerodynamic model that reflects contemporary golf ball aerodynamics.
- Characterization of the trailing arm's kinematic role in the golf swing.
- Characterization of the translational role of the pelvis in the golf swing.
- Insights into how several proposed solutions to golf's distance debate could affect driving distance for elite players.
- Insights into how club design choices can influence mishit tendencies and performance.
- Insights into how the optimal biomechanics of a golfer change in the presence of wind.

Chapter 2

Background and Literature Review

Before describing the outcomes of this research, it is prudent to first provide some background on the subject at hand. To begin, the golf drive will be discussed generally from a non-modeling perspective to introduce key terminology and concepts to the reader. Next, both existing multibody dynamic models of the golf swing and dynamic models of golf ball flight will be reviewed, providing context for the contributions of this research in these two areas. For brevity, only select contributions with particular relevance to this work will be reviewed here. A comprehensive golf review paper focusing on dynamic modeling and measurements was recently published by McPhee [9], and is an excellent resource for further reading.

2.1 The Golf Drive

The golf drive is a specialized type of golf shot taken off the teeing ground as the first shot of a hole. The ball is elevated off the ground using a tee, and a club known as the driver is used. The driver is commonly the longest club in a golfer's bag (typically 46 inches), the club with the largest head volume (typically 460 cubic centimeters), and the club that a golfer is able to hit the farthest (216 yards for the median male golfer [10]). This type of shot is chosen when distance is required, such as on par four and par five holes where more than one shot is required to reach the green. On these holes, the farther the drive travels, the shorter (and therefore easier) the second shot into the green becomes. While distance is the overriding goal of the drive, accuracy is also important as hazards such as long grass, sand traps, and water often surround the landing area. Generally speaking, the golf drive can be decoupled into three phases: the golf swing, impact, and ball flight.

Figure 2.1: Golf drive swing sequence of a professional golfer. Adapted from [11].

The golf swing with a driver is a complex full-body movement that aims to deliver the clubhead to the golf ball in an orientation that promotes favorable ball launch conditions. The golf swing begins at the static address position (Fig. 2.1 frame 1) with the clubhead behind the ball. The golfer then begins the backswing (also known as the takeaway) where they rotate their pelvis, torso, and arms away from the target to the top of the backswing (frame 4). From the top of the backswing position, the downswing commences, rotating in the direction opposite to the backswing until impact (frame 6). After impact, the ball is launched and the follow through begins until the completion of the swing. The follow through does not directly contribute to the outcome of the shot as impact has already occurred, although a balanced follow through is often an indicator of a successful swing. The duration of the swing from takeaway to impact is approximately 1.1-1.2 seconds, with a backswing to downswing "tempo" ratio of generally between 2:1 and 3:1 [12, 13].

The impact between the clubhead and ball is brief and violent, subjecting the golf ball to upwards of 50,000 g's of acceleration over a contact duration of approximately half a millisecond [14]. The regulations surrounding club design limit the coefficient of restitution (COR) between the club and ball to 0.83 [15], reducing the "trampoline effect" and therefore outbound ball velocity. The location of the impact on the clubface is critical to the outcome of the shot; impacts closer to the center of the clubface benefit from a higher COR and favorable launch conditions, while impacts away from the center of the face result in non-optimal ball speed, launch angle, and spin (see the "gear effect" [16]).

The preceding phases of the golf drive serve to generate a successful ball flight: the quantifiable outcome of the shot. At the professional level, the ball routinely flies more

than 300 yards in the air and lands in a target fairway area just 30 yards wide. Even on shots landing in the target area, it is quite rare for a ball to fly perfectly straight. Sidespin imparted to the ball during impact will result in a draw (curving right to left for a right-handed player), or a fade (curving left to right). The ball flight also encounters perhaps the most significant extraneous variable in the golf drive: wind, which must be accounted for in the golfer's alignment and prediction of how far the ball will carry.

2.2 Multibody Dynamic Models of the Golf Swing

Modeling the golf swing is an endeavour that spans several disciplines ranging from multibody dynamics to biomechanics. Fundamentally, the most important aspect of such a model is the interaction between the golfer and their club, although recent models have expanded to include impact and the flight of the ball. Here, several models of the golf swing that have been developed since the mid-twentieth century will be presented, serving as a platform upon which to discuss the model developed in this thesis.

2.2.1 One-Armed Multibody Models

The first rigorous scientific model the golf swing came in 1967 from Williams [17] who used a double-pendulum representation (see Fig. 2.2). The upper lever combined the upper and lower lead arm into a single rigid body, while the lower lever represented the golf club. The upper lever was hinged at one end to a fixed point approximating the shoulder joint, and at its other end to the lower lever, approximating the wrist joint. From the model, Williams was able to deduce the grip forces as well as the work done by the golfer throughout the swing. Williams also suggested that by locking the wrist at the beginning of the downswing, followed by a free release, clubhead speed could be maximized at impact.

One year later in 1968, Cochran and Stobbs [18] published their works entitled *The Search for the Perfect Swing*. The authors also proposed a planar double pendulum representation of the golfer and their club. At the wrist joint, a 90 degree stop was affixed to ensure that the wrist angle was maintained at the beginning of the downswing. This prevented the biomechanical equivalent of infeasible radial deviation or excessive "cocking" of the wrist. The single active component of the model was an applied torque at the shoulder joint. Beginning at the top of the backswing (position one in Fig. 2.2), the applied torque rotated the upper lever towards the ball. As the upper lever rotated, the centrifugal force began to rotate the lower lever off the stop and towards the ball (position two). Pursuant to the conservation of angular momentum, as the angular velocity of

the lower lever increased, the angular velocity of the upper lever decreased until impact was reached (position three) with the upper and lower levers approximately aligned. The authors recognized that additional clubhead speed could be extracted by actively driving the wrist, but discussed how doing so would introduce complexity in sequencing the torque applications between the shoulder and wrist. Despite the passive release of the wrist, the model compared favorably to real golf swings captured using stop-motion photography.

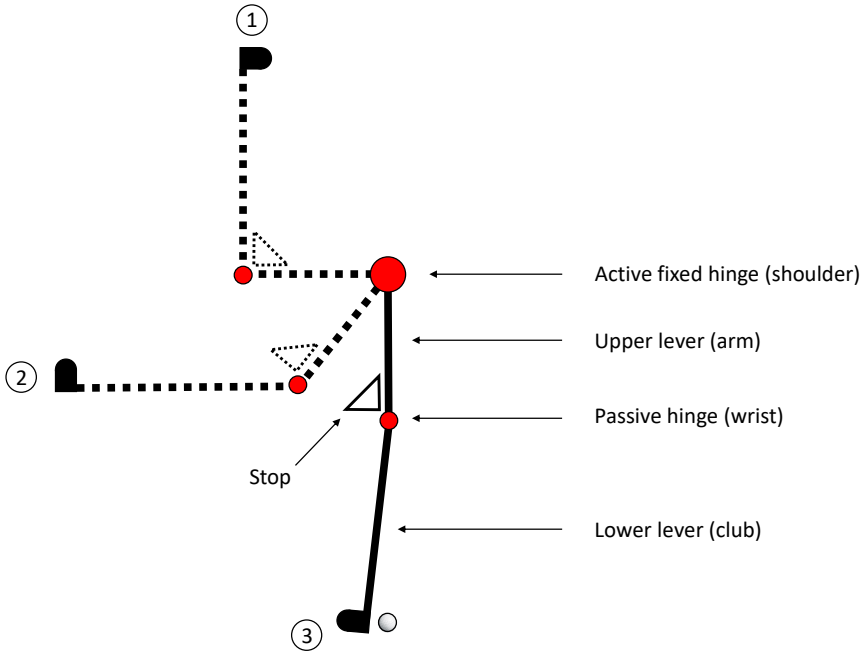

Figure 2.2: Author-created figure representing the double pendulum golf swing model first proposed by Williams [17]. Note that the explicit "stop" at the wrist joint proposed by Cochran and Stobbs [18] has been added.

The planar double pendulum concept proved to be quite robust, and several other studies stemmed from the models of Williams and Cochran & Stobbs [19, 20, 21, 22, 23, 24]. Notably, in 1975 Lampsa [20] employed a double pendulum model in an attempt to optimize the golf swing using optimal control of the torque applied at the shoulder and wrist joints. Using the method of steepest ascent, Lampsa used a cost function maximizing clubhead speed at impact with penalties for the two levers not being aligned at impact or exceeding feasible relative angles at any point in the swing. The optimized swing of the model produced an estimated carry distance of 320 yards; the PGA Tour did not track driving distance in 1975, but in 1980 the leader averaged 274 yards [6]. A key finding of Lampsa

that agreed with the prior work of Jorgensen [19] was that the uncocking of the wrists in the downswing should be delayed as long as possible, a trait nearly universal among elite golfers today.

In 2002, Sprigings and MacKenzie [25] used the model of Sprigings and Neal [26] to further investigate this concept of "delayed release" in optimized golf swing models. The authors felt that exploring this concept with more biofidelity was necessary to definitively draw the conclusion that a delayed release is advantageous. The biomechanical model followed that of Sprigings and Neal [26], including three segments: the club, arm, and torso. Furthering the theme of improved biofidelity, the muscle torque generators (MTG)s of Sprigings and Neal [26] were implemented at the spine, shoulder, and wrist joints (see [27] for a contemporary review of MTGs). These MTGs encompassed the activation rates and force-velocity relationships of the muscles spanning these joints. With this improved model, the authors found that delaying the release of the wrist was advantageous in generating clubhead speed (44.7 vs. 44.0 m/s) but not to the degree that was previously reported. Applying a wrist torque after the release of the wrist was also found to be advantageous when compared to a free release (44.7 vs. 38.9 m/s).

Nine years later, MacKenzie and Sprigings published a first of its kind three-dimensional forward dynamic model of the golf swing [28], shown in Fig. 2.3. The biomechanical model included the torso, lead arm, and hand with four total degrees of freedom: torso rotation, shoulder abduction, wrist ulnar deviation, and arm pronation-supination. The pronation-supination degree of freedom was key to this study as it allowed the clubhead to move outside of the lead arm plane, making it a three-dimensional model. The shaft of the golf club was modeled as four rigid segments connected by rotational spring-damper elements. The muscle torque generators used by Sprigings and Neal [26] in their planar three-segment model were updated to include the muscle deactivation time (in addition to the activation time). The model was validated by comparing the kinematics and kinetics to those of a low-handicap golfer, with both showing strong agreement ($R^2 > 0.98$). When optimized to maximize impact clubhead speed, the model produced a clubhead speed of approximately 96 mph. This was lower than PGA Tour players [6], but still within the normal range of an elite golfer [21]. The optimized model employed proximal to distal sequencing of the segments to generate this clubhead speed, and approached impact with a upwards and inside-to-out clubpath—all characteristics of elite golfers.

Improving upon the work of MacKenzie and Sprigings, Balzerson et al. [30] introduced their own 4-DOF golfer model in 2016, shown in Fig. 2.4. Notably, passive joint torques were added to the muscle torque generators to represent the torque contributions of stretching tendons, ligaments, and other tissue at these joints. Additionally, the segmented shaft model was replaced with a continuous model developed in MapleSim (Maplesoft, Waterloo,

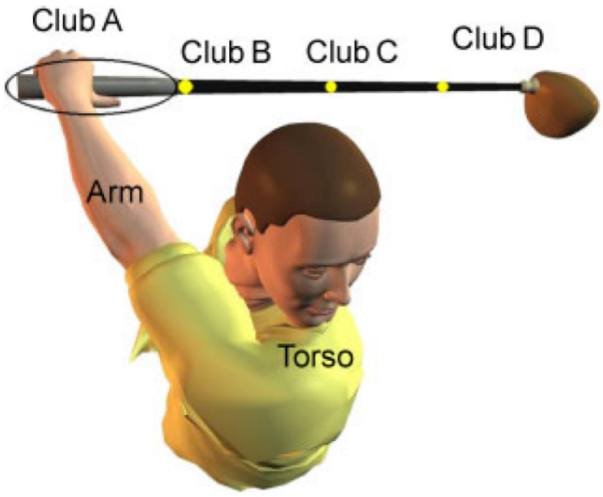

Figure 2.3: The 4-DOF golfer model of MacKenzie and Sprigings [29]. Degrees of freedom: torso rotation, shoulder add-abduction, wrist ulnar-radial deviation, and arm pronation-supination.

Canada) [31]. Perhaps the largest improvement was the addition of an impulse-momentum based clubhead-ball impact model [32] and a dynamic golf ball aerodynamic model [33]. The inclusion of these two additional sub-models allowed the cost function of the optimization to include the carry distance and offline deviation of the shot rather than just the clubhead speed. Solving for the MTG activation and deactivation timings using MATLAB's (MathWorks, Natick, USA) `patternsearch` algorithm, the optimized swing was found to have a carry distance of 214 yards and a clubhead speed of 93 mph, similar to the results of MacKenzie and Sprigings.

The work of McNally and McPhee [35] built upon the model of Balzerson et al. to extend the biofidelity and applications of the model. Notably, a flexion-extension degree of freedom was added to the model's leading shoulder, and a pelvis segment with its own rotational degree of freedom separate from that of the torso was included, bringing the total number of biomechanical degrees of freedom to six (see Fig. 2.5). For the first time in a predictive forward dynamic golf swing model the backswing was included, allowing the nuances of the backswing-to-downswing transition (specifically the storing of energy in the shaft and joints) to be modeled directly. This inclusion of the backswing necessitated two muscle torque generators for each joint: a maximal speed/torque concentric contraction MTG for the downswing, and a scaled speed/torque eccentric contraction MTG to represent the slower nature of the backswing. With two degrees of freedom at the shoulder, McNally and

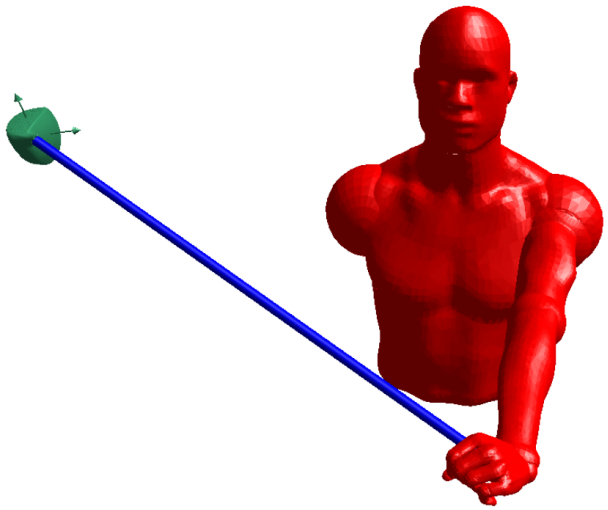

Figure 2.4: The 4-DOF golfer model of Balzerson et al. [34]. Degrees of freedom: torso rotation, shoulder add-abduction, wrist ulnar-radial deviation, and arm pronation-supination.

McPhee proposed using a single MTG that split the torque between these two DOFs, with this ratio of torques being an optimization variable. The biomechanics in conjunction with flexible shaft, clubhead-ball impact, and golf ball aerodynamic models formed the basis for several predictive "what-if?" simulations. In these simulations, parameter optimization was used to determine the activation and deactivation timings of each joint's backswing and downswing MTGs subject to a cost function typically maximizing the carry distance of the golf ball. Studies were conducted to find the optimal shaft balance point [36], clubhead inertial properties [37], and clubhead geometric properties [38] for a given hypothetical golfer, showing the power of a predictive forward dynamic model. It is this state-of-the-art model of McNally and McPhee upon which much of the work presented in this thesis is predicated.

2.2.2 Two-Armed Multibody Models

Multibody models of the golf swing published in the literature have been predominantly one-armed models, with just the leading arm considered. It is hypothesized that this is for several possible reasons. The simplest reason is that the golf swing is generally considered to be lead-arm dominant, with the trailing arm playing a more passive role. However, any golfer can attest that making a swing with solely their lead arm provides neither the power nor control of a two-armed swing. From a modeling perspective, another

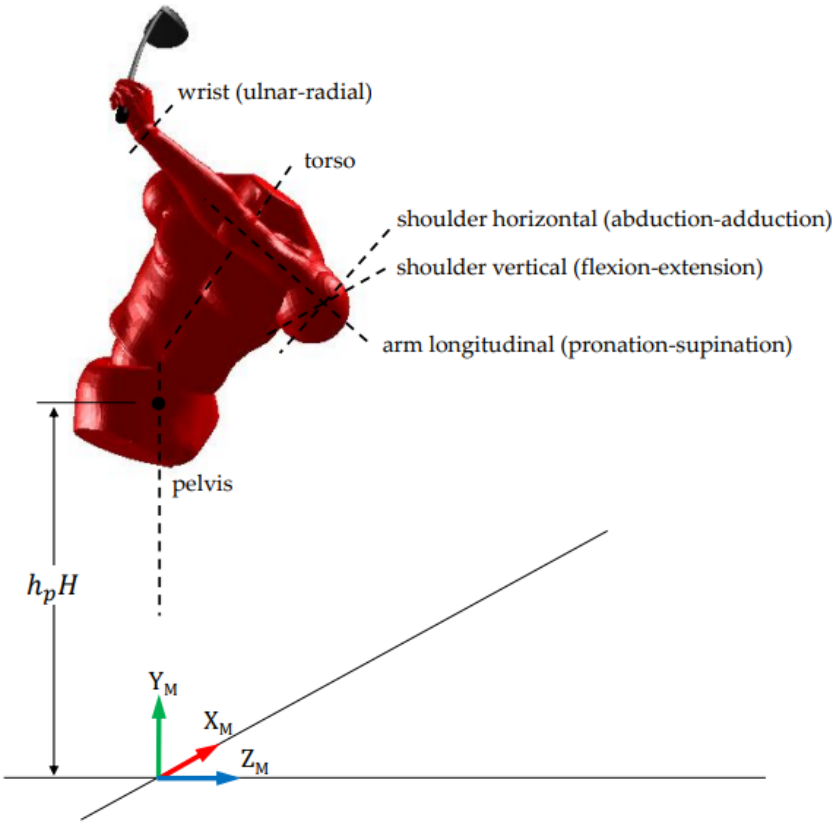

Figure 2.5: The 6-DOF golfer model of McNally and McPhee [37].

reason for excluding the trailing arm has been general model complexity. Although not as currently relevant with today's computational resources, in the past, the additional degrees of freedom associated with the trailing arm could have posed significant simulation time increases that made its inclusion untenable. However, the undoubted most constraining and challenging reason for excluding the trailing arm is the closed kinematic chain that it creates. That is, the two arms, torso, and club form a chain of segments where the last segment is connected through the chain back to the first segment. This arrangement means that the equations of motion for the system are a set of differential-algebraic equations (DAE)s, which are more difficult to solve than the ordinary differential equations for open-loop (one-armed) models [39]. In an inverse dynamics sense, this challenge has primarily been tackled by using force measurements to resolve the indeterminacy at the grip, such as the work by Takagi et al. [40] and Choi and Park [41].

In 2007, Nesbit [42] developed a full-body inverse dynamic model of the golf swing with

the aid of ADAMS software (Hexagon, Stockholm, Sweden). Biomechanically, the model included the head, torso, arms, pelvis, and legs which in total comprised 15 rigid segments connected by 15 unique joints (see Fig. 2.6). Notably, the inclusion of the legs in this model captures the contribution of the legs in the golf swing (see [43]). The joints were modeled as perfect connections without relative motion or damping, and the joint torques were applied at the joint centers. The hands of the golfer were not explicitly defined in the model and were instead lumped with the club's grip, meaning the distal ends of the forearms were connected directly to the grip using spherical-type joints. To solve the potential indeterminacy of the closed kinematic chain between the club and hands, flexible connectors were used and an equal load distribution between the hands was assumed. The shaft was modeled as 15 sub-segments connected by massless three-dimensional beam elements. Flexibility and mass properties of the shaft segments were calculated using analytical methods for a hollow cylinder while damping was determined experimentally by measuring the rate of amplitude decay following deflection of the clubhead with the butt end of the grip fixed. Spring-damper systems were used to model both the clubhead-ball impact forces, and the contact between the feet and ground (along with frictional forces to provide traction).

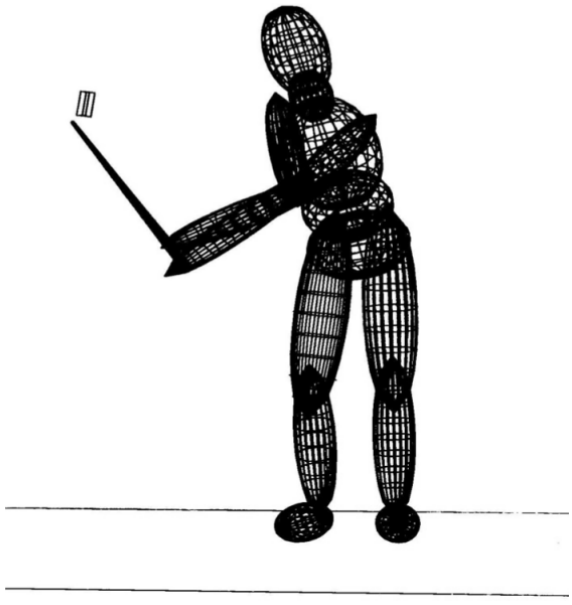

Figure 2.6: The full-body golfer model of Nesbit [42].

The model was driven kinematically using experimental motion capture data from sub-

ject golf swings. From this data, the global angular motions of the body segments and club were determined then transformed into local relative joint motions. Verification of the model was first performed kinematically, then dynamically by comparing ground reaction forces between the model and experiments, and finally by comparing model outputs (3D club trajectories and kinematics, joint kinematics and kinetics, golfer/club interaction forces, etc.) for several subjects to available published data. Nesbit found the model to show good agreement with experimental results for ground reaction forces along with club kinematics and kinetics, although verification of the internal joint torques and forces was difficult due to the lack of published data for comparison.

Although the work of Nesbit was a leap forward in the biomechanical fidelity of multibody golf swing models, it was not an explicit forward dynamic model capable of performing the "what-if?" simulation experiments that make forward dynamic approaches appealing. In 2014, MacKenzie and Normore [44] proposed a forward dynamic model of the golf swing including the trailing arm. Biomechanically, eight segments were included: the pelvis, torso, two upper arms, two forearms, and two hands. Biomechanical joints included those typical for the arms (excluding lead arm flexion/extension), torso twist and lateral bend, pelvis twist, and pelvis translation about the three global axes for a total of 19 joints. The hands of the golfer were connected to the grip of the club using three-dimensional spring-damper elements, avoiding the modeling of closed kinematic chains and their associated differential algebraic equations. Similarly to the work of MacKenzie and Sprigings [28] in 2009, torque generators capturing muscle properties were implemented for each of the rotational joints while a simple Fourier series representation was used for the pelvis translational joints. The backswing was not modeled, and instead the optimization began at the top of the backswing.

A genetic algorithm was used to optimize the activation timings of the torque generators and the coefficients of the Fourier series to maximize clubhead speed at impact, with penalties for deviations in club path and face angle. A typical optimized swing yielded a clubhead speed of 125 mph with a nearly square club path (0.5 degrees left) and angle of attack (0.8 degrees up). The authors found that the trail arm had a smaller kinetic contribution than the leading arm throughout the swing, although the trailing arm contributed more kinetic energy approaching impact. Regarding the equal hand load distribution assumption of Nesbit [42], MacKenzie and Normore found that at many points in the downswing the leading and trailing hands were applying forces to the grip different in magnitude and direction. It should be noted that details of this model are scarce in the available one-page abstract, with no figures, plots, or experimental validation. It is therefore difficult to ascertain the applicability of this model.

2.2.3 Opportunities for Improvement

After an extensive review of the literature, it was found that a significant opportunity exists to build upon the work of prior publications and develop a single forward dynamic golfer model that includes the trailing arm, pelvis translation, and optimization routine including impact and the flight of the ball. While these concepts and implementations have been scattered across several papers in the literature, there has yet to be a full golfer model published including all of these features.

Succinctly illustrating the need for a single model encompassing many of the individual contributions in this space is the work of McNally and McPhee [35] and MacKenzie and Normore [44]. The work of McNally and McPhee modeled the backswing, included a continuous analytical shaft model, impulse-momentum impact model, and golf ball aerodynamic model but did not include the trailing arm or pelvis translational degrees of freedom. On the other hand, MacKenzie and Normore included the trailing arm and pelvis translation but did not model the backswing or consider the impact and flight of the ball, nor present experimental model validation.

2.3 Dynamic Models of Golf Ball Flight

While a technically sound and aesthetically pleasing golf swing is a pleasure to watch, it is completely meaningless in competition if the swing does generate a successful ball flight—the quantifiable outcome of the shot. For this reason, the ability to accurately model the aerodynamic forces contributing to the ball's flight is essential to develop a robust model of a golf drive.

2.3.1 Early Studies of Golf Ball Aerodynamics

Like many sports balls, the study of golf ball aerodynamics is not a new endeavour. In the late 1890s prior to the inclusion of dimples on golf balls, Peter Tait [45] was the first to model golf ball lift force. Importantly, Tait attempted to quantify the effect of spin on this lift force. This would later come to be widely known as the Magnus effect, named after the 1852 work of Heinrich Magnus pertaining to rotating cylinders. Although Tait's model under-predicted the maximum driving distance that was observed to be achievable at the time, it laid the groundwork for future studies in this area (see McPhee [9]).

Fast-forward a half-century, and dimpled golf balls had become commonplace in the sport. The presence of these dimples creates a turbulent boundary layer surrounding the ball that decreases flow separation on the downstream side. This reduces the low-pressure wake region following the ball, and therefore the pressure drag acting on it [46]. The first foray into quantifying the aerodynamic forces of both smooth and dimpled golf balls was undertaken by John Davies in 1949 [47]. Davies understood that the aerodynamic forces acting on the ball could be decoupled into lift $\boldsymbol{L}$ (acting perpendicular to the wind and axis of rotation) and drag $\boldsymbol{D}$ (acting in the direction of the wind)

$$\boldsymbol{L} = \frac{1}{2}\rho A_b \left|\boldsymbol{v}_b\right|^2 C_L(\hat{\boldsymbol{\omega}}_b \times \hat{\boldsymbol{v}}_b) \tag{2.1}$$

$$\boldsymbol{D} = \frac{1}{2}\rho A_b \left|\boldsymbol{v}_b\right|^2 C_D(-\hat{\boldsymbol{v}}_b) \tag{2.2}$$

where ρ is the ambient air density, A_b is the equatorial cross-sectional area of the golf ball, $\boldsymbol{v}_b$ is the linear velocity vector of the ball, C_L and C_D are the coefficients of lift and drag, and $\hat{\boldsymbol{v}}_b$ and $\hat{\boldsymbol{\omega}}_b$ are the unit vectors for the linear and angular velocity of the ball. Using the wind tunnel of tire manufacturer B.F. Goodrich, Davies dropped American specification[1] balls at spin rates of up to 8000 rpm in a horizontal freestream air velocity of 105 ft/s. By measuring the horizontal displacement of the balls, Davies found that the drag of dimpled balls increased linearly from 0.06 lb with no spin to 0.1 lb at 8000 rpm. He also found lift to be an exponential function of spin rate: $L = 0.64(1 - e^{-0.00026|\boldsymbol{\omega}_b|})$ up to a maximum of 0.055 lb.

2.3.2 Quantifying the Dynamic Nature of Aerodynamic Coefficients

Until this point, most experimental studies had focused on quantifying golf ball aerodynamics at a constant freestream velocity. However, lift and drag (and their respective non-dimensional coefficients) are evidently dynamic. The non-dimensional Reynolds number is a logical starting point for dynamic study

$$Re = \frac{v_b 2R}{\nu} \tag{2.3}$$

[1] At the time, both British and American golf balls weighed 1.62 ounces but had diameters of 1.62 and 1.68 inches, respectively. In 1990, the USGA and R&A agreed to proceed with 1.68 inches as the universal minimum diameter standard.

where R is the ball radius and ν is the kinematic viscosity of air. Williams used the Reynolds number in a 1959 study of the relationship between ball speed and drag [48], where under significant assumptions he found that C_D was inversely proportional to Re, making drag a linear function of speed. Expanding scope to both C_L and C_D, in 1976 Bearman and Harvey [49] conducted a wind tunnel study of British specification golf balls across several speeds and spins. Limited by the maximum speed of their wind tunnel, they used a 2.5 times scaled golf ball in order to study the Reynolds numbers of interest. Measurements of lift and drag were performed at speeds ranging from 14 to 90 m/s and spins ranging from 1000 to 6250 rpm. From these experiments, the authors found that the drag crisis[2] for a dimpled ball occurred at approximately $Re = 40,000$, much lower than that of a smooth sphere. Bearman and Harvey also found that the relationship between lift and spin was non-linear, non-dimensionalizing spin as the spin ratio S:

$$S = \frac{\omega_b R}{v_b} \tag{2.4}$$

In 1992, Smits and Smith [50] conducted further wind tunnel experiments to develop their own aerodynamic model. Importantly, the authors included a spin rate decay term SRD

$$SRD = \frac{d\omega_b}{dt}\frac{R^2}{v_b^2} \tag{2.5}$$

which captured the reduction in spin throughout the flight of the ball as it encounters aerodynamic loading. With the aid of a trajectory program from Lieberman [51] developed using USGA trajectory data, Smits and Smith proposed the following dynamic model for the aerodynamic coefficients and SRD

$$C_L = C_{l_1} S^{0.4} \tag{2.6}$$

$$C_D = C_{d_1} + C_{d_2} S + C_{d_3} sin\left\{\pi(Re - A_1)/A_2\right\} \tag{2.7}$$

$$SRD = R_1 S \tag{2.8}$$

[2]The drag crisis is a significant reduction in drag that occurs when flow begins to transition from laminar to turbulent, energizing the boundary layer, and reducing the low-pressure wake region trailing the object. Gustave Eiffel found this to occur between approximately $Re = 200,000$ and $Re = 300,000$ for a smooth sphere.

where C_{d_1} through C_{d_3}, A_1 and A_2, C_{l_1}, and R_1 are constant coefficients. The authors noted that based on the data used to develop this model, it is applicable only for driver shots with Reynolds numbers between 70,000 and 210,000 and spin ratios between 0.08 and 0.20.

In 2002, Quintavalla [33] proposed his own model with curve fits for C_L and C_D based on experimental data from the USGA's indoor test range:

$$C_L = a + bS \tag{2.9}$$

$$C_D = c + dS^2 \tag{2.10}$$

where a through d are non-linear functions of the Reynolds number containing a total of twelve constant parameters.

With the improved computing tools of the last two decades, high-fidelity computational fluid dynamics (CFD) has become a valuable tool in the study of ball aerodynamics. R.K. Hanna [52] provided an excellent review of CFD in sports more broadly, while T.J. Chung [53] provided details of the CFD problem-solving approach. Specific to golf balls, CFD studies have been conducted by Aoki et al. [54] and Crabill et al. [55], with both showing general agreement with historical experimental observations. While CFD is an excellent tool for the granular design of dimple patterns and covers, the level of detail and associated simulation time is excessive for inclusion in optimization-based forward dynamic golfer models, such as the one presented in this thesis.

2.3.3 Opportunities for Improvement

There have been no shortage of investigations into golf ball aerodynamics since the work of Tait [45] in the 1890s. In fact, the search query "golf ball aerodynamics" returns more than 12,000 results on Google Scholar. However, advances in dimple pattern and golf ball cover design mean that the aerodynamics of today's balls are not reflective of even those as recent as ten years ago. This means that parameter-based aerodynamic models such as those presented by Smits and Smith in 1992 [50] and Quintavalla in 2002 [33] would not reflect contemporary aerodynamics if used in a golf drive model. McNally recognized this in his 2018 golf drive model which used the model of Quintavalla, and expressed the need for an updated parameter-based model.

Chapter 3

Dynamic Model of a Golf Drive

The overall model of a golf drive presented here is a synthesis of four sub-models:

1. A model of the golfer's biomechanics including body segments and the torques that drive them
2. A continuous analytical flexible shaft model
3. An adjusted impulse-momentum clubhead-ball impact model
4. A golf ball aerodynamic model to simulate ball flight

The development and functionality of these sub-models is discussed in the subsequent subsections, while validation is presented in Chapter 4.

3.1 Golfer Biomechanics

3.1.1 Segments and Degrees of Freedom

The biomechanical model of the golfer includes eight segments that are represented by rigid bodies: the pelvis, torso, and bilateral upper arms, lower arms, and hands. The size and inertial properties of the segments are based upon the experimental measurements made by Zatsiorsky et al. [56], and modified by de Leva [57] to be in relation to joint centers rather than bony landmarks. In the default configuration of the model, the segments

represent those of an adult male with a height of 174 cm and mass of 73 kg, although the parameterized nature of the model allows for scaling to any height and mass. While the inclusion of the lower limbs in the model would improve its overall biofidelity, the increased model complexity and associated simulation time increase is not justifiable; the primary contribution of the legs is captured in the translation of the pelvis. It should also be noted that the golfer is right-handed.

The pelvis is positioned on a prismatic joint that runs parallel to the global X axis (downrange, refer to Fig. 3.1) at a height h above the global origin (the default value of h is half the golfer's height). This translation encompasses the weight shift that occurs in the frontal plane during the golf swing. The pelvis also has a rotational joint about a local axis passing through the centroid of the pelvis and parallel to the global Y axis. The connection between the pelvis and torso is a universal joint that allows for two adjustment rotational joints: torso tilt in the sagittal plane towards the golf ball (approximately 35 degrees), and torso tilt in the frontal plane away from the target (approximately 10 degrees). The torso has its own rotational joint about its long axis that passes through the sternum, effectively reproducing rotation of the trunk.

The arms connect to the torso at shoulder joint centers that are nominally positioned bilaterally across the torso and at the height of the suprasternal notch in the frontal plane. Both shoulder joint centers have three linear adjustment joints that model small scapular adjustments during the address position (see Section 3.1.4). Both shoulders are connected to the torso using universal joints, allowing flexion-extension and adduction-abduction. The lead arm has a pronation-supination rotational joint about its long axis and an ulnar-radial deviation rotational joint at the wrist. In following the work of McNally and McPhee [35], the lead arm elbow and wrist flexion-extension rotational joints are omitted given their rarity of use in the swings of elite golfers. The trailing arm has an active flexion-extension rotational joint and a passive pronation-supination rotational joint at the elbow to facilitate the "folding" and "unfolding" of the arm during the swing. In addition to active ulnar-radial deviation, the trail wrist also has a passive flexion-extension rotational joint that helps facilitate the movement of the lead arm (primarily pronation-supination).

In total the golfer has 13 biomechanical joint coordinates, which are outlined in Fig. 3.1. Twelve of these coordinates are rotational and modeled using revolute joints, while the other is translational and modeled using a prismatic joint. Much like in many human motions, here the system is heavily overactuated; the 13 dynamic biomechanical joint coordinates give the system seven degrees of freedom once the six algebraic constraint equations are applied as a result of the closed kinematic chain between the two arms, club, and torso.

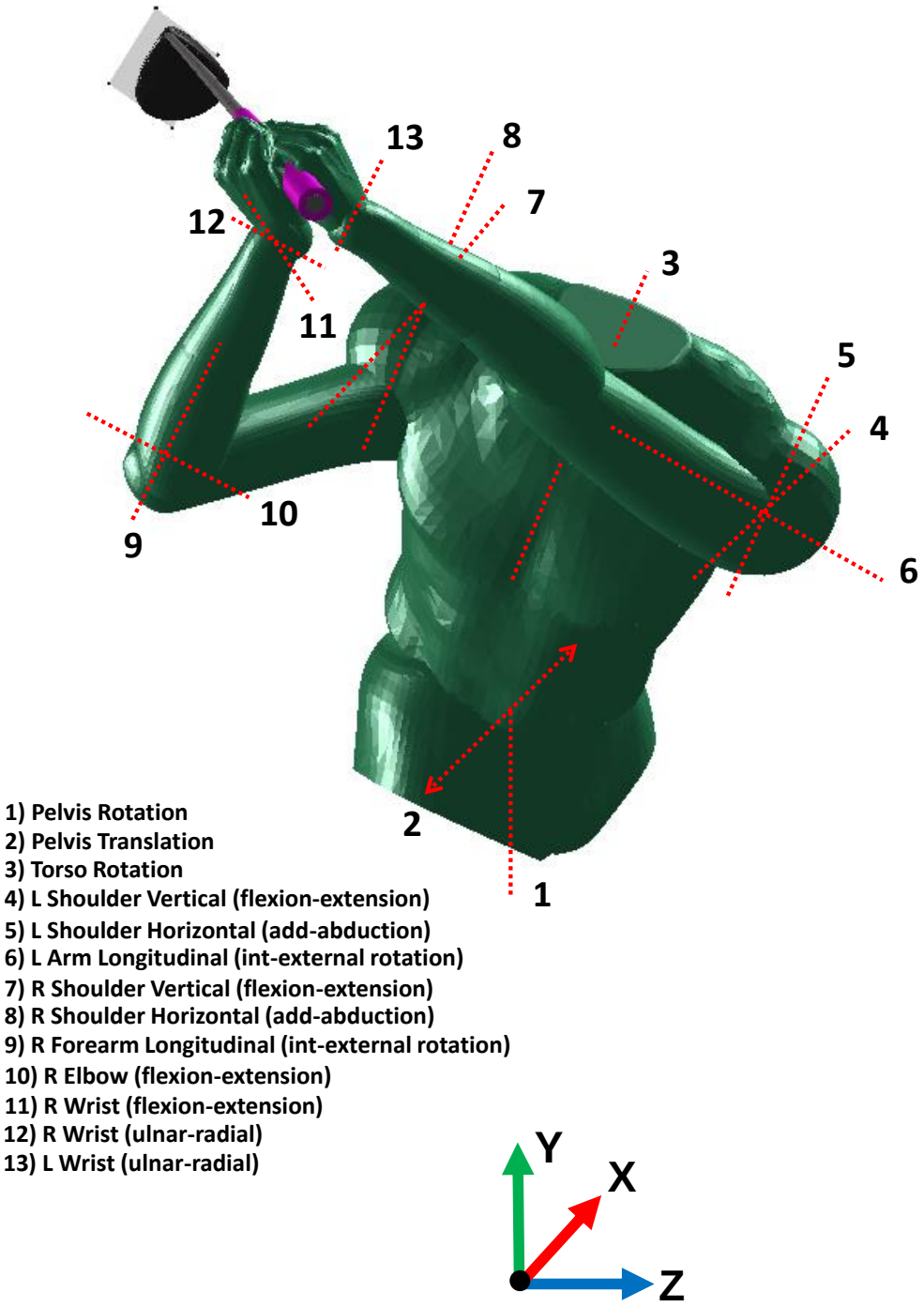

Figure 3.1: Golfer biomechanical model joint coordinates.

The hands of the model connect to the shaft of the golf club using fixed rigid constraints, where they both work to contribute to the motion of the grip (see "bimanual manipulation" [58]). The orientations at which the hands connect to the shaft are adjustment joints determined at address (see Section 3.1.4). Because the hands in a golf grip are typically arranged in an interlocked configuration, the connection points are spaced 60 mm apart axially along the shaft, which is less than the half-width of a male hand [59]. Connecting both hands to the club in the model forms a closed kinematic chain. That is, the two arms, torso, and club form a chain of segments where the last segment is connected through the chain back to the first segment. This arrangement means that the equations of motion for the system are a set of differential-algebraic equations (DAE)s, which can be difficult to solve in real-time. Fortunately, MapleSim's symbolic computing approach is quite robust in handling sets of DAEs—in this model the CK45 semi-stiff solver with constraint projection is used. Furthermore, because this model is used in a forward dynamic sense, it is not necessary to determine a load-sharing relationship between the hands as has been necessary in previous inverse dynamic models [42].

3.1.2 Muscle Torque Generators

Modeling muscles in forward dynamic simulations is a balancing act between biofidelity and model complexity. In models where quantifying the forces in each individual muscle is requisite (such as evaluating injury risk [60]), a Hill-type model [61] for each muscle is a necessary evil. In a model such as this where there are 12 rotational joints with several muscles spanning each, the prospect of modeling each muscle individually is untenable due to the associated simulation time. Rather than modeling each muscle, muscle torque generators (MTG)s combine the effects of each muscle crossing the joint to reduce complexity while still capturing important phenomena such as the force-velocity relationship [62]. MTGs have been used in several forward dynamic models of athletic motions, ranging from golfer models [30, 35] to Olympic track cyclists [63] and wheelchair-athletes [64].

Each MTG can be broken down into two components: active and passive. The active component can be thought of as the torque generated at the joint through voluntary muscle activation and deactivation via neural input. The passive component encompasses the contribution of ligaments, tendons, and muscles stretching to store elastic energy. These contributions are most notable at the edges of the joint range of motion.

Active Torque

The fundamental building block of the active portion of the MTG is the isometric torque generation curve, which models the ramp-up, peak, and ramp-down of the isometric torque produced at the joint. These ramp periods represent the non-instantaneous contraction and relaxation of the muscles crossing the joint, as well as the latent period following neural input. The isometric torque equation of MacKenzie and Sprigings [28] was modified by McNally and McPhee [35] to reduce its numerical stiffness, and is given by

$$T_{isometric} = T_{max}\left(1 - e^{\frac{-t}{\tau_{act}}}\right)^n - T_{max}\left(1 - e^{\frac{-t'}{\tau_{deact}}}\right)^n \tag{3.1}$$

where T_{max} is the maximum isometric torque of the joint, τ_{act} and τ_{deact} are the activation and deactivation time constants (0.06 seconds in this model), t is the time from the start of activation, t' is the time from the start of deactivation, and n is a positive integer used to smooth the curve during activation and deactivation (3 is used in this model). Figure 3.2 shows four sample isometric torque curves for varying activation and deactivation times and smoothness.

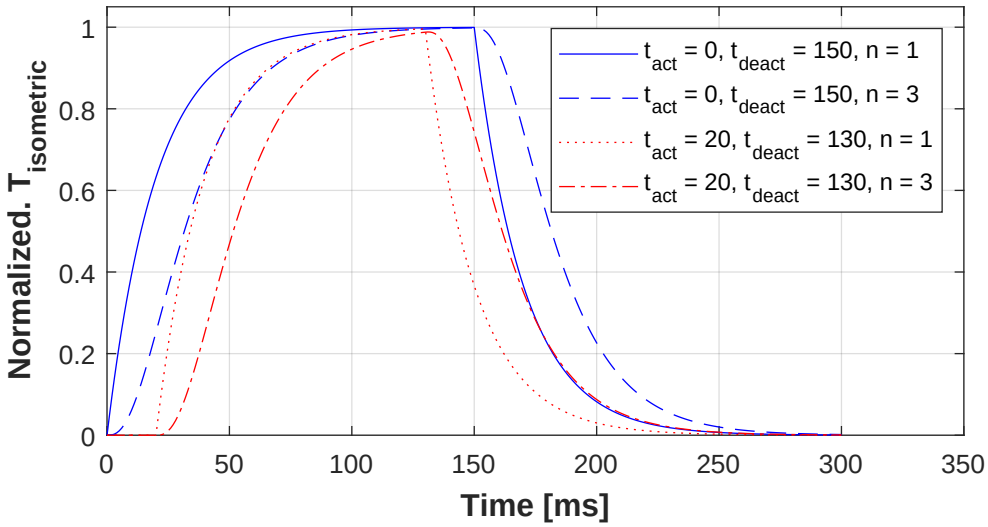

Figure 3.2: Sample isometric torque generation curves for varying activation/deactivation times and smoothness coefficient (n).

The isometric torque is then scaled according to the angular velocity of the joint, which equates to the force-velocity relationship of a Hill-type muscle model. The piecewise

equation for this scaling was proposed by McNally and McPhee [35], and based upon the work of Katz [65] and van Soest et al. [66]. It is given by

$$T = \begin{cases} T_{isometric}\left(\frac{\omega_{max}-\omega}{\omega_{max}+\Gamma\omega}\right) & \text{if } \omega \geq 0 \\ \\ T_{isometric}\left(\frac{(1-T_r)\omega_{max}+S\omega T_r(\Gamma+1)}{(1-T_r)\omega_{max}+S\omega(\Gamma+1)}\right) & \text{if } \omega \leq 0 \end{cases} \tag{3.2}$$

where ω is the current rate of shortening of the joint, ω_{max} is the maximum rate of shortening of the joint, Γ is a shape factor controlling curvature, T_r is the ratio between the maximum eccentric and isometric force (1.5 used in this model), and S is the ratio between the eccentric and concentric derivatives of force with respect to velocity at maximum isometric force as defined by van Soest et al. [66] (2 used in this model). Importantly, this piecewise scaling equation accounts for the fact that because of the backswing, some of the MTGs may still be lengthening at the time of downswing activation. Figure 3.3 shows a sample angular velocity scaling curve generated by Eq. 3.2 for the elbow flexion-extension MTG.

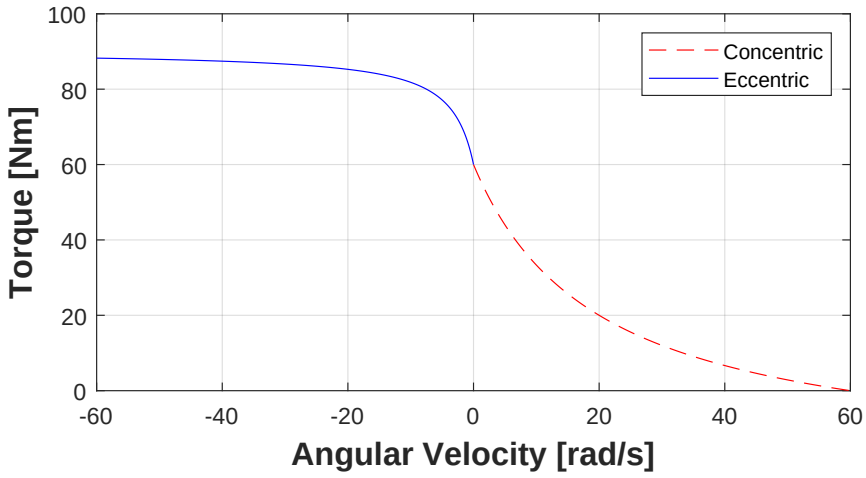

Figure 3.3: Sample velocity-scaled concentric and eccentric torque curves for elbow flexion-extension. $T_{isometric} = 90$ Nm, $\omega_{max} = 60$ rad/s, $\Gamma = 3$, $S = 2$, $T_r = 1.5$.

Each shoulder has two rotations and two corresponding MTGs: horizontal adduction/abduction, and flexion/extension. To split the total active isometric shoulder torque between the two MTGs, the concept of the shoulder torque ratio proposed by McNally and McPhee [35] is implemented here. This shoulder torque ratio is a separate optimization

variable for each of the shoulders, and controls the swing plane. Building upon the work of McNally and McPhee, separate shoulder torque ratios are used for the backswing and downswing to allow for a dual-plane swing if the optimization finds it advantageous. The adduction/abduction isometric torque of the shoulder is given by

$$T_{s,add/abd} = \sqrt{\frac{T_s^2}{(1+r)^2}} \tag{3.3}$$

where T_s is the total active isometric shoulder torque, and r is the shoulder torque ratio. Similarly, the flexion/extension isometric torque of the shoulder is given by

$$T_{s,flex/ext} = rT_{s,add/abd} \tag{3.4}$$

Of the 12 dynamic rotational joints, all but two contain active MTG components; the trail wrist flexion-extension and trail arm pronation-supination joints are purely passive. The decision was made to remove the active components of these joints in order to reduce number of optimization variables, a necessary concession given the complexity of the system. In particular, the trail wrist flexion-extension joint was chosen given its relative lack of contribution [67] while the trail arm pronation-supination joint was chosen given the redundancy provided by the lead arm pronation-supination joint in the downswing. The ten remaining rotational joints have separate active components for the backswing and downswing, as these motions occur in opposite directions and at different speeds. Table 3.1 outlines the active parameters for the downswing portion of the MTGs. For common joints between the models, the same maximal isometric torque values as McNally and McPhee [35] were used; only the trail elbow flexion-extension joint required new data from Millard et al. [68]. Despite the addition of the trailing arm in this model, several of the "doubled" torques used in the single arm model of McNally and McPhee are replicated here. This was done to produce model swing speeds and characteristics commensurate with elite golfers—this is especially important during validation (see Chapter 4) where comparing swings with vastly different clubhead speeds would not be meaningful. The active parameters for the backswing MTGs are the same as the downswing except for the maximum angular velocities and isometric torques. Per McNally and McPhee [35], the maximum angular velocities are scaled to 7% of the downswing values while the maximum isometric torques are scaled to 65% of the downswing values.

Table 3.1: Active joint torque function parameters for rotational joints.

Joint	$T_{isometric}$ [Nm]	ω_{max} [rad/s]	Γ	T_r	S	n
Pelvis rotation	250	30	3	1.5	2	3
Torso rotation	200	30	3	1.5	2	3
Shoulder flex/extension	160*	60	3	1.5	2	3
Shoulder add/abduction	160*	60	3	1.5	2	3
Elbow flex/extension	90	60	3	1.5	2	3
Forearm pro/supination	60	60	3	1.5	2	3
Wrist unlar/radial	90	60	3	1.5	2	3

*160 Nm is split between the two joints per the shoulder torque ratio

Passive Torque

The passive joint torques encompass the contributions from ligaments, joint capsules, and surrounding tissues. These contributions are prevalent primarily towards the edges of the joint range of motion where these tissues begin to stretch. The passive joint torque modeling for the rotational joints is based upon the function proposed by Yamaguchi [69]

$$T_{passive}(\theta, \dot{\theta}) = k_1 e^{-k_2(\theta-\theta_1)} - k_3 e^{-k_4(\theta_2-\theta)} - c_1\dot{\theta} \tag{3.5}$$

where θ is the joint angle, $\dot{\theta}$ is the joint angular speed, k_1 through k_4 are shape parameters, θ_1 and θ_2 are angular breakpoints, and c_1 is a damping coefficient. The breakpoints θ_1 and θ_2 set the angles at which the passive torque contribution begins to significantly increase (near the limits of the joint range of motion), while k_2 and k_4 control the sharpness of the break. Parameters k_1 and $-k_3$ are roughly equal to the passive torque at $\theta = \theta_1$ and $\theta = \theta_2$, respectively.

The damping coefficient c_1 is assumed to be 0.1 Nms/rad per the recommendation of Yamaguchi, while the angular breakpoints and shape parameters were fit to experimental data using MATLAB's `nlinfit` nonlinear regression algorithm. For the pelvis, torso, shoulder, forearm, and ulnar/radial deviation of the wrist, the passive torque data used by McNally and McPhee [35] was utilized. For the new elbow flex/extension joint, data

from Millard et al. [68] and Kental et al. [70] was used. For wrist flex/extension, data from Formica et al. [71] was used. A summary of the fitted parameters can be found in Table 3.2 along with the source of data for each joint. Figure 3.4 plots these passive torque curves.

Table 3.2: Passive joint torque function parameters for rotational joints.

Joint	θ_1 [rad]	θ_2 [rad]	k_1 [Nm]	k_2	k_3 [Nm]	k_4	Source
Pelvis rotation	-0.09	0.09	5.56	1.97	5.57	2.01	[72]
Torso rotation	-0.09	0.09	5.56	1.97	5.57	2.01	[72]
Shoulder flex/extension	-1.14	1.27	7.03	2.31	4.30	1.65	[73, 74]
Shoulder add/abduction	-1.35	1.23	3.22	2.13	4.38	1.62	[73, 74]
Elbow flex/extension	-2.01	0.03	0.39	7.85	3.55	20.6	[68, 70]
Forearm pro/supination	-1.24	1.34	3.21	2.62	2.22	1.75	[75]
Wrist unlar/radial	-0.51	0.42	0.55	5.81	0.92	10.4	[71]
Wrist flex/extension	-1.12	1.14	1.01	2.03	1.74	2.01	[71]

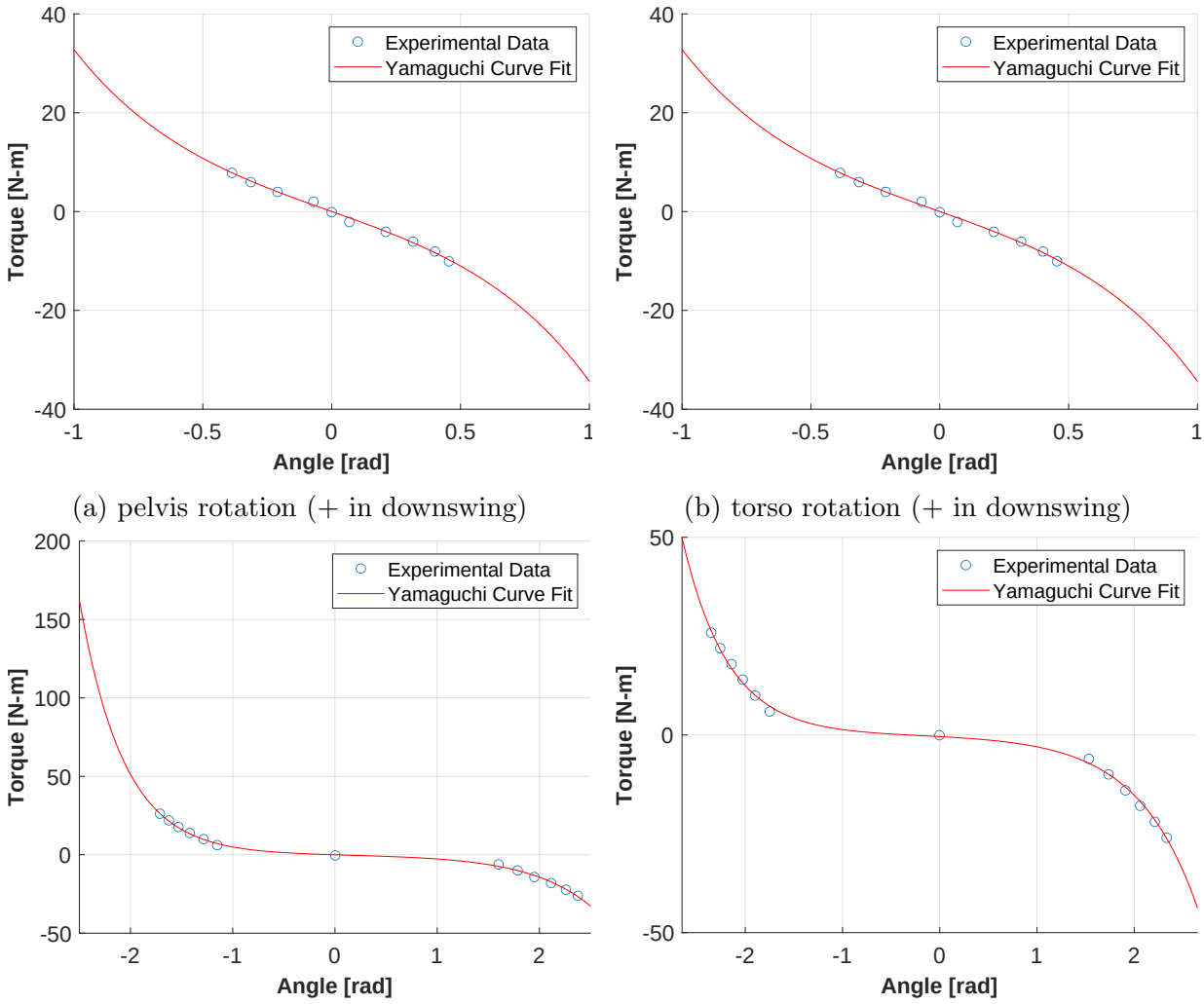

(a) pelvis rotation (+ in downswing)

(b) torso rotation (+ in downswing)

(c) shoulder flex (+)/extension

(d) shoulder adduction/abduction (+)

Figure 3.4: Passive joint torque curves for the biomechanical model. Anatomical polarity of the angles indicated under each subfigure.

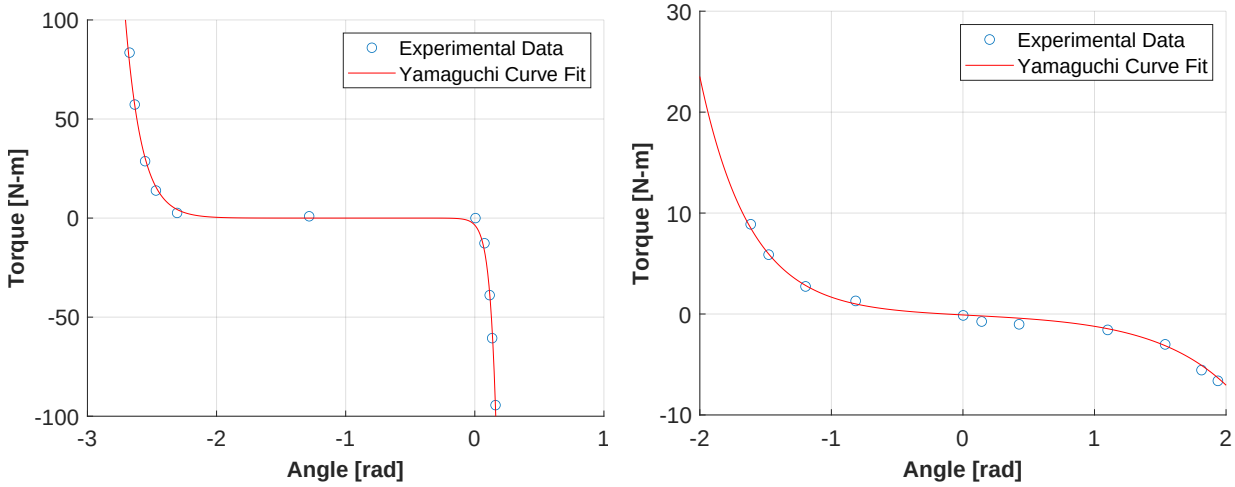

(e) elbow flex/extension (+)

(f) forearm pro/supination (+)

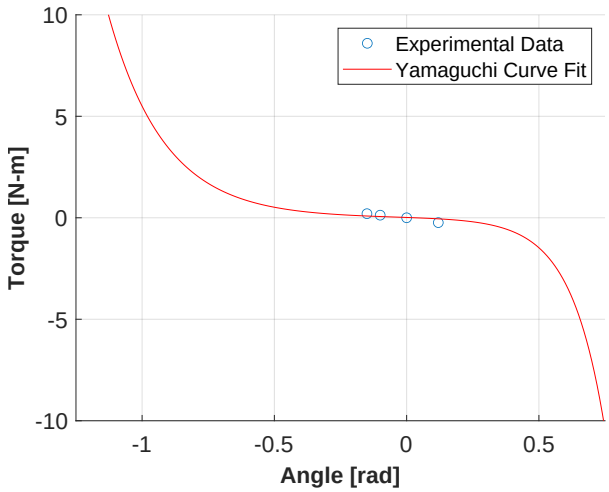

(g) wrist ulnar/radial (+) deviation

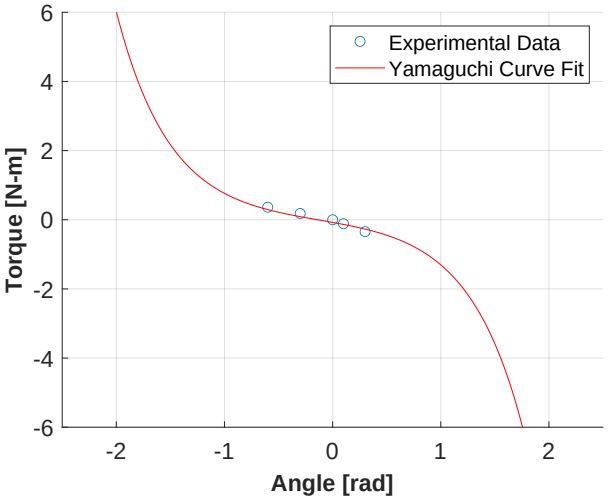

(h) wrist flex/extension (+)

Figure 3.4: (continued) Passive joint torque curves for the biomechanical model. Anatomical polarity of the angles indicated under each subfigure.

3.1.3 Pelvis Translational Muscle Force Generator

The inclusion of global X direction pelvis translation in the model necessitates a unique method to drive this joint, as rotational MTGs are not suitable. While pelvis translation in the golf swing has been previously studied in the literature [76], these investigations have been primarily kinematic in nature and are not concerned with how to replicate this motion in a forward dynamic modeling sense. Because of this, a custom "muscle force generator" (MFG) is developed here in order to dynamically drive this pelvis translation.

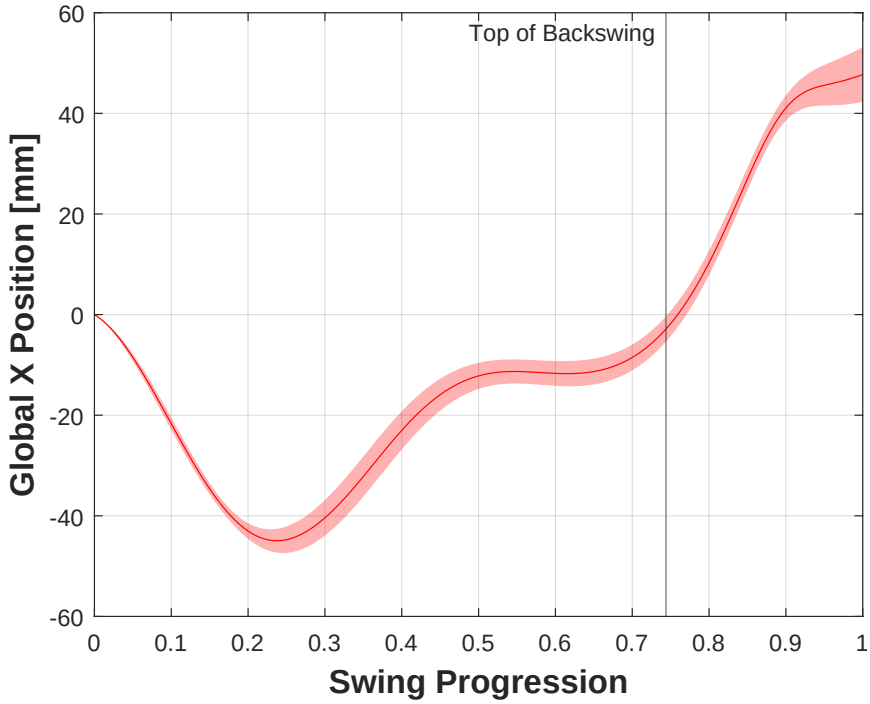

Figure 3.5: Pelvis translational position in the global X direction for Golfer 10 of the motion capture experiment (see Chapter 4 and Appendix E). Note that the pelvis undergoes mutliple changes in direction during the backswing phase before returning to within 6 mm of the address position at the top of the backswing.

As outlined in Chapter 4, a motion capture experiment of ten elite golfers was undertaken; part of this experiment quantified the pelvis translation of participants. Prior to the study, it was assumed that the pelvis would translate away from the target during the backswing, reach its furthest point at the top of the backswing, and then translate towards the target during the downswing. However, it was found that during the backswing the

pelvis often had several small reversals in direction that would be difficult to model dynamically. In addition, the pelvis often ended up near its address position at the top of the backswing (See Fig. 3.5 as an example of this). For the study participants, the average top of the backswing pelvis X position was just 4.8 ± 33.9 mm downrange from the address position. For these reasons, it was decided that pelvis translation could be neglected for the backswing. This is achieved in the MapleSim model using the *Gripper* feature which fixes the pelvis on its prismatic joint until the beginning of the downswing.

For the downswing, the translational movement of the pelvis was found to be much more predictable during the motion capture experiment. For the study participants, the average impact pelvis X position was 51.2 ± 35.4 mm downrange from the top of backswing position. To model this movement, the muscle torque generator isometric torque generation curve (Fig. 3.2) was repurposed to generate a force applied to the pelvis in the positive global X direction instead of a torque. The maximal force of the curve is 600 N which is based upon male hip thrust strength [77]. The damping and stiffness parameters of the prismatic joint were tuned via an optimization routine to produce downswing translation values in line with the experimental results from the motion capture study (see Chapter 4).

3.1.4 Address Position

While the simulation of the system's DAEs throughout the golf swing is possible, the closed kinematic chain means that the determination of the initial conditions of the golfer's biomechanics (the address position) is quite challenging. Moreover, the set of initial conditions that are satisfactory will change depending on factors such as the golf club's length and the height of the tee.

To determine a set of suitable initial conditions for each simulation, an optimization routine is employed using MATLAB's `genetic algorithm`. In total, there are 20 optimization variables that are laid out in Table 3.3 along with a typical solution for a 46 inch club length and a four inch tee height. In addition to the initial conditions of the rotational joints, there are "adjustment" parameters at both the pelvis and shoulders. At the pelvis, the parameter h adjusts the height of the golfer's pelvis above the ground as a proportion of their height; this accounts for knee flexion. At each of the shoulders, the position of the shoulder joint center has a small amount of translational adjustment along all three axes to account for scapular positioning [78, 79]. As demonstrated in Fig. 3.6, professional golfers often perform scapular elevation/depression and retraction/protraction during address, and in many cases this adjustment is physically necessary to close the kinematic chain between the two arms, torso, and club.

The optimization's cost function is shown below

$$J = (r_{CF,X} - r_{b,Z})^2 + (r_{CF,Y} - r_{b,Y})^2 + (r_{grip,X} - r_{CF,X})^2 + (\theta_{elb} - \theta_{elb,opt})^2 + (\phi_c - \phi_{c,opt})^2 \quad (3.6)$$

where $\boldsymbol{r}_{CF}$ is the location of the center of the clubface, $\boldsymbol{r}_b$ is the target location of the clubface, $\boldsymbol{r}_{grip}$ is the location of the butt end of the grip, θ_{elb} and $\theta_{elb,opt}$ are the actual and optimal elbow flexion angle, and ϕ_c and $\phi_{c,opt}$ are the actual and optimal lie angle of the club (the angle between the club shaft and the XZ plane). The cost function seeks to place the clubhead behind the ball while ensuring there is minimal shaft lean (the angle between the club shaft and the YZ plane), the trailing elbow is in a flexion position of approximately 20 degrees, and the club rests at approximately its lie angle. These terms ensure that the approximate address position of a professional golfer is produced (Fig. 3.6) using as few cost function terms as possible.

(a) face-on view (b) down-the-line view

Figure 3.6: Address position of a professional golfer with joint centers indicated. Adapted from [80].

Table 3.3: Address position optimization solution for a nominal driver.

Variable	Typical Solution
Pelvis rotation [rad]	0.09
Torso rotation [rad]	0.09
Shoulder flex/extension [rad]	L -0.55 R -0.57
Shoulder add/abduction [rad]	L -0.43 R -0.33
Elbow flex/extension [rad]	R -0.37
Forearm pro/supination [rad]	L 0 R -1.11
Wrist unlar/radial deviation [rad]	L -0.26 R -0.19
Wrist flex/extension [rad]	R -0.09
Shoulder (x,y,z) adjustment [mm]	L (0,10,20) R (20,-30,-20)
Pelvis height adjustment	0.5

Note: L/R indicate solutions for the golfer's left and right arms where applicable

3.2 Flexible Shaft Model

The club's shaft plays an important role in the golf swing, serving as the connection between the golfer's grip and the clubhead. The shaft's length [38], stiffness [29], and balance point [36] have all been shown to affect the dynamics of the clubhead at impact, making an accurate model of the shaft important for golf swing simulations. While high-fidelity finite element models of the shaft have been published [81], the associated simulation times are untenable for a forward dynamics application.

To bridge the gap between model fidelity and simulation time, the experimentally-validated continuous analytical shaft model presented by McNally et al. [82] is used. The model is developed and deployed in MapleSim using the *Flexible Beam* component, and is based upon a Rayleigh beam formulation. The deformation in the shaft is represented by four variables: axial deformation along the longitudinal axis $u(x,t)$, transverse deformations $v(x,t)$ and $w(x,t)$, and torsional deformation $\phi(x,t)$, where x is the longitudinal position along the shaft axis from the butt end. These variables are approximated by Taylor series polynomial shape functions and time-varying elastic coordinates.

The outer diameter of the shaft combined with its taper and wall thickness are used to determine the cross-sectional area A, second moment of area I, and polar moment of inertia J as continuous functions along the length of the shaft. Bending EI and torsional GJ stiffness profiles provided by the shaft manufacturer are then divided by I and J to determine E and G, which are then fit using third-order polynomials. A sample EI stiffness profile of an archetypal shaft is shown in Fig. 3.7.

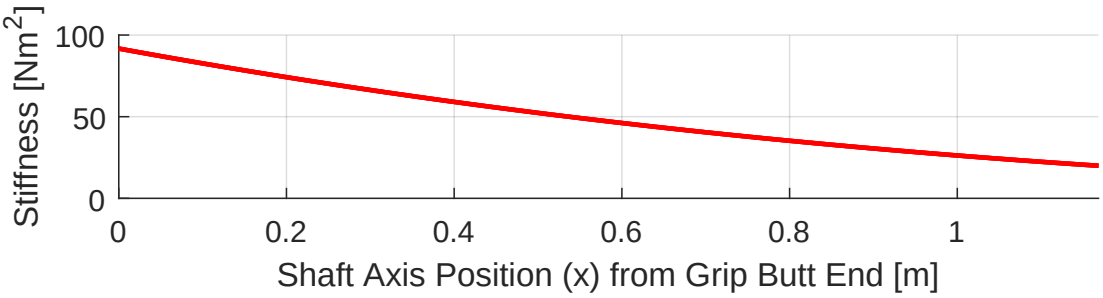

Figure 3.7: Sample shaft EI stiffness profile.

The continuous analytical shaft model was found by McNally et al. to have a root mean square error of 1.14, 0.83, and 0.85 degrees for shaft droop, lag, and twist at impact across several motion capture experiments. Importantly, the simulation time for this model is

on the order of 0.3 seconds, which is suitable for an optimization-based forward dynamic model.

3.3 Clubhead-Ball Impact Model

To simulate the impact between the clubhead and ball, the experimentally-validated adjusted impulse-momentum (IM) impact model proposed by Danaei et al. [83] is implemented (see Fig. 3.8). The model is based upon the IM model of Petersen and McPhee [32], but includes several updates to improve accuracy. The model replaces the ellipsoidal clubface surface with a torus to allow for constant bulge and roll radii, and the clubhead mass and relative impact location are adjusted to address ball speed deficits, and spin rate discrepancies.

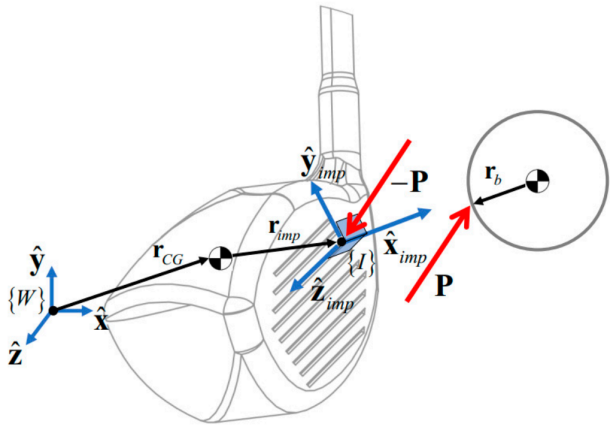

Figure 3.8: Free body diagram of the impact between the clubhead and ball [83].

Importantly for optimization of the full golfer model, this impact model is computationally efficient when compared to alternatives such as finite element models [84]. In a driver-specific application such as this, where the impact between the clubhead and ball is not significantly oblique in nature, the simplifying assumptions of an IM model are suitable (e.g. the pure rolling assumption that assumes the clubhead and ball have equal tangential velocities when the ball leaves the clubface). Using experimental driver data collected by a golf club manufacturer, this model was shown by Caldwell and McPhee [85] to perform better than three other more computationally-intensive contact models, with a ball speed mean absolute error of 1.51 ± 1.27 mph, and backspin and sidespin errors of 213 ± 257 rpm and 150 ± 188 rpm, respectively.

3.4 Golf Ball Aerodynamic Model

Following impact, the launch conditions of the golf ball are passed to a ball flight aerodynamic model. These launch conditions are the initial linear and angular velocities of the ball. In the golf industry, linear velocity is commonly referred to by decoupling into ball speed v_b, vertical launch angle θ_{vert} (relative to the global XZ plane), and horizontal launch angle θ_{hor} (relative to the global X axis), while angular velocity is decoupled into backspin ω_{back} (about the global Z axis), and sidespin ω_{side} (about the global Y axis). A visual representation of these terms is shown in Fig. 3.9. When discussing the linear and angular velocities of the ball in this thesis, these industry-standard terms will often be used.

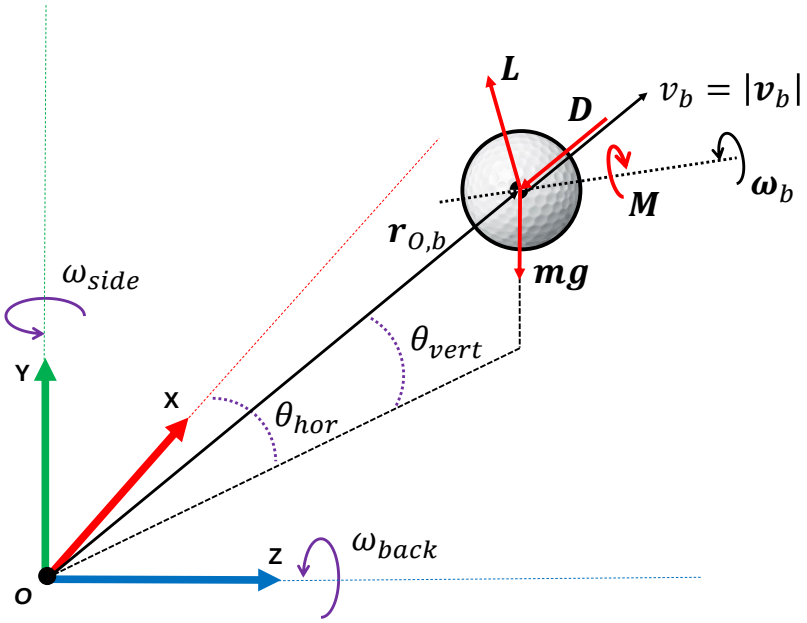

Figure 3.9: Golf industry standard naming conventions of ball launch conditions and aerodynamic forces.

The ball flight aerodynamic model is physics-based and driven by the four loads that act on a spinning spherical projectile: gravity $\boldsymbol{g}$, drag $\boldsymbol{D}$, lift $\boldsymbol{L}$, and spin-decay moment $\boldsymbol{M}$ (see Fig. 3.9). For drag, lift, and spin-decay there is a common dynamic pressure term Q which is given by

$$Q = \frac{1}{2}\rho A_b \left|\boldsymbol{v}_b\right|^2 \tag{3.7}$$

where ρ is the density of air, A_b is the cross-sectional area of the golf ball, and $\boldsymbol{v}_b$ is the linear velocity vector of the golf ball. The lift force $\boldsymbol{L}$ acts perpendicular to the linear and angular velocity vectors as a result of the Magnus effect, and is given by

$$\boldsymbol{L} = QC_L(\hat{\boldsymbol{\omega}}_b \times \hat{\boldsymbol{v}}_b) \tag{3.8}$$

where C_L is the coefficient of lift, and $\hat{\boldsymbol{v}}_b$ and $\hat{\boldsymbol{\omega}}_b$ are unit vectors for the linear and angular velocities of the ball, respectively. The drag force $\boldsymbol{D}$ acts in the direction opposite to the ball's velocity and can be represented as

$$\boldsymbol{D} = QC_D(-\hat{\boldsymbol{v}}_b) \tag{3.9}$$

where C_D is the coefficient of drag. The spin-decay moment $\boldsymbol{M}$ acts in the direction opposite to the ball's angular velocity and is given by

$$\boldsymbol{M} = 2QC_M r_b(-\hat{\boldsymbol{\omega}}_b) \tag{3.10}$$

where C_M is the spin-decay coefficient, and r_b is the radius of the golf ball. From the preceding equations, the ordinary differential equations (ODE)s for the flight of a golf ball can be derived. They are given by

$$\begin{aligned}
\ddot{x} &= \frac{1}{m}\left(\frac{-QC_D v_{b,x} + QC_L\left(\frac{\omega_{b,y}}{\omega_b}v_{b,z} - \frac{\omega_{b,z}}{\omega_b}v_{b,y}\right)}{v_b}\right) \\
\ddot{y} &= \frac{1}{m}\left(\frac{-QC_D v_{b,y} + QC_L\left(\frac{\omega_{b,z}}{\omega_b}v_{b,x} - \frac{\omega_{b,x}}{\omega_b}v_{b,z}\right)}{v_b}\right) - g \\
\ddot{z} &= \frac{1}{m}\left(\frac{-QC_D v_{b,z} + QC_L\left(\frac{\omega_{b,x}}{\omega_b}v_{b,y} - \frac{\omega_{b,y}}{\omega_b}v_{b,x}\right)}{v_b}\right) \\
\ddot{\omega} &= \frac{-2r_b QC_M}{I_b}
\end{aligned} \tag{3.11}$$

Most terms appearing in the equations for the aerodynamic forces (Eq. 3.8 through 3.10) are either known constants (such as the diameter and cross-sectional area of the golf ball), or values that can be directly measured experimentally (such as the linear and angular velocities of the golf ball). Consequently, the differentiating factor between ineffective and effective aerodynamic models is the accurate determination of the aerodynamic coefficients themselves: C_L, C_D, and C_M. For this model, the aerodynamic coefficients are dependent on the non-dimensional spin ratio S, which is given by

$$S = \frac{|\boldsymbol{\omega}_b| \, r_b}{|\boldsymbol{v}_b|} \tag{3.12}$$

The spin ratio is commonly used in projectile aerodynamics applications and has been previously applied to golf by Quintavalla [33]. For this application, the lift and drag coefficients were assumed to be second-order functions of the spin ratio while the moment coefficient was assumed to vary linearly, giving

$$\begin{aligned} C_D &= a + bS + cS^2 \\ C_L &= d + eS + fS^2 \\ C_M &= gS \end{aligned} \tag{3.13}$$

where a through g are constant parameters. In order to determine these unknown constants, a parameter identification study was undertaken as outlined in [86]. Critical to this study was the availability of a dataset of golf shots including both the ball's launch conditions and resultant flight.

To generate a suitable dataset, shots were recorded from golfers of varying skill level with golf clubs ranging from lob wedge to driver. 2021 Titleist Pro-V1 golf balls were used to reflect contemporary golf ball aerodynamics, and wind speeds were verified using an anemometer to be less than 1.3 m/s during all testing.

To record the initial launch conditions of the ball, the GCQuad camera-based launch monitor (Foresight Sports, San Diego, USA) was utilized. The GCQuad is a four-camera stereoscopic high-speed camera system specifically designed for golf applications, and was validated using a separate high-speed camera in internal testing. The initial launch conditions recorded by the GCQuad were: ball speed, vertical launch angle, horizontal launch angle, backspin, and sidespin.

To record the flight of the ball following impact, the FlightScope X3 radar-based launch monitor (FlightScope, Orlando, USA) was utilized. The X3 is a radar-based system de-

signed for sports projectile applications, and is able to track the position of the ball throughout its entire flight. From this position data, three key values were extracted and featured in the dataset: carry distance, apex, and offline landing position.

In total, 1040 shots were recorded over the course of three months. Approximately half of the dataset contains driver shots, while the remaining half is divided relatively equally among the remaining clubs. The minimum spin ratio found in the dataset is 0.02 (a driver shot with high speed and low spin) while the maximum is 0.75 (a lob wedge shot with low speed and high spin). The median carry distance of the dataset is 182 yards while the median offline landing position is 1.1 yards (along the positive Z axis), indicating that the dataset is nearly equally distributed about the fairway center line. Figure 3.10 shows the trajectories of the dataset used to develop the model.

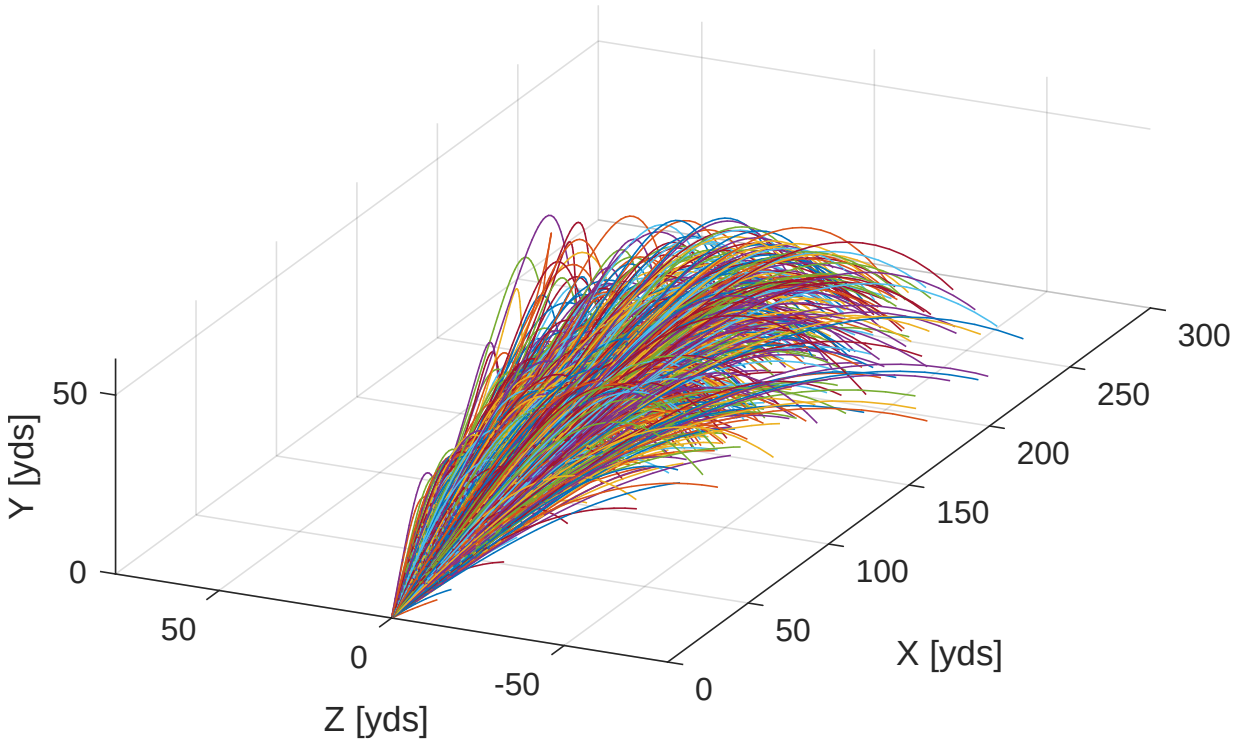

Figure 3.10: Aerodynamic model ball flight trajectories from the collected dataset.

Setting aside 80% of the dataset for training, each set of launch conditions was simulated using the ball flight ODEs (Eq. 3.11) while MATLAB's `fmincon` nonlinear optimization algorithm was employed to determine the unknown constants a through g. Constants a through f were bounded between +2 and -2 while g was bounded between 0.01 and 0.015

to reflect realistic spin decay [50]. The cost function is given by

$$J = \frac{1}{N}\sum_{i=1}^{N}(C_i - C_{i,s})^2 + \frac{1}{N}\sum_{i=1}^{N}(A_i - A_{i,s})^2 + \frac{1}{N}\sum_{i=1}^{N}(O_i - O_{i,s})^2 \tag{3.14}$$

where N is the number of training shots, (C,A,O) denote carry distance, apex, and offline landing position, and the s subscript denotes the simulated value. Several alternate combinations of term weighting and normalization techniques were implemented with the cost function, with insignificant changes to the results. Hence, the presented cost function with equal weighting was chosen for simplicity. With the unknowns determined, Eq. 3.13 can be populated to form the model for the aerodynamic coefficients:

$$\begin{aligned} C_D &= 0.1304 + 0.9287S - 0.8259S^2 \\ C_L &= 0.0504 + 1.2031S - 1.1490S^2 \\ C_M &= 0.01S \end{aligned} \tag{3.15}$$

3.5 Optimal Control

3.5.1 Cost Function

While distance is very important, it is not the only factor that defines a successful golf drive. Shots that travel a far distance but are significantly offline may lead to obstructions for the golfer's next shot such as water, sand traps, trees, or long grass. The optimization cost function that is minimized is primarily based upon maximizing the carry distance of the golf ball, but includes progressive penalization of shots landing too far offline

$$J = -C + \left(\frac{O}{15}\right)^2 \tag{3.16}$$

where C is the ball's carry distance and O is the offline landing position from the fairway center line. The progressive penalization of shots that travel offline is based upon PGA Tour *Strokes Gained* statistics [6]. *Strokes Gained* is a method of numerically quantifying the performance of a golfer on a given shot relative to the other players in the dataset [87]. For example, on a 450 yard par four an average PGA Tour player will hit their drive 295 yards to the fairway, leaving 155 yards to the hole where it takes an average of 2.7 shots to hole out. If the same individual player were to hit a drive the same distance but offline into the long grass instead of the fairway, it would take an average of 2.8 shots to hole out. Because their second shot is from the long grass instead of the fairway, they have lost 0.1 strokes to the field. These *Strokes Gained* statistics demonstrate the importance of the ball coming to rest in the fairway, which on the PGA Tour averages approximately 30 yards in width [88]. This average width of 30 yards gives an acceptable offline landing position of 15 yards on each side of the fairway center line, hence the denominator of the second cost function term.

3.5.2 Optimization Variables

The model's optimization variables consist of:

- 19 muscle torque generator activation and deactivation timings. These timings correspond to the "on" and "off" times for the maximal torque activations of the backswing and downswing muscle torque generators.

- Two muscle force generator activation and deactivation timings. These timings correspond to the "on" and "off" times for the maximal force activation of the downswing pelvis translational muscle force generator.
- Four shoulder torque ratios. Each shoulder has a unique shoulder torque ratio for the backswing and downswing. These ratios split the total shoulder torque between the adduction-abduction and flexion-extension rotational joints.

A keen observer would note that the 25 optimization variables are less than the 46 that would be present if each muscle torque generator/muscle force generator had its four full unique timings. Similarly to McNally and McPhee [35], a series of assumptions and couplings were made to reduce the scope of the solution space to an acceptable level:

1. The pelvis, torso, and shoulder backswing MTGs were all assumed to activate at $t = 0$ to begin the backswing. All three of these joints are typically activated immediately in a human golf swing to ensure a proper takeaway path of the club (see Appendix E for motion capture results confirming this).
2. The pelvis and torso backswing deactivation timings were assumed to also be the downswing activation timings. While some golfers have a brief pause near the top of the backswing for both of these joints, the pause is brief enough [89] that assuming no pause in this model does not significantly affect biofidelity, and crucially removes two optimization variables.
3. The right shoulder and wrist were assumed to follow the activation and deactivation timings of the left shoulder and wrist. In a human golf swing, the bilateral shoulder joints [90] and wrists are typically sequenced together, and any small difference in this sequencing is not significant enough to justify the additional optimization variables.

In addition to the aforementioned assumptions, linear constraints were imposed to ensure proper sequencing of the swing (i.e. the downswing MTGs do not activate before the backswing MTGs, and activation occurs before deactivation). Table 3.4 lists the optimization variables along with their upper and lower bounds in the optimization; the bounds are sufficiently generous so as not to influence the outcome of the optimization. The timings are expressed as a multiple of the total simulation time t_{sim}, which is 1.2 seconds based upon the work of McNally and McPhee [35]. Impact occurs at approximately $t = 1.1$ seconds for a typical optimized swing, and the results were found to be insensitive to increasing simulation time.

Table 3.4: Golf drive model optimization variable bounds.

Joint		Parameter	Lower Bound	Upper Bound
Pelvis	rotation	MTG off backswing	$0.2t_{sim}$	$0.8t_{sim}$
		MTG off downswing	$0.4t_{sim}$	$1.1t_{sim}$
Torso	rotation	MTG off backswing	$0.2t_{sim}$	$0.8t_{sim}$
		MTG off downswing	$0.4t_{sim}$	$1.1t_{sim}$
L Shoulder	flex/ext, add/abd	MTG off backswing	$0.2t_{sim}$	$0.8t_{sim}$
		MTG on downswing	$0.4t_{sim}$	$1.1t_{sim}$
		MTG off downswing	$0.4t_{sim}$	$1.1t_{sim}$
R Elbow	flex/extension	MTG on backswing	0	$0.8t_{sim}$
		MTG off backswing	0	$0.8t_{sim}$
		MTG on downswing	$0.4t_{sim}$	$1.1t_{sim}$
		MTG off downswing	$0.4t_{sim}$	$1.1t_{sim}$
L Forearm	pro/supination	MTG on backswing	0	$0.2t_{sim}$
		MTG off backswing	0	$0.8t_{sim}$
		MTG on downswing	$0.4t_{sim}$	$1.1t_{sim}$
		MTG off downswing	$0.4t_{sim}$	$1.1t_{sim}$
L Wrist	ulnar/radial	MTG on backswing	0	$0.2t_{sim}$
		MTG off backswing	0	$0.8t_{sim}$
		MTG on downswing	$0.4t_{sim}$	$1.1t_{sim}$
		MTG off downswing	$0.4t_{sim}$	$1.1t_{sim}$
L Shoulder	flex/ext, add/abd	$r_{backswing}$	0.3	1.2
		$r_{downswing}$	0.3	1.2
R Shoulder	flex/ext, add/abd	$r_{backswing}$	0.3	1.2
		$r_{downswing}$	0.3	1.2
Pelvis	Translation	MFG on downswing	$0.2t_{sim}$	$0.8t_{sim}$
		MFG off downswing	$0.4t_{sim}$	$1.1t_{sim}$

3.5.3 Optimization Methodology

While the primary objective of the model is to hit the golf ball as far as possible with a certain degree of accuracy, a system as complex as this is not guaranteed to produce a swing that is biomechanically feasible or even capable of hitting the golf ball at every optimization iteration. Because of this, an initial cost function structure must first be employed to guide the optimization to a feasible swing before the swings are evaluated for how far they can hit the ball. Given the nature of this `if/else` structure, it is best to describe it using an enumerated list that mimics the code structure for a given swing:

1. Is the biomechanical range of motion exceeded for any joint at any point in the swing? If yes, penalties increase with the number of joints exceeding limits and with how much they are exceeded by. If no, proceed.

2. Do any body segments intersect each other at any point in the swing? If yes, penalties increase with the number of intersections and their duration. If no, proceed.

3. Does the clubhead make contact with the ground at any point during the swing even with a hip height adjustment of up to 5% of the golfer's height? If yes, penalties are proportional to the depth of clubhead penetration. If no, proceed.

4. After the beginning of the downswing, are there instances where the clubhead passes through a point that is: (a) between zero and 40 cm forward of the clubhead address position in the positive global X direction, (b) within 15 cm of the clubhead address position in the global Z direction, and (c) reachable by the specified tee height in the global Y direction. If no, penalties are proportional to how far the club is from this geometric window. If yes, a center-face impact between the ball and clubhead is imposed at each of these points and the resulting ball flight is evaluated using the final cost function presented in Section 3.5.1.

3.5.4 Optimization Algorithms

To generate sets of variables at each optimization iteration, a dual-algorithm approach similar to that of McNally and McPhee [35] is employed. First, MATLAB's `genetic algorithm` (`ga`) is used to converge upon the general area in which the global optimum resides. The `ga` does not require an initial guess and mimics biological evolution in developing the populations of successive iterations. These characteristics make the `ga` desirable for the highly nonlinear nature of this problem, and give a high degree of confidence that

a global optimum is being converged upon. However, the downside of this algorithm is its speed; it is much slower than alternatives.

As a result, once the cost function's (see section 3.5.1) average relative change across the maximum number of stall generations is less than one for the initial `ga` optimization, the second step of the process is initialized. In this second step, the best candidate from the `ga` is used as the initial guess and a new set of bounds are created. These bounds are the best candidate muscle torque/muscle force generator timings ± 75 ms and the best candidate shoulder torque ratios ± 0.1. MATLAB's `patternsearch` algorithm is then employed to find the final set of optimization values using its efficient convergence methods. For a typical optimization on a six-core CPU at 3.8 GHz, this dual-algorithm method converges upon a solution in approximately six hours when compared to eight hours using solely the `genetic algorithm`.

Chapter 4

Model Validation

A quote often repeated in the modeling world is that "all models are wrong, but some are useful," generally attributed to statistician George Box. Ensuring that a model is useful is often accomplished through experimental validation, and this golfer model is no exception. This chapter outlines the validation of the biomechanical model, flexible shaft model, and golf ball aerodynamic model. The validation of the first two was accomplished with a golf drive motion capture experiment in partnership with two golf club manufacturers. The validation of the aerodynamic model was conducted concurrently with development of the model using the collected dataset.

4.1 Golf Drive Motion Capture Experiment

To validate the biomechanical and flexible club models experimentally, a motion capture study was undertaken. Prior to participant recruitment, the study was given ethics approval by the University of Waterloo's Human Research Ethics Board (Office of Research Ethics #44578). The participants in the experiment were ten right-handed male golfers with official handicap better than -3.0 (approximately 95th percentile [91]). The mean handicap of the participants was +0.4, while the highest was -3.0 and the lowest was +3.5[1]. Six of the participants possessed handicap indices of zero or better. Table 4.1 outlines key self-reported data from the participants.

[1]The presence of a '+' preceding a handicap indicates that the participant's handicap is better than zero; their expected score for a given round is below the course rating. A '-' preceding a handicap indicates their expected score is above the course rating.

Table 4.1: Motion capture study participant data. Note that all data was self-reported.

Golfer	Sex	Age	Handicap	Height [cm]	Mass [kg]
1	M	24	-1.0	185	73
2	M	27	-3.0	180	100
3	M	54	-1.5	175	86
4	M	22	-0.7	188	93
5	M	35	+3.5	185	93
6	M	20	0.0	185	82
7	M	20	+2.0	185	64
8	M	21	+2.6	185	102
9	M	20	+2.3	178	70
10	M	20	+1.3	175	66
avg.		25.9 ± 11.0	$+0.4 \pm 2.0$	182.1 ± 4.7	82.9 ± 14.1

4.1.1 Experimental Protocol

Participants were asked to hit ten shots with three unique drivers into a hitting net, for a total of 30 shots. Specific details of the drivers are discussed in Section 4.1.3. New 2021 Titleist Pro-V1 golf balls were used for all shots in the experiment, and participants were free to tee the ball at their preferred height for each swing. Participants were instructed to complete the swings at their normal playing speed, and not to swing harder than they typically would on the course. Following each swing, the participants were asked to rate the quality of their shot from one to ten where one was unacceptable, and ten was the best shot the participant was realistically capable of hitting. Shots the participants were not satisfied with were discarded, and additional swings were made to bring the number of acceptable shots with each club to ten. Figure 4.1 shows the experimental setup with a participant at the top of their backswing.

Passive reflective markers were affixed to the golf club and the golfers themselves. On the golf club, marker clusters were placed on the shaft just below the grip and on the

clubhead. On the golfer, markers were affixed to bony landmarks. For each swing, a 13-camera passive Vantage V5 optical camera system (VICON, Oxford, UK) recorded the position of the passive markers at a frequency of 1000 Hz. The position data of these markers was then post-processed using the VICON Nexus 2.12 software (VICON, Oxford, UK). Following impact, the launch conditions of the ball were recorded using the GCQuad stereoscopic camera-based launch monitor (Forsesight Sports, San Diego, USA).

Figure 4.1: Motion capture study participant Golfer 5 at the top of backswing position. Markers can be seen affixed to the participant's pelvis, torso, and upper extremities as well as on the grip and head of the golf club. A Foresight Sports GCQuad launch monitor is present to the right of the golf ball to record launch conditions. Five of the 13 VICON Vantage cameras used are visible along the upper wall and mounted on tripods.

4.1.2 Golf Club Marker Placement and Clubframe Calibration

Markers were attached to the top surface of the clubhead (the "crown") at four positions: forward near the center-face alignment decal, rear along the center line of the club, and approximately aligned with the heel and toe of the clubface halfway between the forward and rear markers (see Fig. 4.2). The markers were affixed using custom 3D-printed PETG bases and VHB tape. When used with a primer, VHB tape offers excellent absorption of the vibrations experienced during impact—especially when compared to hard-drying liquid adhesives such as epoxy and super glue that fractured nearly immediately during pre-study testing.

To accommodate the calibration wand of the Vantage system, the global reference frame for the motion capture experiment is different than that of the golfer model introduced in Chapter 3. The global X axis points in the direction of the target line where the participants were aiming, the Z axis is perpendicular to the ground, and the Y axis follows the right-hand rule. For each of the three drivers, three separate reference frames (see Fig. 4.3) on the golf club were statically calibrated: clubface (CF), lower shaft (LS), and grip (G).

The clubface frame was calibrated using a custom 3D-printed marker cluster temporarily affixed to the clubface (see Fig. 4.2). The origin lies at the center of the clubface with the X_{CF} axis normal to the clubface and the Y_{CF} axis running parallel to the clubface's grooves. The grip frame's origin lies at the midpoint of the three upper markers of the grip cluster (see Fig. 4.4), which is coincident with the shaft's longitudinal axis just below the grip. The Z_G axis runs along the shaft's longitudinal axis and the X_G axis lies in a plane parallel to the $X_{CF}Z_{CF}$ plane. The origin of the lower shaft frame is at the intersection of the Z_G axis and the $X_{CF}Y_{CF}$ plane; this is approximately where the tip of the shaft is located within the hosel. The Z_{LS} axis runs along the shaft's longitudinal axis and the X_{LS} axis lies in a plane parallel to the $X_{CF}Z_{CF}$ plane. The position and orientation of these frames relative to the clubhead and grip marker clusters during static calibration were used during post-processing to reconstruct these frames in the dynamic trials. In this reconstruction, the clubface and lower shaft frames were assumed to lie on a single rigid body, i.e. the small deformations of the clubhead were neglected.

4.1.3 Golf Club Properties

Three different drivers from two manufacturers were used in the experiment, with the nominal properties of these drivers outlined in Table 4.2. Both manufacturers supplied

Figure 4.2: Clubface calibration marker cluster.

these clubs to the Motion Research Group for the purposes of the experiment under a research agreement. Full inertial properties of the clubheads, as well as stiffness and geometric profiles of the shafts were provided by the manufacturers but are not disclosed explicitly in this thesis for reasons of confidentiality.

Table 4.2: Motion capture experiment nominal driver properties.

Manufacturer	Driver	Loft [deg]	Length [in]	Shaft Stiffness	Swingweight
'A'	A1	10.5	45.75	'Stiff'	D3
	A2	10.5	44.75	'Stiff'	D0
'B'	B1	9.0	45.75	'Stiff'	D3

It should be noted that driver A2 uses the same clubhead, shaft, and grip as driver A1, but is one inch shorter and omits an eight gram counterweight in the butt end of the shaft, hence the lighter swingweight of D0[2]. All three drivers feature adjustable loft sleeves that

[2]Swingweight is a method of quantifying the apparent weight of the clubhead to the golfer using a scale

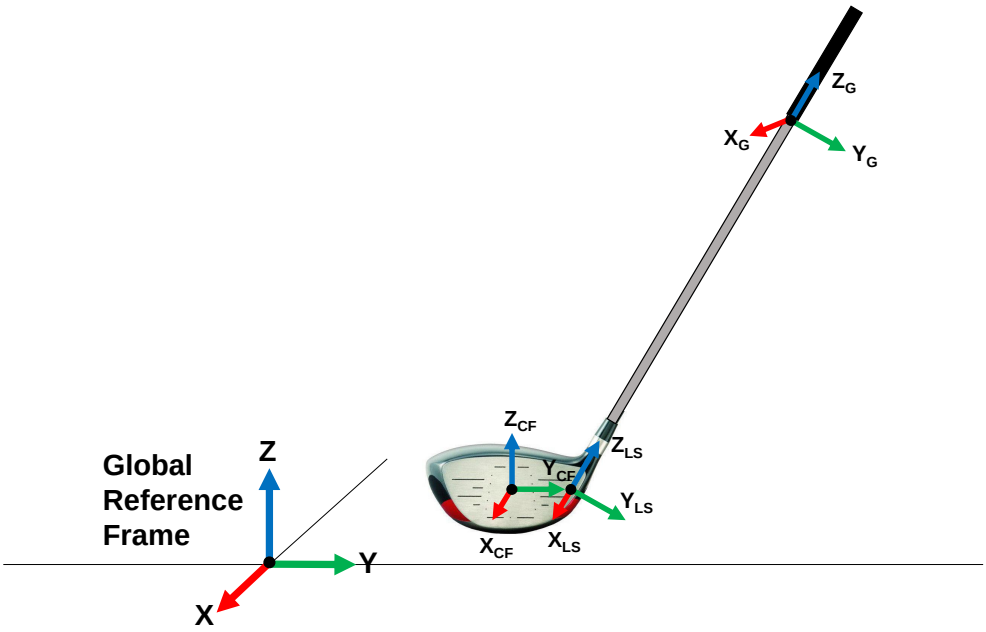

Figure 4.3: Golf club reference frames calibrated in the motion capture experiment.

were kept in their neutral position, and the adjustable 26 gram mass on the clubhead of driver B1 was kept in its neutral position.

4.1.4 Participant Marker Placement and Calibration

Markers were affixed to the participant on bony landmarks to limit the effects of skin artifacting [92]. Markers were affixed to the arms bilaterally on the shoulder acromia, medial and lateral epicondyles of the elbow, radial and ulnar styloids, and 2nd and 5th metacarpals. On the torso, markers were affixed to the C7 cervical vertebra, suprasternal notch, xiphoid process, T8 thoracic vertebra, and L5 lumbar vertebra. On the pelvis, markers were affixed bilaterally on the posterior and anterior superior iliac spines. See Fig. 4.5 for a visual representation of the marker locations. The marker arrangement chosen allowed the three-dimensional tracking of the segments of interest to the golfer model (arms, torso, and pelvis) using the minimum number of markers possible so as not to encumber the

ranging from A0 to F9; increasing letters and numbers indicate a 'heavier' feeling clubhead. This value is a measure of the club's center of mass position along the shaft's longitudinal axis relative to the butt end of the grip.

Figure 4.4: Marker cluster used to determine the club's grip frame.

swing of the participants, or add unnecessary setup time to the study. A static calibration trial was taken for each participant to generate a skeletal labeling template based on this marker configuration.

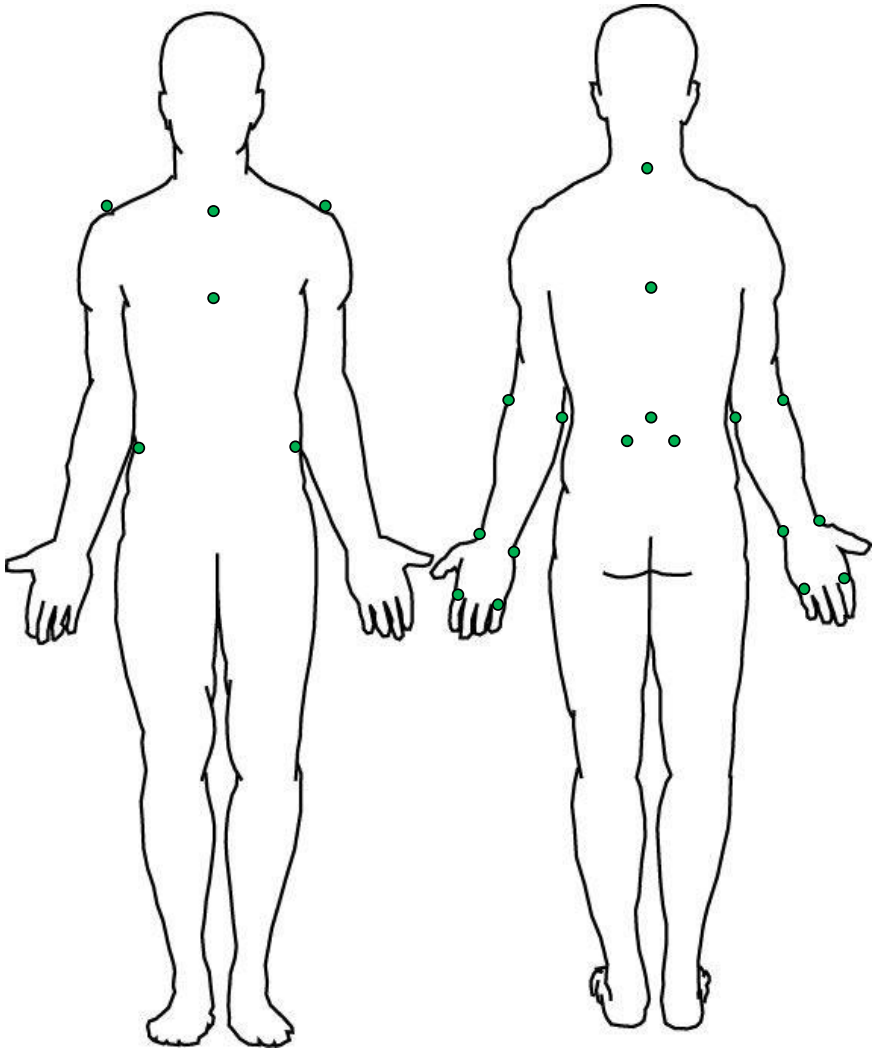

Figure 4.5: Motion capture marker positioning on the participants. Green circles represent individual motion capture markers affixed to bony landmarks.

4.1.5 Post-Processing

Following collection, the motion capture data of recorded swings was first post-processed in VICON Nexus in order to resolve the marker position data into labelled trajectories. Using a labelling skeleton template, marker trajectories were labelled using a hybrid approach with Nexus' auto-labelling algorithms being augmented by manual intervention where necessary. Gaps present in the data due to occlusion were filled using donor trajectories or spline interpolation. Processing then moved to MATLAB, where the marker trajectories were first filtered using a second-order low-pass Butterworth filter. The filter was implemented using MATLAB's `filtfilt` function to ensure zero phase distortion. Following a convergence study, club markers were filtered at a cutoff frequency of 30 Hz while biomechanical markers were filtered at a cutoff frequency of 6 Hz based upon general consensus in the literature [93].

Because several of the participants did not keep their club completely still prior to commencing the swing, simply defining the beginning of the swing as the first instance of movement was not feasible. Instead, a custom event detection algorithm was developed that could differentiate between a pre-swing club movement and the actual beginning of the swing. The algorithm began by chronologically searching for a candidate frame in which all eight of the golf club markers were moving away from the target (the takeaway direction). If the five frames following this candidate frame also contained homogeneous movement away from the target, this eliminated the possibility that the candidate frame was the result of systematic marker position noise. It then verified that 300 frames (0.3 seconds) following the candidate frame, the clubhead and grip had left the address position area. Meeting all three of these criteria confirmed that the candidate frame was the beginning of the swing. The top of the backswing frame was defined as the frame in which the second global X direction reversal of the grip occurred following the beginning of the swing; the first reversal occurs when the grip reaches the "halfway back" position (9 o'clock from a face-on perspective). Even at a sampling rate of 1000 Hz, the discrete nature of the collected data meant that impact occurred nearly exclusively between frames. Knowing the position of the ball and clubhead in the global coordinate system, the frame immediately preceding impact was used to linearly extrapolate the club kinematics to the position of impact.

With the bounds of each swing determined, several quantities of interest were determined for each frame. For the club, the global position and body-fixed YXZ Euler angles of all three club reference frames were calculated, allowing for the quantification of shaft deflection. Toe-down deflection was defined as the displacement of the lower shaft frame in the Y_G direction, lead deflection was the displacement of the lower shaft frame in the X_G direction, and twist was the Z Euler angle between the lower shaft and grip frames.

For the biomechanics of the participants, focus was placed upon kinematically quantifying the novel biomechanical joints of this model. Translation of the pelvis was quantified in all three global directions, as was the rotation of the pelvis about the global Z axis. Torso rotation was quantified using the rotation of the vector between the two shoulder acromia about the global Z axis. The trailing shoulder's flexion-extension and adduction-abduction angles as well as the trailing elbow's flexion-extension angle were determined based on the coordinate systems and guidelines set out by Wu et al. [94]. It should be noted that these biomechanical quantities were only determined for the swings made with driver B1 in an effort to reduce the substantial post-processing time associated with VICON data. Despite the slight differences between the three clubs tested, it is reasonable to expect that the general biomechanical trends of the golfers are similar between clubs.

4.2 Continuous Analytical Shaft Model

Shaft intertial, geometric, and stiffness properties for each of the clubs were experimentally determined by the driver manufacturers before the clubs were provided for the motion capture experiment. As outlined in Section 3.2, the continuous analytical flexible beam model used to model the shaft requires third-order polynomials for the Young's modulus E, shear modulus G, cross-sectional area A, and second area moment I of the shaft as functions of its length. For driver B1, the manufacturer provided experimental EI, GJ and cross-sectional measurements for the untrimmed shaft. From this data, third-order polynomials were fit to the properties of interest, shown in Fig 4.6. The magnitude of these curves is occluded in the figure for reasons of confidentiality.

The study of McNally et al. [82] demonstrated that the continuous analytical shaft model used here is quite robust in accurately replicating experimental shaft deflections when developed using experimental stiffness and geometric profiles. However, the profiles provided by manufacturers cannot be guaranteed to represent the true stiffness of the shaft. It was therefore determined that the shaft properties used in the model should be validated using experimental results from the motion capture experiment.

Similar to the method used by McNally [37], the kinematics of the grip marker cluster from each of the motion capture experiment swings for driver B1 were extracted into translational (XYZ) and rotational (YXZ Euler) components. These discrete datasets were then transformed into continuous functions using cubic spline interpolation. Using an isolated shaft and clubhead model (i.e. the full golfer model without biomechanics, impact, or golf ball aerodynamics), the experimental grip kinematics were prescribed to the grip in the model and the duration of the swing was simulated. A one-second static

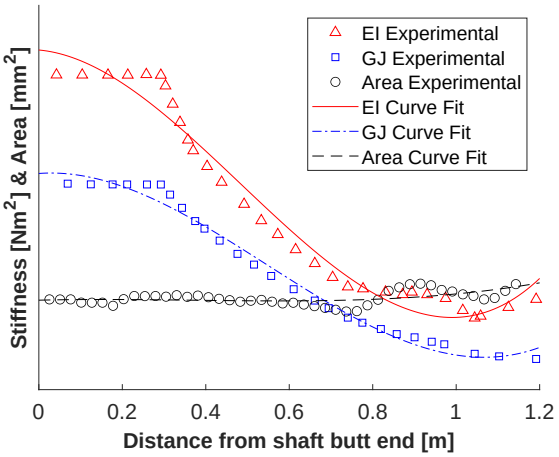

Figure 4.6: Driver 'B1' shaft property curve fits. Note that the constant experimental properties at the butt end of the grip are the result of the uniform geometry and material properties in this section of the shaft that exist to accommodate trimming.

pause preceding the beginning of the swing was added to ensure internal equilibrium of the shaft was reached prior to takeaway.

MATLAB's `genetic algorithm` was used to tune the coefficients of the third-order polynomials in order to minimize the sum of the squared deflection errors between the shaft model and the motion capture experiment across each time step. The total dataset of motion capture swings was split 80%/20% for training/testing in this optimization. In addition to the coefficients, the damping coefficient of the shaft in the bending and shear directions was also allowed to vary in the optimization. Table 4.3 outlines the mean absolute deflection errors of the tuned shaft for driver B1 at the moment of impact for the 20% of the dataset reserved for testing. Also included are the mean absolute deflection errors for the common shaft (trimmed to different lengths) shared between drivers A1 and A2, which was tuned using a similar process to driver B1.

Table 4.3: Continuous shaft model mean absolute deflection errors (MAE) at impact.

Shaft	Toe-up/Toe-down MAE [mm]	Lead/Lag MAE [mm]	Twist MAE [deg]
A1/A2	18.6±6.7	19.9±9.8	1.5±1.0
B1	17.1±5.8	19.4±10.1	1.5±1.1

Note: ± indicates standard deviation

4.3 Biomechanical Model

The results generated from the motion capture experiment are kinematic in nature, as techniques (such as inverse dynamics via force plates) to estimate the muscle forces/joint torques of the participants were not employed. For this reason, validation of the biomechanical side of the model comes from comparing kinematics throughout the swing of the model to those of a human study participant.

To generate a model swing for comparison, the model was given driver B1 and optimized using the cost function outlined in Section 3.5.1. The simulated drive carried a total of 283 yards with a clubhead speed of 109 mph. The downswing swing sequence of this optimized drive is shown in Fig. 4.7 while the optimized variables for this swing are outlined in Table 4.4. Because the trail arm and pelvis translation are novel features of this model, they are focused upon in this validation. Figure 4.8 plots joint angle/position comparisons between the combined mean of the motion capture experiment participants and the optimized model swing for the trailing shoulder and elbow rotational joints, pelvis translational and rotational joints, and torso rotational joint. Individual comparisons for all motion capture study golfers can be found in Appendix E.

Table 4.4 reveals that the optimized swing follows a swing pattern that employs proximal-to-distal downswing sequencing where the downswing muscle torque generators of the pelvis, torso, shoulder, forearm, and wrist activate in succession. This sequencing is common among elite golfers [89] due to its effectiveness in generating clubhead speed. Referring to Fig. 4.8, the model and human golfers show similar shoulder flex-extension and add-abduction trends throughout the swing. Both the model and golfers start in flexion/adduction and move in the flexion/abduction directions until the top of the backswing before returning to their approximate address positions at impact. Similarly, the elbow flexion-extension joint for both the model and golfers follows the traditional "folding" (flexion) in the backswing followed by "unfolding" (extension) in the downswing approaching impact. In the later half of the downswing (beyond 80% swing progression), the simulated and experimental movements of the elbow joint are nearly identical. The pelvis and torso rotation angles reach peaks at the top of the backswing for both the model and golfers. It is quite evident that the torso is rotated much more in the backswing by the golfers than the model, creating a large angular separation with the pelvis—known as the X-factor. The golfer model (which has a rigid torso) is likely unable to achieve this position without modeling the lower back as a separate entity from the torso. Also of note is how much more "open" the pelvis angle at impact is for the golfers; again this is likely a result of the rigid model torso restricting this movement. The pelvis translational joint is not active for the backswing of the model, but compares quite well for the downswing with the golfers.

Table 4.4: Golf drive model sample optimized variables.

Joint		Parameter	Solution
Pelvis	rotation	MTG off backswing	0.742 s
		MTG off downswing	1.129 s
Torso	rotation	MTG off backswing	0.745 s
		MTG off downswing	1.087 s
L Shoulder	flex/ext, add/abd	MTG off backswing	0.563 s
		MTG on downswing	0.862 s
		MTG off downswing	1.129 s
R Elbow	flex/extension	MTG on backswing	0.094 s
		MTG off backswing	0.317 s
		MTG on downswing	0.992 s
		MTG off downswing	1.069 s
L Forearm	pro/supination	MTG on backswing	0.024 s
		MTG off backswing	0.400 s
		MTG on downswing	0.990 s
		MTG off downswing	1.263 s
L Wrist	ulnar/radial	MTG on backswing	0.083 s
		MTG off backswing	0.399 s
		MTG on downswing	1.001 s
		MTG off downswing	1.254 s
L Shoulder	flex/ext, add/abd	$r_{backswing}$	0.927
		$r_{downswing}$	0.647
R Shoulder	flex/ext, add/abd	$r_{backswing}$	1.143
		$r_{downswing}$	0.965
Pelvis	Translation	MFG on downswing	0.742 s
		MFG off downswing	1.254 s

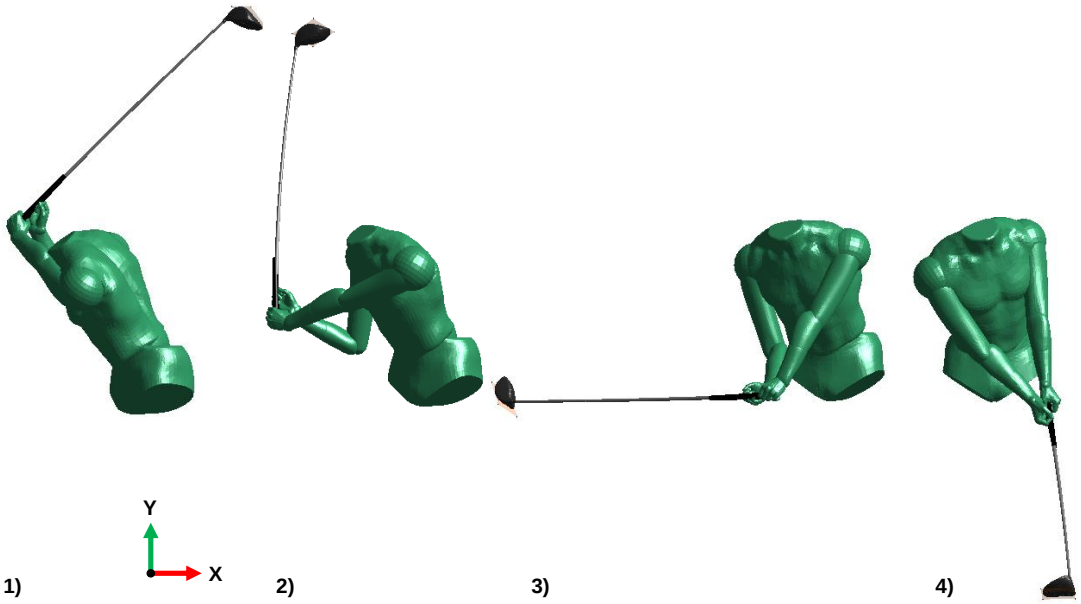

(a) face-on view

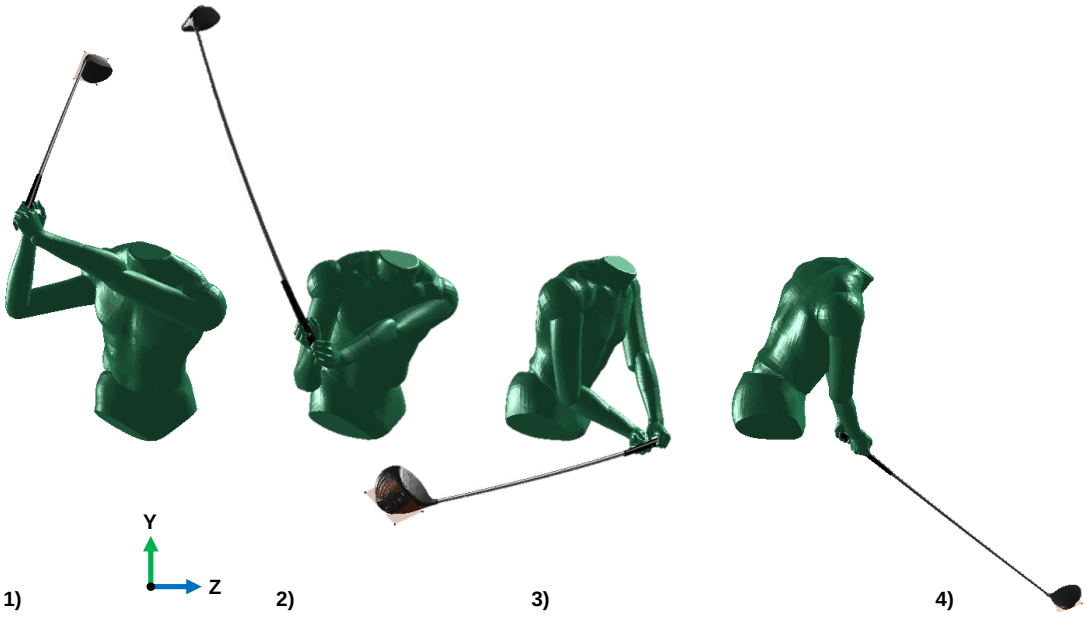

(b) down-the-line view

Figure 4.7: Downswing sequence of the optimized golfer model swing.

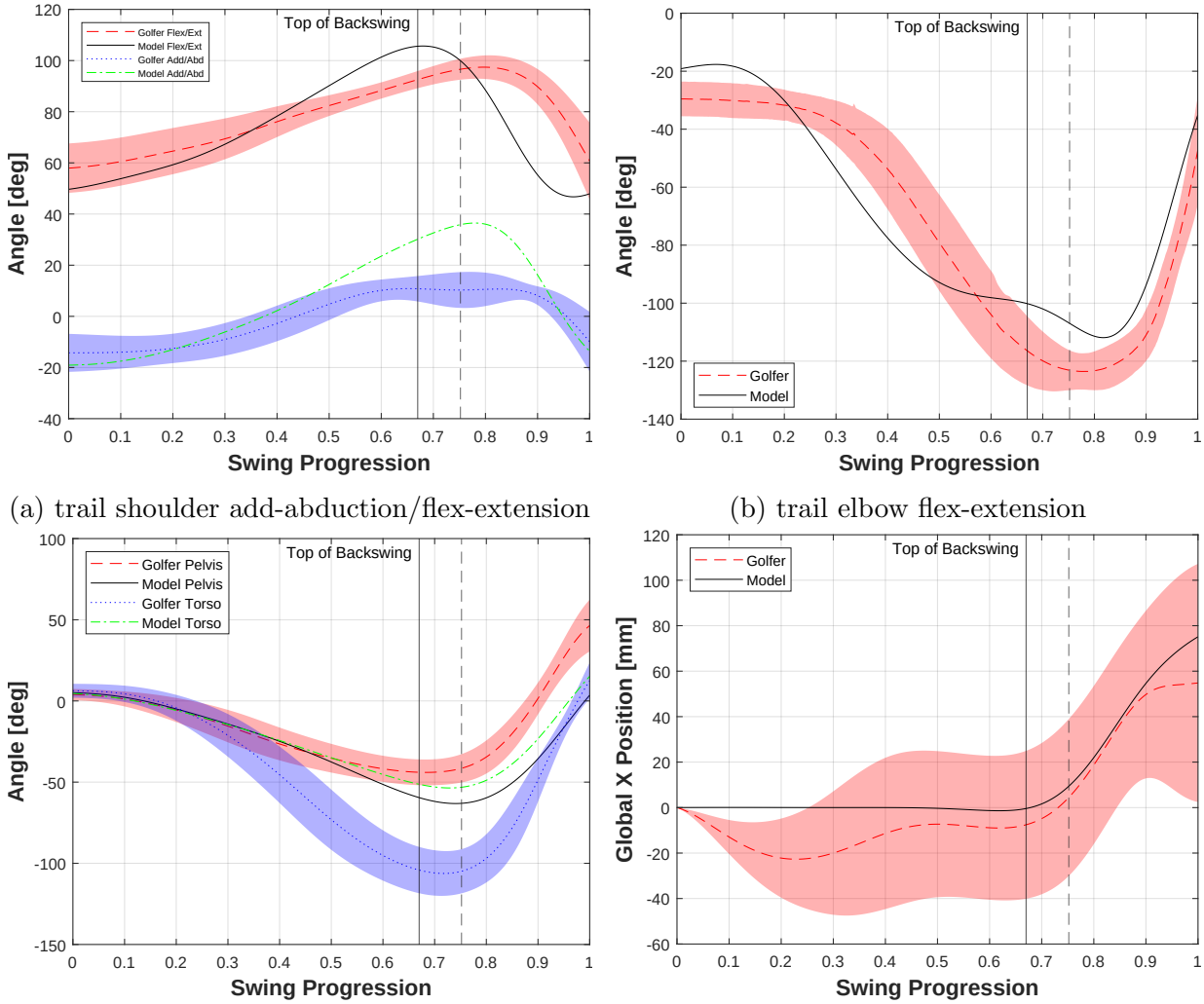

(a) trail shoulder add-abduction/flex-extension

(b) trail elbow flex-extension

(c) torso/pelvis rotation angle

(d) pelvis translation

Figure 4.8: Joint angle/position comparison between the optimized golfer model and the mean of the motion capture experiment golfers. The solid line represents the mean kinematics while the shaded region represents one standard deviation. Shoulder flex-extension is zero with the golfer's arm at their side, and add-abduction is zero with the golfer's arm perpendicular to their chest. Elbow flex-extension is zero at full extension. Torso and pelvis rotation angles are positive about the model global Y axis. The pelvis translation values of the golfers were offset to begin at zero for direct comparison to the golfer model. Vertical lines indicate the top of the backswing for the model (solid line) and the golfers (dashed line). See Section 4.1.5 for determination of the top of the backswing.

Overall, the results from the golfer model biomechanics are promising, and show similarities to elite golfers. While the swing traits are similar, there are some observable differences—especially in the backswing. These differences could be the result of several generalized factors:

- When constructing their golf swing, a player needs to be cognizant of repeatability. A swing technique that has low variance and garners an acceptable result 9/10 times is much more valuable than a technique that has high variance with an exceptional result 1/10 times but poor results otherwise. This can be summarized in the common trope "golf is a game of managing misses." On the other hand, the golfer model is perfectly repeatable to millisecond precision and can exploit techniques that human golfers may find difficult to consistently repeat.

- The simplifications to the model may be preventing it from replicating a human swing. For example, the absence of an explicit model of the spine may cause the model's pelvis-torso rotation to differ from experiments as the relative displacement of the vertebrae in a human swing contributes substantially to this motion.

- Much like repeatability, something a human golfer needs to consider in their swing is injury prevention and fatigue. Musculoskeletal injuries are quite prevalent among both recreational and elite golfers with common sources being the back, shoulders, elbows, wrists, and knees [95]. Between practice time and competitive rounds, it is not unreasonable to expect a PGA Tour player to make on the order of 30,000 swings in a calendar year. This means that their swing technique must not only avoid acute injuries on a single swing, but cumulative injuries as well. The golfer model does not need to consider these factors and is instructed solely to maximize performance for the given shot.

- The tee height was not specified in the motion capture experiment, and participants were free to tee the ball at their preferred height. This means that the human participants and golfer model could be using different tee heights, which could cause discrepancies in biomechanics (see Section 5.1.2).

- The model is generic, and not specific to an individual golfer or set of golfers. This means it is not likely the model will perfectly replicate the swing of any golfer (even elite ones) despite producing similar shot outcomes.

4.4 Golf Ball Aerodynamic Model

As discussed in Section 3.4, 80% of the collected ball flight dataset was used to train and determine the unknown constants of the physics-based aerodynamic model. The remaining 20% of shots were reserved for validation of the model. Each of the launch conditions for the validation shots were passed through the aerodynamic model, with the extracted results for carry, apex, and offline landing position compared to those from the ground truth in the dataset. Table 4.5 outlines the mean absolute error (MAE) and mean absolute percentage error (MAPE) between the aerodynamic model and ground truth.

Table 4.5: Aerodynamic model mean absolute error (MAE) and mean absolute percentage error (MAPE).

Output	MAE [yds]	MAPE [%]
Carry	2.74±2.46	1.52±1.28
Offline	1.68±1.77	28.4±4.39
Apex	1.28±1.20	5.08±64.8

Note: ± indicates standard deviation

The aerodynamic model performs very well in predicting the primary ball flight metric of concern (carry) with a mean absolute error of just 2.74 yards or 1.52%. Results for offline and apex are also encouraging, with means absolute errors of 1.68 and 1.28 yards, respectively. It should be noted that the mean absolute percentage error for offline is higher than one might expect because 12% of the shots in the validation dataset have an offline landing position within one yard of zero. This means that several aerodynamic model predictions that are close to the ground truth in an absolute sense produce very large errors in the relative (or percentage) sense due to the small nature of these numbers.

The results are especially promising when compared to the previous aerodynamic model utilized in the most recent iteration of the dynamic golfer model [35]. Simulating the launch conditions of the validation dataset using this prior model resulted in mean absolute errors of 7.00 ± 5.60, 2.27 ± 2.04, and 2.52 ± 1.53 yards for carry, offline, and apex, respectively.

Chapter 5

Simulation Experiments

Much of the utility of a forward dynamic model is its ability to be used in "what-if?" simulation experiments. These simulations allow for quantitative results to hypothetical questions in a matter of hours without expensive and time-consuming physical experimental setups. In this section, three different simulation experiments are conducted:

1. An investigation into equipment regulations that could be implemented to reduce driving distance at golf's elite level.
2. A study of how the addition of random noise to the optimal swing timings of a golfer will affect the results of a drive using two different drivers.
3. An exploration of the effect of wind on the optimal launch conditions and biomechanics of a golf drive.

These simulation experiments span several topical issues in the game of golf, and show the breadth with which this model can be used. Each of the following subsections will begin with a brief overview of the topic, proceed to detail the simulation experiment setup, and discuss the results.

5.1 Golf's Distance Debate

Since the 1990s, driving distance at the elite level of the game has been increasing at an unprecedented rate; the average driving distance on the PGA Tour increased from 262 yards to 296 yards between 1990 and 2021 [6] (see Fig. 5.1).

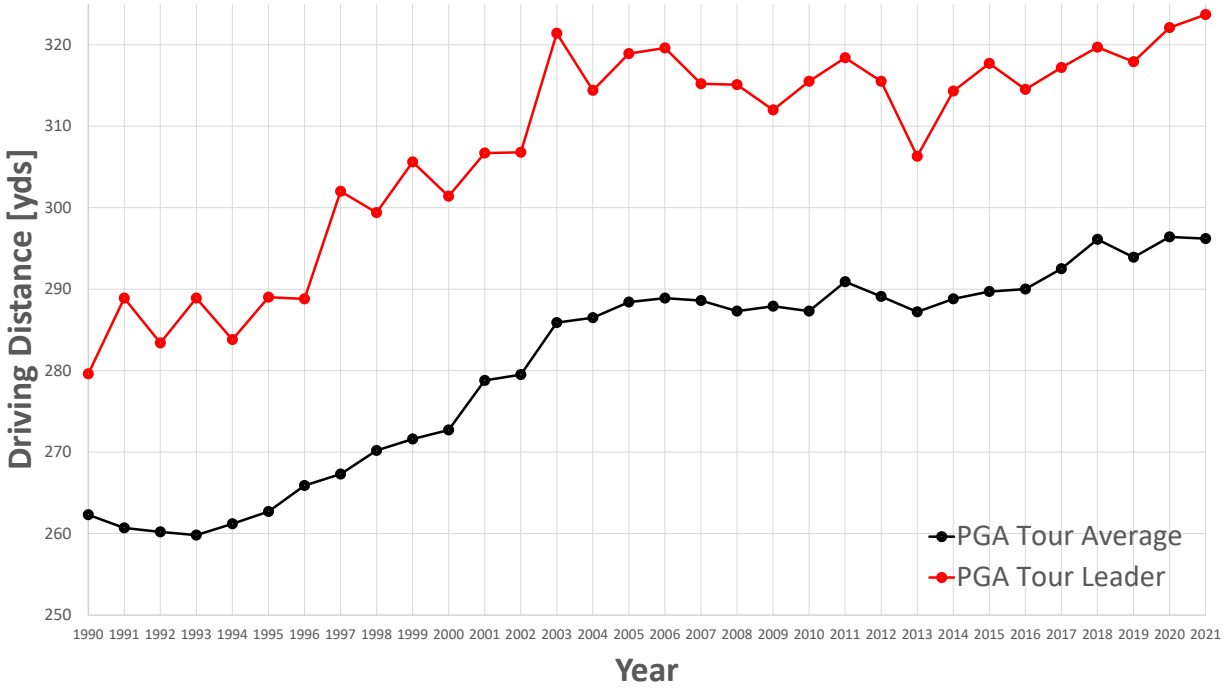

Figure 5.1: PGA Tour leading and average driving distance by year [6].

The cause of these increases can be broken down into two broad categories: innovation in equipment design, and improved understanding of the golf swing. In terms of equipment innovation, changes in driver head design are perhaps the most apparent. For nearly all of the game's history until the late 20th century, driver heads were crafted from wood. In the 1960s through 1980s, these "persimmon woods" as they were known had a head volume of ∼225 cubic centimeters, center of face coefficient of restitution (COR) of ∼0.77, and moment of inertia (MOI) of ∼1700 g-cm^2. Since the introduction of the first metal driver head in 1979, the game has not looked back. Contemporary driver heads are nearly exclusively manufactured from composite materials and titanium alloys, have head volumes of 460 cubic centimeters, CORs of ∼0.83, and MOIs of ∼4500 g-cm^2. Put simply, modern driver heads are larger, "hotter" off the clubface, and more forgiving on mishits while maintaining a nearly identical mass of ∼200 g to their persimmon counterparts. These advancements in driver head design, coupled with the transition from steel to graphite shafts and increase in standard driver shaft length mean that the driver is much more advanced and conducive to distance than it was just 30 years ago.

Perhaps an equal contributor to the rise in driving distance is the golf ball itself, which

much like the driver has undergone significant advancements in the last 30 years. In the 1990s the wound golf ball was the preference of most PGA Tour players, containing a rubber thread wound around a liquid-filled or synthetic rubber core. These balls were encased in a soft balata or surlyn cover, and were known to be high-spinning – especially on wedge shots. With the introduction of the Titleist Pro-V1 golf ball in October of 2000, golf balls transitioned from wound cores to solid cores. Modern solid core golf balls can have upwards of five rubber inner layers and a urethane cover, offering improved energy retention at impact, low long-game spin, and high short-game spin. This improved energy retention at impact combined with low long-game spin leads to significant distance increases with the driver.

Informing the aforementioned innovations in equipment is an improved understanding of the golf swing. From a biomechanics perspective, motion capture systems such as VICON have allowed biomechanists to numerically quantify the golf swing and understand the swing characteristics that elite players possess. From an equipment perspective, launch monitors such as the CGQuad (a stereoscopic high-speed camera system that quantifies clubhead and ball kinematics during impact) and Trackman (a radar-based system that tracks the entire flight of the golf ball) allow for direct numerical quantification of the performance of equipment and the result of the shot (see McPhee [9]).

So why is increased driving distance an issue in golf? Put simply, in most other sports athletes are competing directly against another competitor who has access to the same advanced equipment and training that they do. In golf, athletes compete against the golf course itself and then compare scores with other competitors. Many golf courses were built upwards of 100 years ago when athletes and equipment were not nearly as advanced, meaning they have become much less challenging for today's best players. In an attempt to rectify this, several courses have resorted to lengthening holes [96], increasing the height of rough, narrowing fairways, and keeping the course in firmer playing condition. Not only is this costly, but it is also resource-intensive from an agronomy perspective.

Because it is not practical to modify every golf course on earth or regulate athlete performance outside of prohibiting the use of performance-enhancing drugs, the most logical solution to golf's distance debate involves modifications to the regulations surrounding equipment. In this vein, a myriad of possible solutions have been proposed. In this simulation experiment, two of the proposed equipment regulations deemed meritorious are tested with the golfer model to determine their effectiveness in reducing driving distance.

5.1.1 A Reduction in Allowable Driver Length

For much of golf's modern history the maximum allowable length of any non-putter has been 48 inches, although it is exceedingly rare for a player to actually use a club of this length. On the LPGA Tour, Brooke Henderson has used a 48 inch driver for her entire professional career [97]. In 2020 and 2021, PGA Tour players Phil Mickelson and Bryson DeChambeau began experimenting with 48 inch drivers [98] in the midst of already tense discourse surrounding golf's distance debate. Shortly after, the United States Golf Association and Royal & Ancient introduced a model local rule[1] setting the maximum allowable club length at 46 inches, with the intent for this rule to be used in elite competitions. In theory, a longer club allows the player to generate more clubhead speed and therefore hit the ball farther. This hypothesis was tested by Ferguson et al. [38] with the previous generation of the forward dynamic golfer model [35], and it was found that a 48 inch driver offered a 4.4 yard carry distance increase when compared to a 46 inch driver.

The experiment of Ferguson et al. was repeated here with the updated golfer model to confirm the qualitative results, and discover if the addition of the trailing arm and pelvis translation would change the results in a significant way. The golfer model was given length-scaled versions of driver A1 with lengths of 44, 46, and 48 inches. The maximum allowable tee height of 4 inches was used, translating to 3.5 inches of usable length with 0.5 inches assumed to be submerged in the ground. The biomechanical timings of the golfer were optimized to maximize carry distance subject to the cost function presented in Section 3.5.1. The clubhead deliveries of the optimized drives are presented in Table 5.1 while launch conditions and resultant landing positions are presented in Table 5.2.

Table 5.1: Optimal clubhead deliveries for three different driver lengths.

	44 Inches	46 Inches	48 Inches
CHS [mph]	105.1	108.2	110.3
AOA [°]	13.0	13.4	11.7
Azimuth [°]	8.2 R	6.8 R	5.8 R
Face Angle [°]	4.3 R	3.1 R	2.5 R

[1] A model local rule can be implemented at the discretion of the tournament committee for a particular competition, but is not a codified part of the official "rules of golf" that apply to all rounds of golf.

Table 5.2: Optimal launch conditions and landing positions for three different driver lengths.

	44 Inches	46 Inches	48 Inches
v_b [mph]	154.9	159.3	162.3
θ_{vert} [°]	19.1	19.7	18.0
θ_{hor} [°]	5.3 R	4.1 R	3.4 R
ω_{back} [rpm]	2000	2110	2160
ω_{side} [rpm]	396 L	357 L	305 L
Carry [yds]	274	281	286
Offline [yds]	4.0 R	0.5 L	0.2 L

The results indicate that increasing club length is correlated positively with both clubhead speed ($r = 0.999$) and carry distance ($r = 0.995$), showing general agreement with the previous study of Ferguson et al. Like the previous study, the results here also indicate that there is a slight diminishing return in both clubhead speed and carry distance moving from 46 to 48 inches when compared to moving from 44 to 46 inches. The clubhead deliveries and launch conditions across all three driver lengths represent general draw (right-to-left) shot shapes, but it is interesting to note that the azimuth moves progressively further right as the driver length is shortened (5.8 degrees right to 8.2 degrees right moving from 48 to 44 inches). Launch conditions other than ball speed show no major changes between club lengths except for the horizontal launch angle and sidespin which are a direct result of the changing azimuth and face angle. These results indicate that reducing permissible driver length is effective in reducing driving distance at an approximate rate of three yards of carry distance per inch of club length. The model local rule introduced by golf's governing bodies limiting club length to 46 inches may prevent further distance increases in the future, but is unlikely to reduce current driving distance as five of the most recent driving distance leaders on the PGA Tour used clubs less than 46 inches in length [99].

5.1.2 A Reduction in Allowable Tee Length

Like club length, the rules of golf also dictate an upper limit on the length of a tee. Currently, this limit is four inches although the actual "usable" length is slightly less because of the portion of the tee submerged in the ground to keep it upright; in this thesis it is assumed 0.5 inches must remain submerged in the ground. As demonstrated in Fig. 5.2, the upper limit of a player's angle of attack is effectively limited by the length of the tee; the shorter the tee, the lower the possible angle of attack because the bottom of the clubhead's arc in the downswing should not contact the ground before the ball.

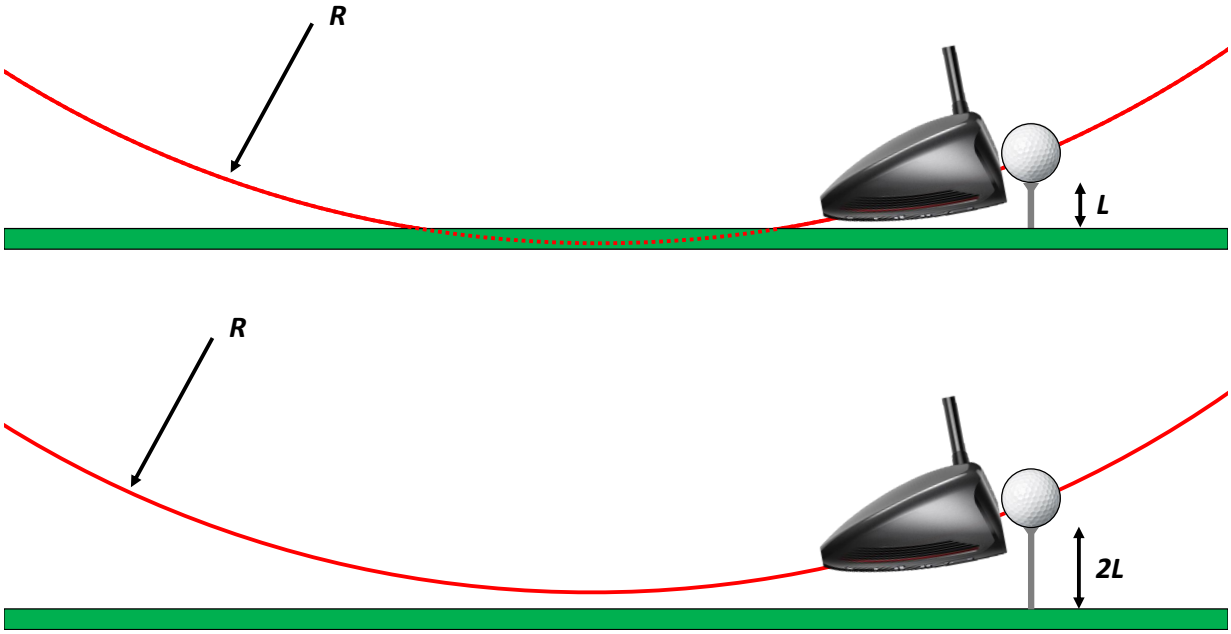

Figure 5.2: Qualitative visualization of how for a given swing arc radius, the length of the tee limits the achievable angle of attack at impact. In the lower image, tee length $2L$ with a swing arc radius R permits the given angle of attack. In the upper image, for the same swing arc radius, the shorter tee length L does not permit this angle of attack due to contact with the ground.

As a general rule, the more a player can increase their angle of attack, the more potential they have to increase driving distance (in combination with their other launch conditions). Therefore, limiting tee length has the potential to reduce driving distance indirectly by limiting the top end of the window of clubhead angles of attack possible for a player. This

is a potentially attractive solution to the distance debate because it requires a change only to one of the least expensive pieces of equipment a golfer owns: the tee. It might cost a golfer a few cents to replace a tee under new rules, but a driver deemed non-conforming because it is too long might cost hundreds of dollars to replace or bring into conformance via shaft trimming.

To test this tee height hypothesis, the golfer model was given tee lengths of two, three, and four inches with the aforementioned assumption that the tee must remained submerged 0.5 inches in the ground. The 46 inch version of driver A1 from the previous simulation experiment was used and the biomechanical timings were once again optimized to maximize carry distance for each tee height subject to the cost function presented in Section 3.5.1. Results for clubhead delivery are presented in Table 5.3 while launch conditions and landing positions are presented in Table 5.4.

The four inch tee height produces the greatest angle of attack (13.4 degrees) and the greatest carry distance (281 yards); an intuitive result based on the aforementioned description of the swing arc radius. At the other end, the two inch tee produces the lowest angle of attack (7.0 degrees) and the shortest carry distance (252 yards). The clubhead speed for the two inch tee is also noticeably less (by 5.9 mph) than that of the four inch tee; this is likely because the model has to swing in such a way that avoids contact with the ground, limiting the amount of speed that is able to be generated. Also of note is that the four inch tee produces an azimuth to the right and a draw shot shape whereas the two inch tee produces a left azimuth and a fade shot shape; again this is likely because the reduction in angle of attack necessary to accommodate this tee length changes the swing path the model is able to make.

Between the two and four inch tees, the three inch tee produces only three less carry yards than the four inch tee despite noticeable changes in clubhead delivery. The angle of attack is reduced by 3.2 degrees and the azimuth moves 4.1 degrees to the left, while the clubhead speed actually increases by 1.4 mph. Despite the increase in clubhead speed, the three inch tee produces slightly less carry distance than the four inch tee due to the reduction in vertical launch angle (by 2.2 degrees) and increase in backspin (by 353 rpm). Beyond a certain tee length, the producible results for carry distance are likely to be similar no matter the length of the tee. This is backed up by the fact that most professional golfers use a tee length of approximately three inches, and one would think they would certainly switch to a four inch tee if there was a consistent advantage in doing so. The results indicate that reducing the allowable tee length from four to two inches could reduce driving distance by approximately 30 yards by indirectly affecting the golfer's clubhead delivery. However, a lesser reduction in tee length would not be nearly as effective.

Table 5.3: Optimal clubhead deliveries for three different tee lengths.

	2.0 Inches	3.0 Inches	4.0 Inches
CHS [mph]	102.3	109.6	108.2
AOA [°]	7.0	10.2	13.4
Azimuth [°]	0.2 L	2.7 R	6.8 R
Face Angle [°]	1.8 L	0.7 L	3.1 R

Table 5.4: Optimal launch conditions and landing positions for three different tee lengths.

	2.0 Inches	3.0 Inches	4.0 Inches
v_b [mph]	150.1	160.7	159.3
θ_{vert} [°]	14.6	17.5	19.7
θ_{hor} [°]	1.3 L	0.2 R	4.1 R
ω_{back} [rpm]	2420	2460	2110
ω_{side} [rpm]	112 R	334 L	357 L
Carry [yds]	252	278	281
Offline [yds]	1.0 L	16.4 L	0.5 L

5.2 Swing Timing Variation

Much of the foundation of instruction in golf is based upon achieving certain positions in the golf swing. At address, an instructor might encourage a student to have their lead arm in full extension and hanging below their chest perpendicular to the ground. Halfway through the downswing, instructors will often encourage golfers to position the golf club parallel to the target line with the clubface perpendicular to the ground. These are just two of the several positional "checkpoints" throughout what is considered to be the ideal swing. Golfers who play at the professional level evidently understand and have mastered these positional checkpoints. However, even the world's best often go through droughts of poor play—why is this? Often the explanation is centered around "tempo" or "rhythm", which can best be described as the timing of key moments in the swing. For example, if a player normally begins rotating their torso 50 milliseconds after their pelvis during the downswing but does so in 70 milliseconds on a given swing, they are likely to see an undesirable change in the clubhead delivery at impact, and therefore the result of the shot.

Evidently, no athlete is perfectly repeatable to millisecond precision in a motion as complex as the golf swing [13]. It is therefore important to understand how variation in golf swing timing affects the outcome of the shot, and how equipment design choices can change these effects. Drivers A1 and A2 from the experimental validation (see Section 4.1) were given to the golfer model, and the biomechanical timings were optimized to maximize the carry distance of the shot subject to the cost function presented in Section 3.5.1. These two drivers were chosen for this experiment because driver A2 is described as an "accuracy" derivative of driver A1; it is one inch shorter and omits an eight gram counterweight in the butt of the grip. The resultant optimal golf drives for both drivers are presented in Table 5.5.

The optimized swings with both clubs produce draw shot shapes that are launched high (approximately 19 degree vertical launch angle) and have low backspin (approximately 2000 rpm). For comparison, the average vertical launch angle on the PGA Tour is 10.5 degrees and the average spinrate is 2500 rpm [6]. These differences are likely due to the model's tee length of four inches allowing a greater angle of attack than what is typically achievable using a more typical 2.75 inch tee used frequently by professionals. Between driver A1 and A2, the one-inch difference in club length is evident in both the clubhead and ball speeds with differences of 2.1 mph and 2.8 mph, respectively. Both drives land within one yard of center of the fairway with driver A1 carrying 281 yards and driver A2 carrying 277 yards.

To simulate variation in swing timing, the optimal biomechanical timings for each driver were mixed with random noise varying between ± 6 milliseconds using MATLAB's `rand`

Table 5.5: Optimal clubhead deliveries, launch conditions, and ball landing positions for optimized swings with drivers A1 and A2.

	Driver A1	Driver A2		Driver A1	Driver A2
CHS [mph]	108.2	106.1	v_b [mph]	159.3	156.5
AOA [°]	13.4	12.9	θ_{vert} [°]	19.7	18.6
Azimuth [°]	6.8 R	5.7 R	θ_{hor} [°]	4.1 R	3.0 R
Face Angle [°]	3.1 R	2.6 R	ω_{back} [rpm]	2110	1940
			ω_{side} [rpm]	357 L	269 L
			Carry [yds]	281	277
			Offline [yds]	0.5 L	0.7 L

function to generate 100 unique "noisy" swings. The noise range of ±6 milliseconds was chosen because it was the largest tested that would ensure all swings still made contact with the golf ball. From the optimal swings, the impact location between the clubhead and ball in the global coordinate system was known and was fixed in the same place for the 100 noisy swings to represent a fixed tee location. The clubhead kinematics at impact for each of the 100 noisy swings were extracted and sent to the impact model at the moment the x component of the vector between the clubface and ball in the clubface local coordinate system became zero (refer to Fig. 3.8). To achieve this, the step size of the system solver in MATLAB was reduced to 10 microseconds to ensure minimal movement of the clubhead between frames, in this case approximately 0.3 mm. While this significantly increased simulation time when compared to the automatic variable-step solver used for typical optimization runs, it importantly meant that significant interpolation between steps was not required. The mean clubhead deliveries and launch conditions for the noisy shots are shown in Table 5.6 while the impact locations and resultant ball flight landing positions are shown Fig. 5.3 and Fig. 5.4, respectively.

Table 5.6: Mean clubhead deliveries, launch conditions, and ball landing positions for noisy swings with drivers A1 and A2.

	Driver A1	Driver A2		Driver A1	Driver A2
CHS [mph]	108.1	106.0	v_b [mph]	156.7	154.2
	±0.8	±0.7		±3.4	±3.0
AOA [°]	13.6	12.9	θ_{vert} [°]	19.8	18.8
	±0.9	±0.9		±1.5	±1.4
Azimuth [°]	6.9 R	5.8 R	θ_{hor} [°]	4.3 R	3.8 R
	±0.6	±0.7		±1.6	±1.7
Face Angle [°]	3.0 R	2.5 R	ω_{back} [rpm]	2065	1920
	±1.3	±1.2		±555	±508
			ω_{side} [rpm]	429 L	300 L
				±452	±468
			Carry [yds]	270.0	265.6
				±12.5	±13.1
			Offline [yds]	4.2 L	1.2 R
				±18.2	±17.7
			Abs. Offline [yds]	16.0	15.0
				±9.4	±9.4

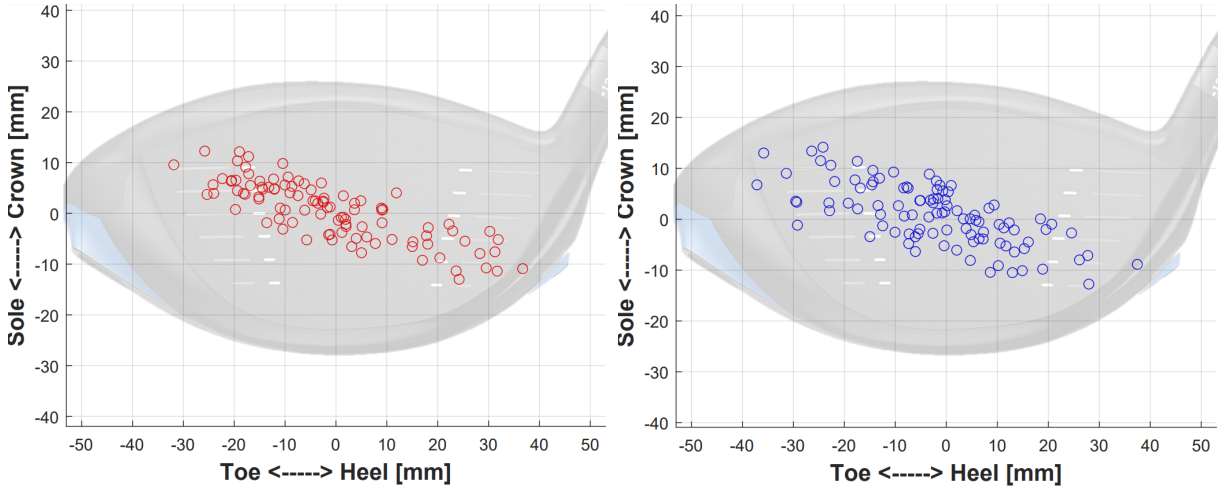

(a) Driver A1 (b) Driver A2

Figure 5.3: Clubface strike locations for swings with noisy joint timings. Note that (0,0) represents the geometric center of the clubface.

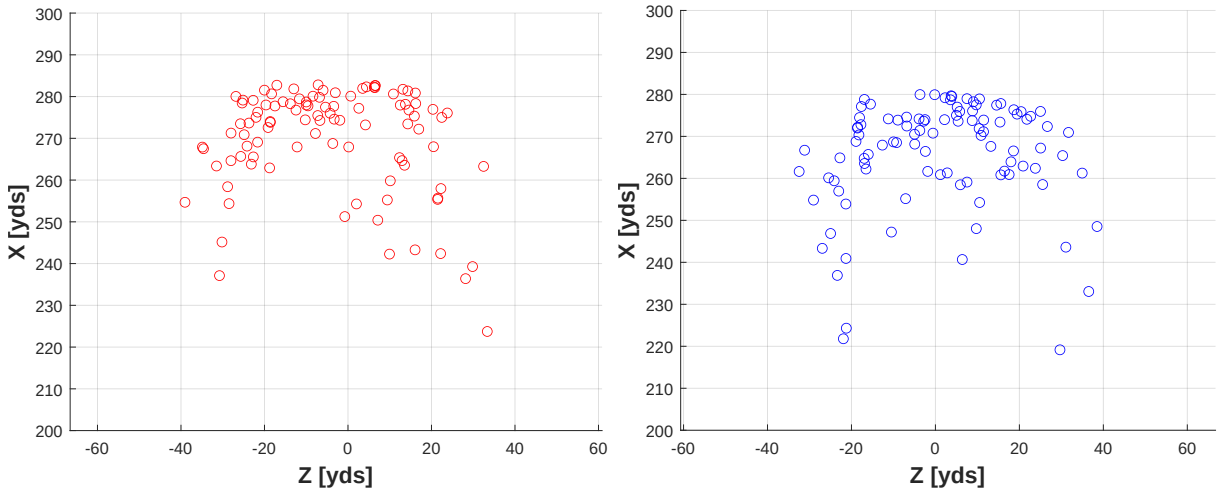

(a) Driver A1 (b) Driver A2

Figure 5.4: Landing locations for swings with noisy joint timings.

For both driver A1 and A2, the mis-hit pattern follows an elliptical-like shape that spans from the high-toe region to the low-heel region of the clubface. The average strike location for driver A1 is 14.0±9.1 mm from the center of the clubface compared to 13.3±9.1

mm for driver A2. In a discussion with an original equipment manufacturer (OEM), it was confirmed that this elliptical impact distribution is also found in real-world experimental testing of golfers. This has led some OEMs to tune their clubface bulge and roll radii [38] specifically to this mishit pattern in order to reduce distance losses and offline dispersion.

The landing positions of both drivers do not follow a distinct geometric pattern. For driver A1, the average carry distance is 270.0±12.5 yds (an 11 yard reduction from optimal) and for driver A2 the average carry distance is 265.6 ± 13.1 yds (an 11.4 yard reduction from optimal). It should be noted that some of the swings with noisy joint timings have a longer carry distance than the optimal drive; this is because these drives travel farther offline and are penalized by the cost function during optimization. Of particular interest is the distribution of offline landing position for the two drivers. Driver A1 has an average offline landing position of 4.2 L ±18.2 yds, compared to 1.2 R ±17.7 yds for driver A2. It is evident that driver A1 has a noticeable draw bias to its mishits while driver A2 has a slight fade bias; this is intuitive based on the difference in length between the two clubs and was confirmed by experimental observations from the OEM. When taking the mean absolute offline landing position, driver A1 has an average absolute offline landing position of 16.0 ±9.4 yds, compared to 15.0 ±9.4 yds for driver A2. These results indicate that at the expense of carry distance, changes to club length and swingweight (through a grip butt counterweight) can reduce mean absolute offline landing position for mishits to a small degree. However, for an individual golfer it is likely best that they engage in a custom-fitting to identify their specific swing and launch condition characteristics, and choose a driver that best accommodates them.

5.3 Effect of Wind on Optimal Launch Conditions

The simulation experiments presented previously have assumed calm conditions with no wind present. This is for obvious reasons; wind is an extraneous variable that is difficult to account for. However, it is extremely rare for a round of golf to occur in completely calm conditions; the sport is played nearly exclusively during the day with the presence of solar heating and subsequent air pressure variations. For context, the average hourly wind speed in Waterloo, Ontario has fallen between 7.4 and 9.5 miles per hour every year since 1997 [100]. The effect of wind on golf shots has been studied in the literature previously, most notably by McPhee and Andrews [101]. However, these studies have explored the launch conditions of the ball exclusively, and not the biomechanics, clubhead delivery, and ball position that create the launch conditions.

It is hypothesized that the presence of wind will lead to a different set of optimal

biomechanical timings, optimal launch conditions, and ball position than a drive with no wind. To test this hypothesis, a headwind (in the negative global X direction) and a tailwind (in the positive global X direction) of 10 miles per hour were imposed on the golfer model. These wind speeds are typical for a summer day and roughly correspond to a "one-club" wind, which golfers generally interpret as the change in club required to hit the ball the distance of the nominal club with no wind present. Using driver A1, the golfer was then optimized subject to the standard cost function presented in Section 3.5.1. The clubhead deliveries of the optimized drives are presented in Table 5.7 while launch conditions and resultant landing positions are presented in Table 5.8. Presented in Table 5.9 are ball positions for the optimized swings while Fig. 5.5 shows the flights of the balls.

Table 5.7: Optimal clubhead deliveries for varying wind conditions.

	Nominal (No Wind)	10 mph Head	10 mph Tail
CHS [mph]	108.2	107.4	108.4
AOA [°]	13.4	13.5	11.0
Azimuth [°]	6.8 R	8.0 R	6.8 R
Face Angle [°]	3.1 R	4.2 R	3.2 R

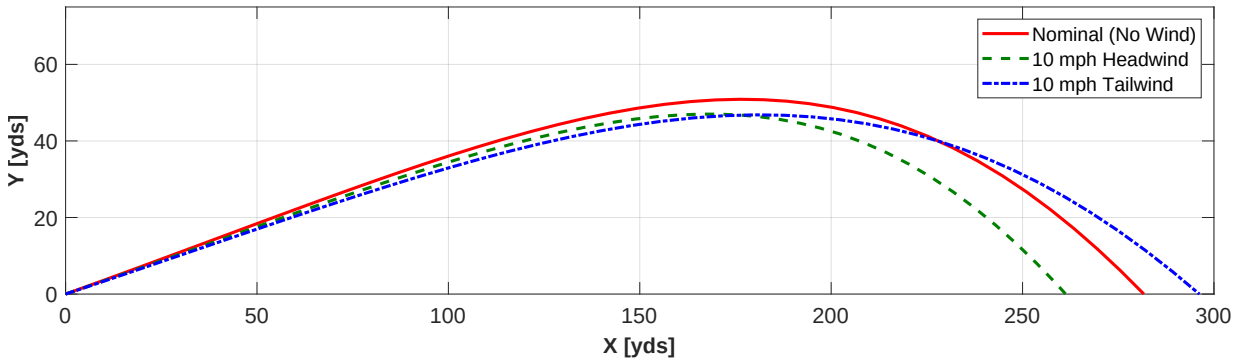

Figure 5.5: Side-profile view of the optimized ball flights with different wind conditions.

Table 5.8: Optimal launch conditions and landing positions for varying wind conditions.

	Nominal (No Wind)	10 mph Head	10 mph Tail
v_b [mph]	159.3	158.4	158.9
θ_{vert} [°]	19.7	18.8	18.4
θ_{hor} [°]	4.1 R	5.2 R	4.2 R
ω_{back} [rpm]	2110	1810	2440
ω_{side} [rpm]	357 L	391 L	379 L
Carry [yds]	281	260	296
Offline [yds]	0.5 L	0.9 L	3.6 R

Table 5.9: Optimal teed ball positions for varying wind conditions.

	Nominal (No Wind)	10 mph Head	10 mph Tail
Ball Position (X) [m]	0.185	0.157	0.140
Ball Position (Z) [m]	1.119	1.135	1.135
Tee Height [inches]	3.4	4.0	3.0

It is interesting to note that the optimal biomechanical timings did not change at all between the three wind conditions despite changes in clubhead delivery and launch conditions. All three swings show a proximal-to-distal sequencing with the pelvis activating first (0.740 s), followed by the torso (0.746 s), shoulder (0.861 s), forearm (0.959 s), and wrist (1.002 s). The changes in clubhead delivery and launch conditions instead came from the teed ball position at which contact was made between the clubhead and ball. Comparing the 10 mph headwind shot to the nominal shot with no wind, the ball position was moved away from the golfer (positive global Z direction) by 1.6 centimeters and back (negative global X direction) by 2.8 centimeters with the tee height increasing to 4 inches from 3.4 inches. These changes critically produced a drive with 300 rpm less backspin than the nominal drive, a desirable characteristic when trying to prevent a shot from "ballooning" when hit into the wind. In total, the drive carried 260 yards when compared to 281 yards for the nominal drive, and had a slightly lower apex height thanks to the reduction in backspin (see Fig. 5.5).

Comparing the 10 mph tailwind shot to the nominal shot with no wind, the ball position was moved away from the golfer (positive global Z direction) by 1.6 centimeters and back (negative global X direction) by 4.5 centimeters with the tee height decreasing to 3.0 inches. These changes produced a drive with 330 rpm more backspin than the nominal drive, a desirable characteristic when trying to prevent a shot from "falling out of the air" due to too little spin when hit with the wind. In total, the drive carried 296 yards when compared to 281 yards for the nominal drive, and had a slightly lower apex height. These results indicate that when hitting drives in the presence of wind, alterations to ball position and tee height can produce desirable launch conditions without the need for changes to biomechanical sequencing.

Chapter 6

Conclusions

6.1 Project Summary

At the outset of this project, the goal was to improve upon the forward dynamic golfer model of McNally and McPhee [35] with the important addition of the trailing arm, validate the improved model experimentally, and to apply the model in "what-if?" simulation experiments surrounding important topics in the game of golf. Notable improvements were made to the model, including the addition of the trailing arm, the addition of a pelvis translational degree of freedom and its associated "muscle force generator", the implementation of a computationally efficient impulse-momentum impact model and continuous analytical shaft model, and the development of a contemporary golf ball aerodynamic model.

The model was then validated as part of a motion capture experiment in which both the club kinematics and golfer biomechanics were of interest. The recorded club kinematics were used to inform and optimize the parameters of the continuous analytical shaft model, while the the biomechanics of the participants were used to make direct comparisons between the swing characteristics of elite golfers, and those of the optimized golfer model.

Using the validated model, simulation experiments were performed that span several topics. The first simulation experiment explored perhaps the most crucial issue presently facing the game of golf: the distance debate. Possible rule changes of limiting club length and limiting tee length were evaluated to determine their efficacy in reducing driving distance; both were deemed successful to varying degrees. The second experiment evaluated the effect of variation in swing timing on the results of a golf drive, finding that a predictable

mishit pattern results from noisy swing timing and that club design choices can affect the results of these mishits. The third experiment investigated the effect of wind on optimal launch conditions, biomechanics, and ball position, finding that different sets of these parameters are ideal in the presence of a headwind or tailwind.

6.2 Opportunities for Future Research

Although the presented work is a significant step forward in modeling the golf drive using forward dynamics, there are several opportunities that exist for additional simulation experiments and improvement to the model through future research.

6.2.1 Simulation Experiments

- Further experiments pertaining to golf's distance debate could be conducted with proposed distance-reducing rules that were not covered here. These include but are not limited to: a reduction in allowable clubhead moment of inertia, a reduction in allowable clubhead volume/clubface surface area, a reduction in allowable clubface coefficient of restitution, and changes to the performance of the golf ball [102].

- There are a number of simulation experiments that have been conducted in the past using one-armed forward dynamic golfer models that could be revisited to compare to the results of this two-armed model. Specific examples include but are not limited to: McNally et al's study of shaft balance point on clubhead speed [36], Ferguson et al's study of clubface bulge and roll radii [38], and McNally's study of optimal clubhead mass [37].

6.2.2 Improvements to the Model

- The focus of this work is modeling golf shots with the driver. This is for good reason; the driver is often the most expensive club in a player's bag, and where equipment manufacturers spend much of their marketing and research and development budgets. However, full swings are not exclusive to the driver and the model could be expanded to consider other clubs including fairway woods, irons, and wedges. Of specific interest would be the development of optimization cost functions for these clubs, which are not likely to be based purely on distance. For example, it is advantageous to hit

an iron shot far, but not if the shot does not have the requisite backspin and descent angle for the ball to remain on the green. The work of Caldwell [103] has recently advanced iron clubhead-ball and clubhead-turf impact modeling, and could form the basis for an iron-specific full golfer model.

- The movement of the shoulder joint center locations to accommodate the address position is necessary to close the kinematic chain between the arms and club. In this model, the shoulder joint center locations are moved within anatomical limits during address position optimization and remain in these positions throughout the swing. Future work could include a full shoulder scapular model that allows the shoulder joint center to translate during the swing, and capture the associated changes in both passive and active muscle forces/torques because of this movement.

- The presented model can use virtual simulation experiments to estimate how a golfer might react to even the smallest design changes to the inertial and material properties of the clubhead, or inertial and stiffness properties of the shaft. However, the presented model does not consider clubhead or shaft aerodynamics. Balzerson [34] considered these forces in his iteration of the model. While these aerodynamic effects are small, nearly all contemporary innovation in driver design is incremental in nature and even seemingly small improvements can justify inclusion in new products. With a clubhead and shaft aerodynamic model, changes to clubhead and shaft geometry could be evaluated from an aerodynamic perspective, rather than from inertial, material, or stiffness perspectives.

- Currently, the model only considers the flight of the ball and not its run phase following landing. Although research has been conducted regarding the impact between the ball and ground [104] and the subsequent roll-out [105], an experimentally-validated model has not yet been presented in the literature. Because agronomic factors such as grass type, moisture levels, and turf compliance vary widely across fairways, a model considering the run of a golf ball should be developed for a single fairway that is deemed representative. The inclusion of a run model could allow the biomechanical timings of the golfer to be optimized for the total (carry + run) distance of the driver rather than just the carry distance, possibly resulting in different optimal launch conditions.

- At the expense of model complexity and simulation time, additional segments and biomechanical degrees of freedom could be added to the model. The most apparent choices are the legs and the associated hip, knee, and ankle joints. Modeling the lower body in this fashion would eliminate the need for the muscle force generator

developed to drive pelvis translation in this model, and would allow for translation of the pelvis in the other two directions not modeled here; these directions were found to move predictably during the motion capture experiment.

- If it is decided that modeling the lower body fully is not prudent, the muscle force generator developed to drive the pelvis translation in this work could be improved through an experimental study that quantifies the dynamics of this pelvic motion. This could be achieved through inverse dynamics via a force plate, or a custom biomechanical dynamometer experiment in which the force output of the pelvis is directly measured.

- The backswing of the optimized swing in this model was found to differ from those of elite golfers. A separate optimization structure for the backswing that focuses on minimizing excess movement or guiding the club to a "typical" position at the top of the backswing would likely result in a backswing more closely mimicking those of elite players.

References

[1] "National Golf Foundation," 2023. https://www.ngf.org/. Accessed 15 Jan 2023.

[2] "Record numbers now playing golf worldwide," 2021. https://api.randa.org/en/news/2021/12/record-numbers-now-playing-golf-worldwide. Accessed 15 Jan 2023.

[3] "Round played reporting – October 2021," 2021. https://files.ngcoa.ca/files/ngcoa/files/rounds-played-report/en-rpr-oct2021-national.pdf. Accessed 15 Jan 2023.

[4] "Taylormade R7 drivers," 2004. https://www.taylormadegolf.com/on/demandware.static/-/Sites-TMaG-Library/default/v1459859109590/docs/productspecs/05_r7_drivers_SS.pdf. Accessed 15 Jan 2023.

[5] J. Achenbach, "2002: Business - Callaway's C4 looking to break sound barrier," 2002. https://golfweek.usatoday.com/2002/11/02/2002-business-callaways-c4-looking-break-sound-bar/. Accessed 15 Jan 2023.

[6] PGA Tour, "PGA Tour Statistics," 2023. https://www.pgatour.com/stats.html. Accessed 15 Jan 2023.

[7] M. Stachura, "Golf's ruling bodies take next step in limiting driver length," 2021. https://www.golfdigest.com/story/driver-length-limit-usga-ra-news. Accessed 15 Jan 2023.

[8] "Golf Laboratories," 2023. https://www.golflabs.com/. Accessed 15 Jan 2023.

[9] J. McPhee, "A review of dynamic models and measurements in golf," *Sports Engineering*, vol. 25, no. 22, 2022. https://doi.org/10.1007/s12283-022-00387-0.

[10] Royal & Ancient and the United States Golf Association, "The 2021 annual driving distance report," tech. rep., Royal & Ancient, St Andrews, Fife, Scotland, 2022. https://www.usga.org/content/dam/usga/pdf/Equipment/2021%20Distance%20Report%20Final%2010-03-2022.pdf.

[11] R. Kaspriske, "Swing sequence: Kevin Tway," 2019. https://www.golfdigest.com/story/swing-sequence-kevin-tway. Accessed 15 Jan 2023.

[12] W. McNally, K. Vats, T. Pinto, C. Dulhanty, J. McPhee, and A. Wong, "GolfDB: A video database for golf swing sequencing," In: *Proceedings of the IEEE/CVF Conference on Computer Vision and Pattern Recognition (CVPR) Workshops*, Long Beach, USA, 2019.

[13] M. Cheon, B. Khuyagbaatar, J.-H. Yeom, and Y. H. Kim, "Analysis of swing tempo, swing rhythm, and functional swing plane slope in golf with a wearable inertial measurement unit sensor," *Journal of Mechanical Science and Technology*, vol. 34, no. 7, pp. 3095–3101, 2020. http://doi.org/10.1007/s12206-020-0640-3.

[14] K. Arakawa, T. Mada, H. Komatsu, T. Shimizu, M. Satou, K. Takehara, and G. Etoh, "Dynamic deformation behavior of a golf ball during normal impact," *Experimental Mechanics*, vol. 49, no. 4, pp. 471–477, 2009. https://doi.org/10.1007/s11340-008-9156-y.

[15] Royal & Ancient and the United States Golf Association, "The equipment rules," tech. rep., Royal & Ancient, St Andrews, Fife, Scotland, 2019. https://www.usga.org/content/dam/usga/pdf/Equipment/Equipment%20Rules%20Final.pdf.

[16] W. McNally, D. Balzerson, D. Wilson, and J. McPhee, "Effect of clubhead inertial properties and driver face geometry on golf ball trajectories," *Procedia Engineering*, vol. 147, pp. 407–412, 2016. https://doi.org/10.1016/j.proeng.2016.06.329.

[17] D. Williams, "The dynamics of the golf swing," *The Quarterly Journal of Mechanics and Applied Mathematics*, vol. 20, no. 2, pp. 247–264, 1967. https://doi.org/10.1093/qjmam/20.2.247.

[18] A. J. Cochran and J. Stobbs, *The Search for the Perfect Swing: An account of the golf society of great Britain scientific study.* Heinemann, 1968.

[19] T. Jorgensen, "On the dynamics of the swing of a golf club," *American Journal of Physics*, vol. 38, no. 5, pp. 644–651, 1970. https://doi.org/10.1119/1.1976419.

[20] M. Lampsa, "Maximizing distance of the golf drive: an optimal control study," *Journal of Dynamic Systems, Measurement, and Control, Transactions ASME*, vol. 97, no. Series G, pp. 362–367, 1975.

[21] R. D. Milne and J. P. Davis, "The role of the shaft in the golf swing," *Journal of Biomechanics*, vol. 25, no. 9, pp. 975–983, 1992. https://doi.org/10.1016/0021-9290(92)90033-w.

[22] W. Pickering and G. Vickers, "On the double pendulum model of the golf swing," *Sports Engineering*, vol. 2, no. 3, pp. 161–172, 1999. https://doi.org/10.1046/j.1460-2687.1999.00028.x.

[23] K. Miura, "Parametric acceleration–the effect of inward pull of the golf club at impact stage," *Sports Engineering*, vol. 4, no. 2, pp. 75–86, 2001. https://doi.org/10.1046/j.1460-2687.2001.00071.x.

[24] C. Chen, Y. Inoue, and K. Shibara, "Numerical study on the wrist action during the golf downswing," *Sports Engineering*, vol. 10, no. 1, pp. 23–31, 2007. http://dx.doi.org/10.1007/BF02844199.

[25] E. J. Sprigings and S. J. MacKenzie, "Examining the delayed release in the golf swing using computer simulation," *Sports Engineering*, vol. 5, no. 1, pp. 23–32, 2002. https://doi.org/10.1046/j.1460-2687.2002.00094.x.

[26] E. J. Sprigings and R. J. Neal, "An insight into the importance of wrist torque in driving the golfball: a simulation study," *Journal of Applied Biomechanics*, vol. 16, no. 4, pp. 356–366, 2000. http://dx.doi.org/10.1123/jab.16.4.356.

[27] K. A. Inkol, C. Brown, W. McNally, C. Jansen, and J. McPhee, "Muscle torque generators in multibody dynamic simulations of optimal sports performance," *Multibody System Dynamics*, vol. 50, pp. 435–452, 2020. https://doi.org/10.1007/s11044-020-09747-9.

[28] S. J. MacKenzie and E. J. Sprigings, "A three-dimensional forward dynamics model of the golf swing," *Sports Engineering*, vol. 11, no. 4, pp. 165–175, 2009. http://dx.doi.org/10.1007%2Fs12283-009-0020-9.

[29] S. J. MacKenzie, "Understanding the role of shaft stiffness in the golf swing," Doctoral thesis, University of Saskatchewan, 2005.

[30] D. Balzerson, J. Banerjee, and J. McPhee, "A three-dimensional forward dynamic model of the golf swing optimized for ball carry distance," *Sports Engineering*, vol. 19, pp. 237–250, 2016. https://doi.org/10.1007/s12283-016-0197-7.

[31] P. Shi, J. McPhee, and G. R. Heppler, "A deformation field for Euler–Bernoulli beams with applications to flexible multibody dynamics," *Multibody System Dynamics*, vol. 5, no. 1, pp. 79–104, 2001. https://doi.org/10.1023/A%3A1026433909962.

[32] W. Petersen and J. McPhee, "Comparison of impulse-momentum and finite element models for impact between golf ball and clubhead," In: *Science and Golf V: Proceedings of the World Scientific Congress of Golf*, Phoenix, USA, 2008.

[33] S. J. Quintavalla, "A generally applicable model for the aerodynamic behaviour of golf balls," In: *Science and Golf IV: Proceedings of the 2002 World Scientific Congress of Golf*, St. Andrews, Scotland, pp. 341–348, 2002.

[34] D. Johnson, "A three-dimensional forward dynamic model of the golf swing," Master's thesis, University of Waterloo, 2015.

[35] W. McNally and J. McPhee, "Dynamic optimization of the golf swing using a six degree-of-freedom biomechanical model," *Proceedings*, vol. 2, no. 6, 2018. https://doi.org/10.3390/proceedings2060243.

[36] W. McNally and J. McPhee, "Investigating the influence of shaft balance point on clubhead speed: A simulation study," *Proceedings*, vol. 49, no. 1, 2020. https://doi.org/10.3390/proceedings2020049156.

[37] W. McNally, "Forward dynamic simulation of a golf drive: Optimization of golfer biomechanics and equipment," Master's thesis, University of Waterloo, 2018.

[38] S. Ferguson, W. McNally, and J. McPhee, "The effect of club length, face bulge radius, and center of gravity depth on optimal golf drives – a simulation study," In: *Engineering of Sport 14: Proceedings of the 14th Conference of the International Sports Engineering Association*, West Lafayette, USA, 2022 https://doi.org/10.5703/1288284317486.

[39] T. K. Uchida, "Real-time dynamic simulation of constrained multibody systems using symbolic computation," Doctoral thesis, University of Waterloo, 2011.

[40] T. Takagi, M. Murata, T. Yokozawa, and H. Shiraki, "Dynamics of pelvis rotation about its longitudinal axis during the golf swing," *Sports Biomechanics*, vol. 20, no. 5, pp. 583–602, 2019. https://doi.org/10.1080/14763141.2019.1585472.

[41] H. Choi and S. Park, "Three dimensional upper limb joint kinetics of a golf swing with measured internal grip force," *Sensors*, vol. 20, no. 13, 2020. https://doi.org/10.3390/s20133672.

[42] S. M. Nesbit, "Development of a full-body biomechanical model of the golf swing," *International Journal of Modelling and Simulation*, vol. 27, no. 4, pp. 392–404, 2007. https://doi.org/10.1080/02286203.2007.11442442.

[43] M. P. McNally, N. Yontz, and A. M. Chaudhari, "Lower extremity work is associated with club head velocity during the golf swing in experienced golfers," *International Journal of Sports Medicine*, vol. 35, no. 9, pp. 785–788, 2014. https://doi.org/10.1055/s-0034-1367010.

[44] S. MacKenzie and R. C. Normore, "How the golfer transfers energy to the club: a two-armed forward dynamics approach," *International Journal of Golf Science*, vol. 4, no. Suppl. 1, pp. S57–S58, 2015. http://dx.doi.org/10.1123/ijgs.2015-0007.

[45] C. Denley and C. Pritchard, "The golf ball aerodynamics of Peter Guthrie Tait," *The Mathematical Gazette*, vol. 77, no. 480, pp. 298–313, 1993. https://doi.org/10.2307/3619769.

[46] J. Choi, W. P. Jeon, and H. Choi, "Mechanism of drag reduction by dimples on a sphere," *Physics of Fluids*, vol. 18, no. 4, 2006. https://doi.org/10.1063/1.2191848.

[47] J. M. Davies, "The aerodynamics of golf balls," *Journal of Applied Physics*, vol. 20, no. 9, pp. 821–828, 1949. https://doi.org/10.1063/1.1698540.

[48] D. Williams, "Drag force on a golf ball in flight and its practical significance," *The Quarterly Journal of Mechanics and Applied Mathematics*, vol. 12, no. 3, pp. 387–392, 1959. https://doi.org/10.1093/qjmam/12.3.387.

[49] P. W. Bearman and J. K. Harvey, "Golf ball aerodynamics," *Aeronautical Quarterly*, vol. 27, no. 2, pp. 112–122, 1976. https://doi.org/10.1017/S0001925900007617.

[50] A. J. Smits and D. R. Smith, "A new aerodynamic model of a golf ball in flight," In: *Science and Golf II: Proceedings of the 1992 World Scientific Congress of Golf*, St. Andrews, Scotland, pp. 411–420, 1992.

[51] B. B. Lieberman, "Estimating lift and drag coefficients from golf ball trajectories," In: *Science and Golf: Proceedings of the 1990 World Scientific Congress of Golf*, St. Andrews, Scotland, pp. 187–192, 1990.

[52] R. K. Hanna, "CFD in sport - a retrospective; 1992 - 2012," *Proceedings*, vol. 34, pp. 622–627, 2012. https://doi.org/10.1016/j.proeng.2012.04.106.

[53] T. J. Chung, *Computational Fluid Dynamics*. Cambridge University Press, 2002.

[54] K. Aoki, K. Muto, and H. Okanaga, "Aerodynamic characteristics and flow pattern of a golf ball with rotation," *Procedia Engineering*, vol. 2, no. 2, pp. 2431–2436, 2010. https://doi.org/10.1016/j.proeng.2010.04.011.

[55] J. Crabill, F. Witherden, and A. Jameson, "High-order computational fluid dynamics simulations of a spinning golf ball," *Sports Engineering*, vol. 22, no. 9, 2019. https://doi.org/10.1007/s12283-019-0300-y.

[56] V. Zatsiorsky, V. Seluyanov, and L. Chugunova, "Methods of determining mass-inertial characteristics of human body segments," *Contemporary Problems of Biomechanics*, pp. 272–291, 1990.

[57] P. de Leva, "Adjustments to Zatsiorsky-Seluyanov's segment inertia parameters," *Journal of Biomechanics*, vol. 29, no. 9, pp. 1223–1230, 1996. https://doi.org/10.1016/0021-9290(95)00178-6.

[58] Y. Liu, C. Günter, R. Leib, and D. W. Franklin, "Bimanual manipulation of a complex object with internal dynamics," In: *44th Annual International Conference of the IEEE Engineering in Medicine Biology Society (EMBC)*, Glasgow, UK, 2022, pp. 4119-4122 https://doi.org/10.1109/EMBC48229.2022.9871098.

[59] S. Komandur, P. W. Johnson, R. L. Storch, and M. G. Yost, "Relation between index finger width and hand width anthropometric measures," In: *Proceedings of the 31st Annual International Conference of the IEEE EMBS*, Minneapolis, USA, 2009 https://doi.org/10.1109/IEMBS.2009.5333195.

[60] J. H. Buffi, K. Werner, T. Kepple, and W. M. Murray, "Computing muscle, ligament, and osseous contributions to the elbow varus moment during baseball pitching," *Annals of Biomedical Engineering*, vol. 43, no. 2, pp. 404–415, 2014. https://doi.org/10.1007/s10439-014-1144-z.

[61] M. Millard, T. Uchida, A. Seth, and S. L. Delp, "Flexing computational muscle: modeling and simulation of musculotendon dynamics," *Journal of Biomechanical Engineering*, vol. 135, no. 2, 2013. https://doi.org/10.1115/1.4023390.

[62] R. W. Gülch, "Force-velocity relations in human skeletal muscle," *International Journal of Sports Medicine*, vol. 15, no. Suppl. 1, pp. S2–S10, 1994. https://doi.org/10.1055/s-2007-1021103.

[63] C. Jansen and J. McPhee, "Predictive dynamic simulation of olympic track cycling standing start using direct collocation optimal control," *Multibody System Dynamics*, vol. 49, no. 1, pp. 53–70, 2020. https://doi.org/10.1007/s11044-020-09723-3.

[64] C. Brown and J. McPhee, "Predictive forward dynamic simulation of manual wheelchair propulsion on a rolling dynamometer," *Journal of Biomechanical Engineering*, vol. 142, no. 7, 2020. https://doi.org/10.1115/1.4046298.

[65] B. Katz, "The relation between force and speed in muscular contraction," *The Journal of Physiology*, vol. 96, no. 1, pp. 45–64, 1939. https://doi.org/10.1113%2Fjphysiol.1939.sp003756.

[66] A. J. van Soest and M. F. Bobbert, "The contribution of muscle properties in the control of explosive movements," *Biological Cybernetics*, vol. 69, no. 3, pp. 195–204, 1993. https://doi.org/10.1007/bf00198959.

[67] H. Choi and S. Park, "Three dimensional upper limb joint kinetics of a golf swing with measured internal grip force," *Sensors*, vol. 20, no. 13, pp. 3672–3686, 2020. https://doi.org/10.3390/s20133672.

[68] M. Millard, A. L. Emonds, M. Harant, and K. Mombaur, "A reduced muscle model and planar musculoskeletal model fit for the simulation of whole-body movements," *Journal of Biomechanics*, vol. 89, pp. 11–20, 2019. https://doi.org/10.1016/j.jbiomech.2019.04.004.

[69] G. T. Yamaguchi, *Dynamic modeling of musculoskeletal motion: a vectorized approach for biomechanical analysis in three dimensions*. Springer Science & Business Media, 2005.

[70] B. B. Kentel, M. A. King, and S. R. Mitchell, "Evaluation of a subject-specific, torque-driven computer simulation model of one-handed tennis backhand ground strokes," *Journal of Applied Biomechanics*, vol. 27, no. 4, pp. 345–354, 2011. https://doi.org/10.1123/jab.27.4.345.

[71] D. Formica, S. K. Charles, L. Zollo, E. Guglielmelli, N. Hogan, and H. I. Krebs, "The passive stiffness of the wrist and forearm," *Journal of Neurophysiology*, vol. 108, no. 4, pp. 1158–1166, 2012. https://doi.org/10.1152/jn.01014.2011.

[72] S. McGill, J. Seguin, and G. Bennett, "Passive stiffness of the lumber torso in flexion, extension, lateral bending, and axial roatation: Effect of belt wearing and breath holding," *Spine*, vol. 19, no. 6, pp. 696–704, 1994. https://doi.org/10.1097/00007632-199403001-00009.

[73] A. E. Engin and S. M. Chen, "Statistical data base for the biomechanical properties of the human shoulder complex–i: Kinematics of the shoulder complex," *Journal of Biomechanical Engineering*, vol. 108, no. 3, pp. 215–221, 1986. https://doi.org/10.1115/1.3138605.

[74] A. E. Engin and S. M. Chen, "Statistical data base for the biomechanical properties of the human shoulder complex—ii: Passive resistive properties beyond the shoulder complex sinus," *Journal of Biomechanical Engineering*, vol. 108, no. 3, pp. 222–227, 1986. https://doi.org/10.1115/1.3138606.

[75] A. E. Engin, "Passive resistive torques about long bone axes of major human joints," *Aviation, Space, and Environmental Medicine*, vol. 50, no. 10, pp. 1052–1057, 1979.

[76] S. Brown, A. M. Nevill, S. A. Monk, S. R. Otto, W. S. Selbie, and E. S. Wallace, "Determination of the swing technique characteristics and performance outcome relationship in golf driving for low handicap female golfers," *Journal of Sports Sciences*, vol. 29, no. 14, pp. 1483–1491, 2011. https://doi.org/10.1080/02640414.2011.605161.

[77] J. Delgado, E. J. Drinkwater, H. G. Banyard, G. G. Haff, and N. Kazunori, "Comparison between back squat, romanian deadlift, and barbell hip thrust for leg and hip muscle activities during hip extension," *Journal of Strength and Conditioning Research*, vol. 33, no. 10, pp. 2595–2601, 2019. https://doi.org/10.1519/jsc.0000000000003290.

[78] F. Struyf, J. Nijs, J. P. Baeyens, S. Mottram, and R. Meeusen, "Scapular positioning and movement in unimpaired shoulders, shoulder impingement syndrome, and glenohumeral instability," *Scandinavian Journal of Medicine and Science in Sports*, vol. 21, no. 3, pp. 352–358, 2011. https://doi.org/10.1111/j.1600-0838.2010.01274.x.

[79] C. Amabile, A. M. J. Bull, and A. E. Kedgley, "The centre of rotation of the shoulder complex and the effect of normalisation," *Journal of Biomechanics*, vol. 49, no. 9, pp. 1938–1943, 2016. https://doi.org/10.1016%2Fj.jbiomech.2016.03.035.

[80] Taylormade Golf, "Rory McIlroy's Powerful Driver Swing," 2020. https://www.youtube.com/watch?v=P3YksJdejog&ab_channel=TaylorMadeGolf. Accessed 16 Jan 2023.

[81] K. Tanaka and K. Sekizawa, "Construction of a finite element model of golf clubs and influence of shaft stiffness on its dynamic behavior," *Proceedings*, vol. 2, no. 6, pp. 247–252, 2018. https://doi.org/10.3390/proceedings2060247.

[82] W. McNally, E. Henrikson, and J. McPhee, "A continuous analytical shaft model for fast dynamic simulation of the golf swing," *Sports Engineering*, vol. 22, no. 20, 2019. https://doi.org/10.1007/s12283-019-0314-5.

[83] B. Danaei, W. McNally, E. Henrikson, and J. McPhee, "Adjusting a momentum-based golf clubhead-ball impact model to improve accuracy," *Proceedings*, vol. 49, no. 1, 2020. https://doi.org/10.3390/proceedings2020049047.

[84] K. Tanaka, Y. Teranishi, and S. Ujihashi, "Finite element modelling and simulations for golf impact," *Journal of Sports Engineering and Technology*, vol. 227, no. 1, pp. 20–30, 2012. https://doi.org/10.1177/1754337112442117.

[85] A. Caldwell and J. McPhee, "Comparison of three-dimensional dynamic models for golf clubhead-ball impacts," In: *Engineering of Sport 14: Proceedings of the 14th Conference of the International Sports Engineering Association*, West Lafayette, USA, 2022 https://doi.org/10.5703/1288284317484.

[86] S. Ferguson, W. McNally, and J. McPhee, "Predicting the flight of a golf ball: Comparing a physics-based aerodynamic model to a neural network," In: *Engineering of Sport 14: Proceedings of the 14th Conference of the International Sports Engineering Association*, West Lafayette, USA, 2022 https://doi.org/10.5703/1288284317493.

[87] M. Broadie, *Every Shot Counts: Using the Revolutionary Strokes Gained Approach to Improve Your Golf Performance and Strategy*. Penguin Publishing Group, 2014.

[88] S. Weinman, "U.s. open 2017: How wide are these ridiculously wide fairways at erin hills? let's put that in perspective," 2017. https://www.golfdigest.com/story/just-how-wide-are-these-ridiculously-wide-fairways-at-erin-hills-lets-put-that-in Accessed 15 Jan 2023.

[89] F. Tinmark, J. Hellstrom, K. Halvorsen, and A. Thorstensson, "Elite golfers' kinematic sequence in full-swing and partial-swing shots," *Sports Biomechanics*, vol. 9, no. 4, pp. 236–244, 2010. https://doi.org/10.1080/14763141.2010.535842.

[90] A. Verikas, E. Vaiciukynas, A. Gelzinis, J. Parker, and M. Charlotte Olsson, "Electromyographic patterns during golf swing: Activation sequence profiling and prediction of shot effectiveness," *Sensors*, vol. 16, no. 4, pp. 592–618, 2016. https://doi.org/10.3390/s16040592.

[91] J. Berhow, "Here's how your handicap index stacks up against golfers in the united states," 2020. https://golf.com/news/how-your-handicap-index-compares/. Accessed 15 Jan 2023.

[92] V. Camomilla, R. Dumas, and A. Cappozoo, "Human movement analysis: The soft tissue artefact issue," *Journal of Biomechanics*, vol. 62, no. 1, pp. 1–4, 2017. https://doi.org/10.1016/j.jbiomech.2017.09.001.

[93] D. Winter, *Biomechanics and Motor Control of Human Movement*. Wiley, 2009.

[94] G. Wu, F. C. T. van der Helm, H. E. J. Veeger, M. Makhsous, P. Van Roy, C. Anglin, J. Nagels, A. R. Karduna, K. McQuade, X. Wang, F. W. Werner, and B. Buchholz, "Isb recommendation on definitions of joint coordinate systems of various joints for the reporting of human joint motion—part ii: shoulder, elbow, wrist and hand," *Journal of Biomechanics*, vol. 38, no. 2005, pp. 981–992, 2005. https://doi.org/10.1016/j.jbiomech.2004.05.042.

[95] G. Theriault and P. Lachance, "Golf injuries," *Sports Medicine*, vol. 26, no. 1, pp. 43–57, 1998. https://doi.org/10.2165/00007256-199826010-00004.

[96] S. Hennessey, "Latest photos of augusta national's work on the 13th hole reveal how it could play from a new tee in 2023," 2022. https://www.golfdigest.com/story/augusta-national-13th-tee-course-changes. Accessed 15 Jan 2023.

[97] A. Rogers, "Brooke henderson moving to shorter driver for first time at chevron," 2022. https://www.golfchannel.com/news/brooke-henderson-going-miss-48-inch-driver-she-adapts-new-rule. Accessed 15 Jan 2023.

[98] A. Turskey, "Top golf gear stories of 2021: Phil mickelson rips usga for proposed driver limit," 2021. https://golf.com/gear/drivers/phil-mickelson-rips-usga-driver-limit/. Accessed 15 Jan 2023.

[99] J. Wall, "We got exact specs for 5 pga tour bombers. here's 1 thing they all have in common," 2020. https://golf.com/gear/drivers/driver-specs-pga-tour-driving-distance-rory-dustin-johnson-champ/. Accessed 15 Jan 2023.

[100] Environment and Climate Change Canada, "Wind speed - annual data for Kitchener-Waterloo," 2023. https://kitchenerwaterloo.weatherstats.ca/charts/wind_speed-yearly.html. Accessed 15 Jan 2023.

[101] J. McPhee and G. Andrews, "Effect of sidespin and wind on projectile trajectory, with particular application to golf," *American Journal of Physics*, vol. 56, no. 10, pp. 933–939, 1988. https://doi.org/10.1119/1.15363.

[102] M. Stachura, "Golf governing bodies to announce plan to roll back golf ball for elite competition," 2023. https://www.golfdigest.com/story/usga-and-r-a-ball-rollback-proposal. Accessed 17 Mar 2023.

[103] A. Caldwell, "Development and comparison of 3D dynamic models of golf clubhead-ball impacts," Master's thesis, University of Waterloo, 2023.

[104] S. J. Haake, "Apparatus and test methods for measuring the impact of golf balls on turf and their application in the field," Doctoral thesis, Aston University, 1989.

[105] R. A. Penner, "The run of a golf ball," *Canadian Journal of Physics*, vol. 80, no. 8, pp. 931–940, 2002. https://doi.org/10.1139/p02-035.

APPENDICES

Appendix A

Motion Capture Experiment Mean Ball Launch Conditions

Table A.1: Motion capture experiment mean launch conditions (1/2)

G	Club	Ball Speed [mph]	Launch Angle [deg]	Azimuth [deg]	Backspin [rpm]	Sidespin [rpm]
1	A1	150	15.5	−12.6	4170	29.6
		±2.00	±1.32	±2.13	±670	±634
	A2	150	14.7	−13.4	3800	−201
		±2.97	±1.69	±1.69	±502	±639
	B1	146	14.7	−9.33	3680	291
		±2.06	±2.02	±1.69	±512	±643
2	A1	144	10.8	−2.46	3060	205
		±2.40	±2.09	±1.38	±647	±698
	A2	141	11.4	−4.46	2880	−114
		±3.48	±2.17	±1.43	±569	±425
	B1	140	9.29	−0.01	3700	1640
		±2.83	±2.45	±2.23	±410	±562
3	A1	123	21.4	−3.43	2550	−141
		±2.92	±2.24	±2.33	±613	±460
	A2	123	19.2	−4.12	1980	−640
		±3.61	±2.75	±1.63	±424	±377
	B1	123	17.3	−4.63	2110	395
		±3.54	±2.52	±2.31	±435	±437
4	A1	160	14.0	−0.80	4240	185
		±1.82	±1.55	±0.93	±408	±355
	A2	160	11.5	−1.62	3860	141
		±1.84	±4.22	±2.33	±556	±273
	B1	160	11.8	−2.85	3330	168
		±2.04	±1.72	±1.52	±197	±266
5	A1	166	14.8	0.58	3930	−385
		±2.48	±1.63	±1.00	±716	±435
	A2	163	15.6	−2.44	3380	−811
		±2.87	±0.96	±1.25	±404	±345
	B1	166	10.0	−0.86	3660	−131
		±2.26	±2.26	±1.42	±586	±631

Table A.2: Motion capture experiment mean launch conditions (2/2)

G	Club	Ball Speed [mph]	Launch Angle [deg]	Azimuth [deg]	Backspin [rpm]	Sidespin [rpm]
6	A1	165	19.0	−0.96	4620	1370
		±2.25	±1.27	±1.36	±519	±488
	A2	163	18.5	−2.32	4240	1020
		±3.63	±1.09	±1.95	±470	±499
	B1	169	15.9	−3.50	2960	576
		±1.56	±1.04	±0.95	±232	±323
7	A1	152	15.0	3.28	3960	607
		±1.01	±1.31	±1.00	±275	±294
	A2	153	15.3	1.41	3500	118
		±1.32	±1.40	±1.78	±365	±255
	B1	155	13.9	2.01	2860	346
		±1.11	±1.19	±1.99	±236	±299
8	A1	162	13.1	1.61	2750	−742
		±3.21	±1.26	±1.43	±484	±487
	A2	162	12.0	0.52	2880	−975
		±1.98	±0.92	±0.93	±375	±405
	B1	158	12.1	−1.99	2540	−1110
		±7.39	±4.55	±1.80	±1720	±673
9	A1	157	17.9	−1.09	4210	671
		±2.43	±1.11	±0.78	±377	±280
	A2	157	16.9	−2.28	3390	112
		±2.59	±1.59	±1.86	±395	±282
	B1	160	14.9	−2.84	3050	383
		±1.42	±1.15	±0.82	±515	±318
10	A1	147	15.9	−0.93	3360	573
		±2.30	±1.14	±1.36	±363	±259
	A2	147	15.2	−0.55	3350	526
		±1.00	±1.13	±1.21	±255	±218
	B1	147	12.4	−4.63	2330	430
		±1.34	±1.18	±0.97	±260	±243

Appendix B

Motion Capture Experiment Mean Club Kinematics: Driver A1

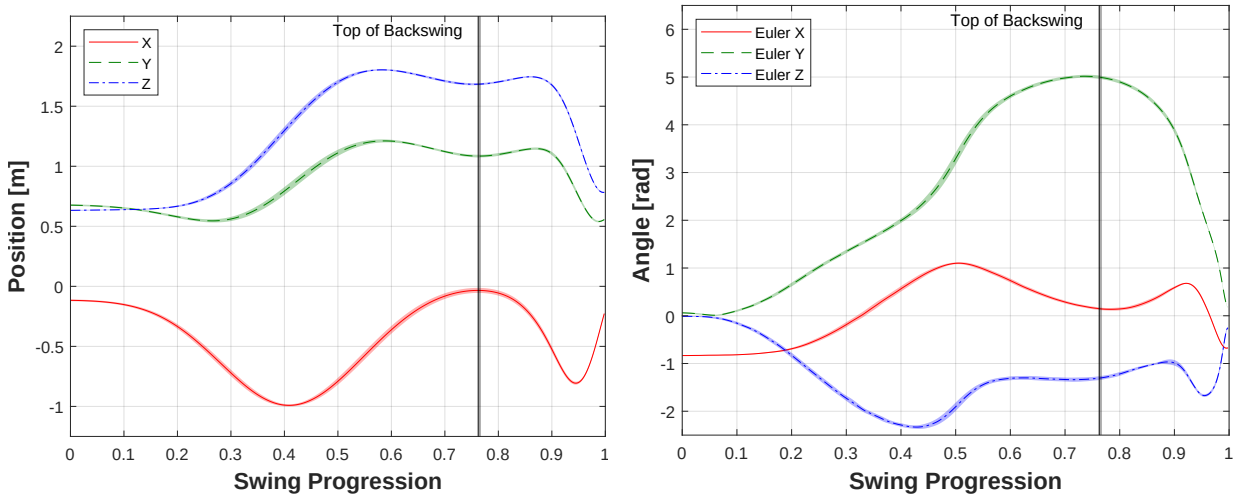

(a) grip position

(b) grip angles (YXZ Euler)

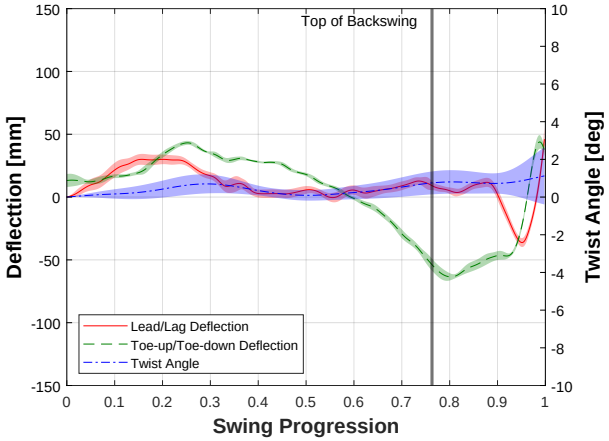

(c) clubhead deflections

Figure B.1: Golfer 1 mean club kinematics: Driver A1

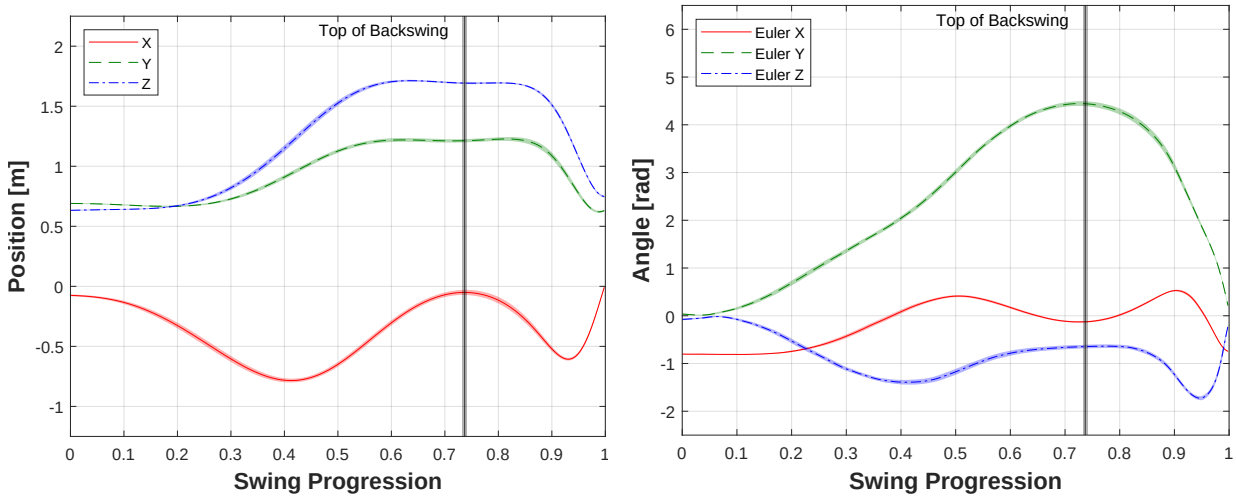

(a) grip position

(b) grip angles (YXZ Euler)

(c) clubhead deflections

Figure B.2: Golfer 2 mean club kinematics: Driver A1

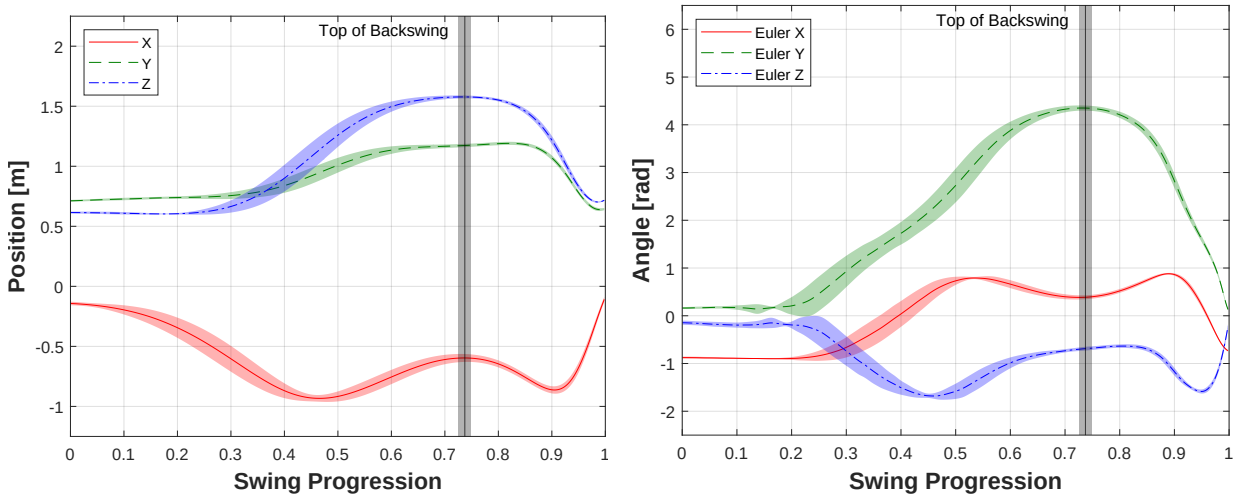

(a) grip position

(b) grip angles (YXZ Euler)

(c) clubhead deflections

Figure B.3: Golfer 3 mean club kinematics: Driver A1

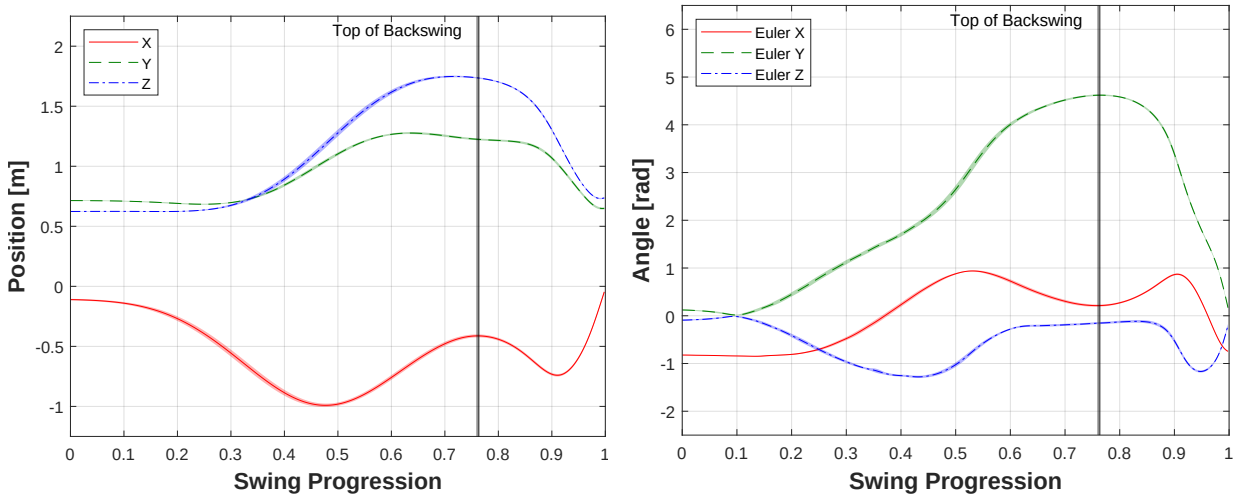

(a) grip position

(b) grip angles (YXZ Euler)

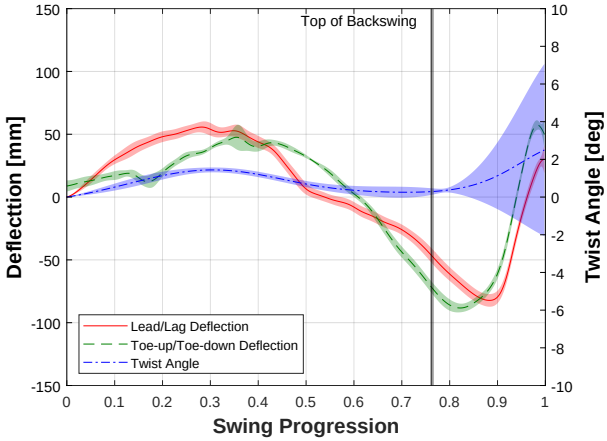

(c) clubhead deflections

Figure B.4: Golfer 4 mean club kinematics: Driver A1

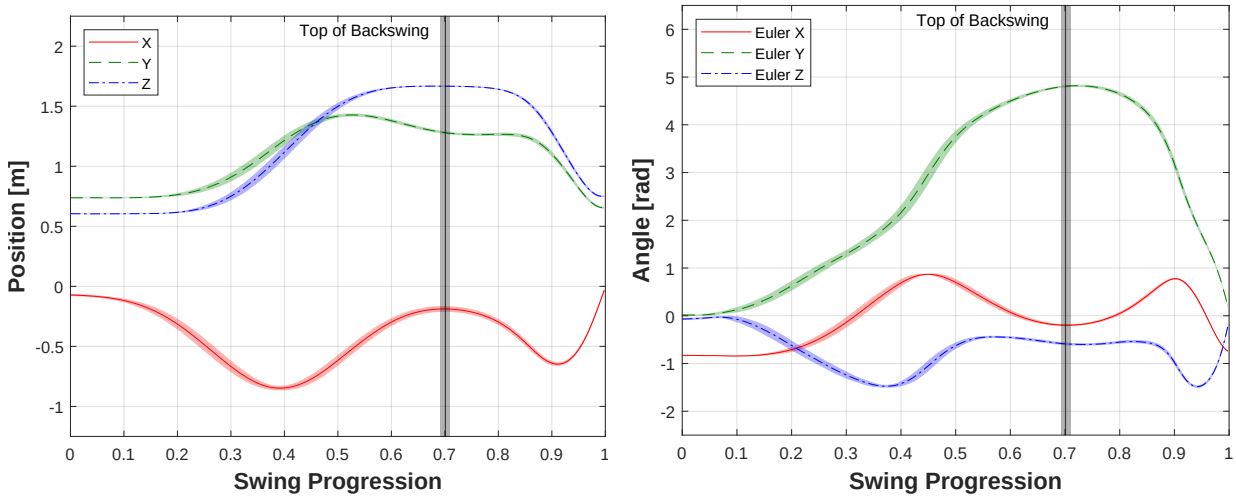

(a) grip position

(b) grip angles (YXZ Euler)

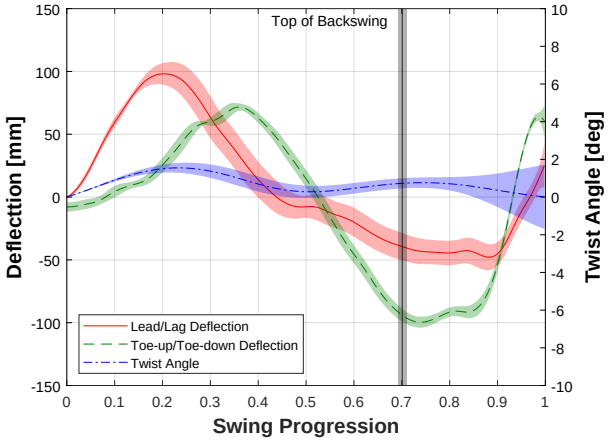

(c) clubhead deflections

Figure B.5: Golfer 5 mean club kinematics: Driver A1

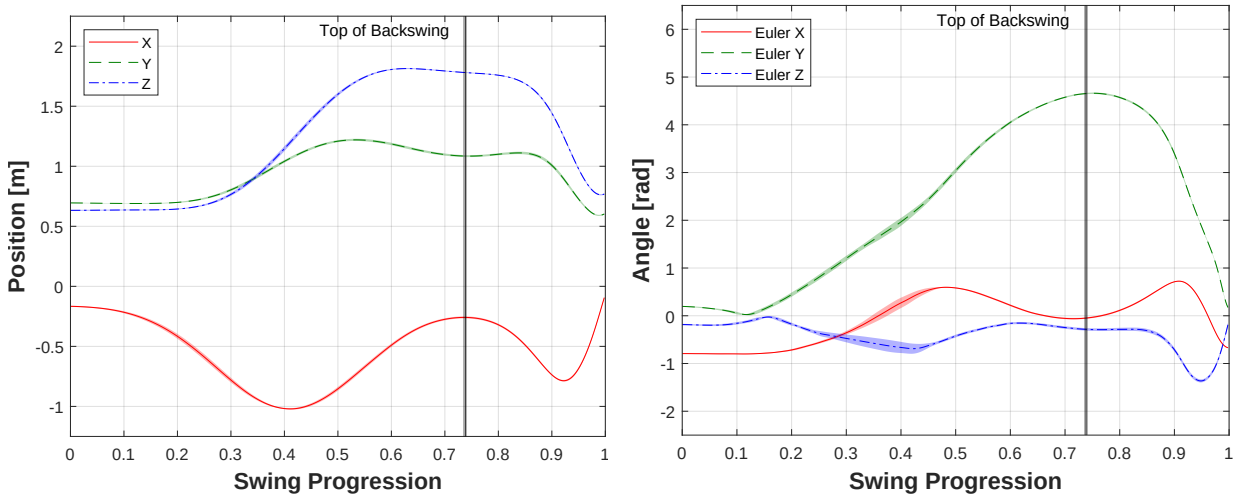

(a) grip position

(b) grip angles (YXZ Euler)

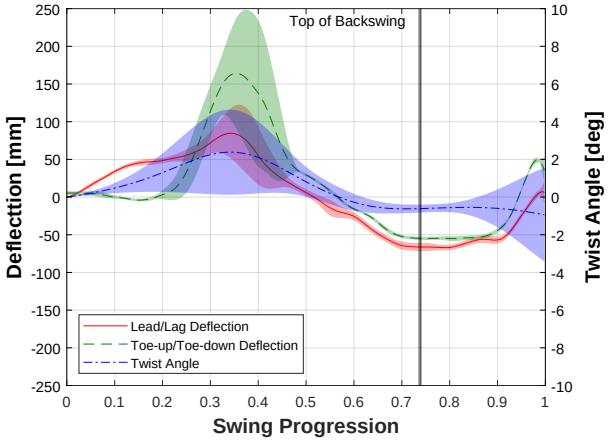

(c) clubhead deflections

Figure B.6: Golfer 6 mean club kinematics: Driver A1

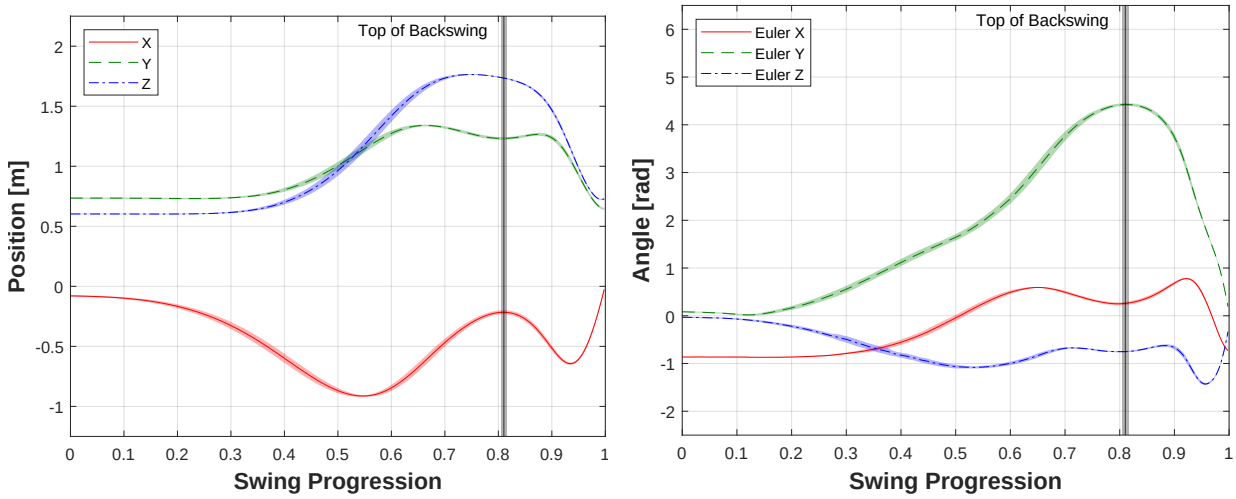

(a) grip position

(b) grip angles (YXZ Euler)

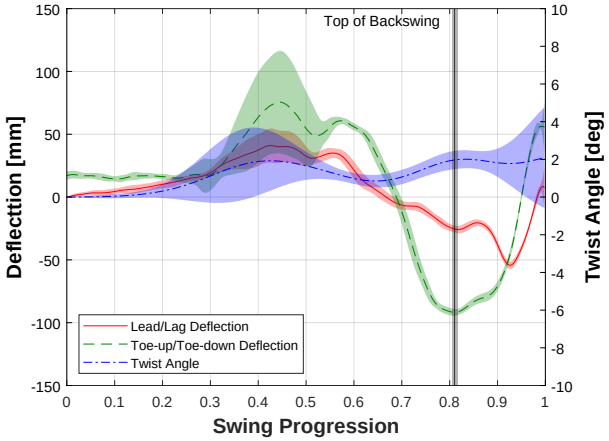

(c) clubhead deflections

Figure B.7: Golfer 7 mean club kinematics: Driver A1

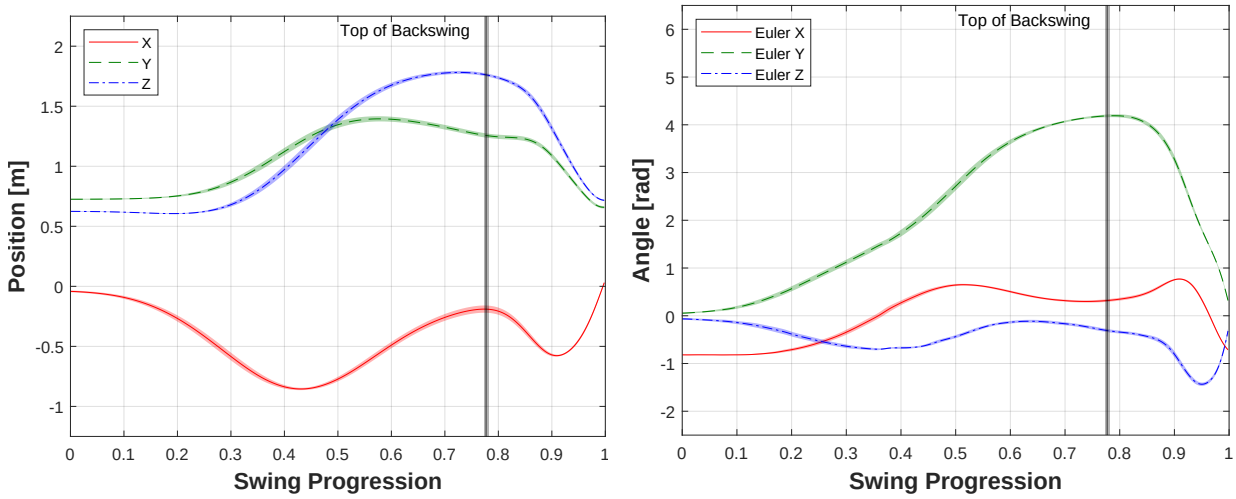

(a) grip position

(b) grip angles (YXZ Euler)

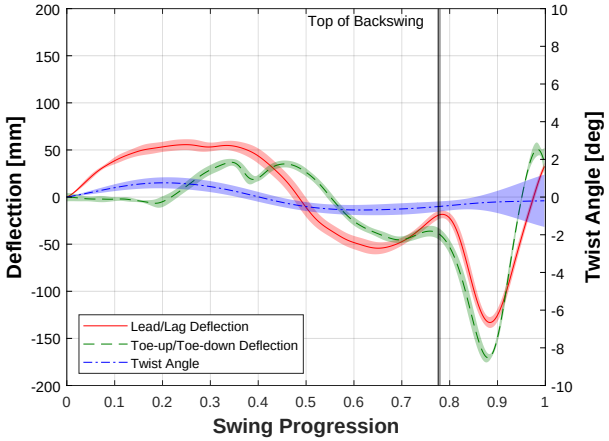

(c) clubhead deflections

Figure B.8: Golfer 8 mean club kinematics: Driver A1

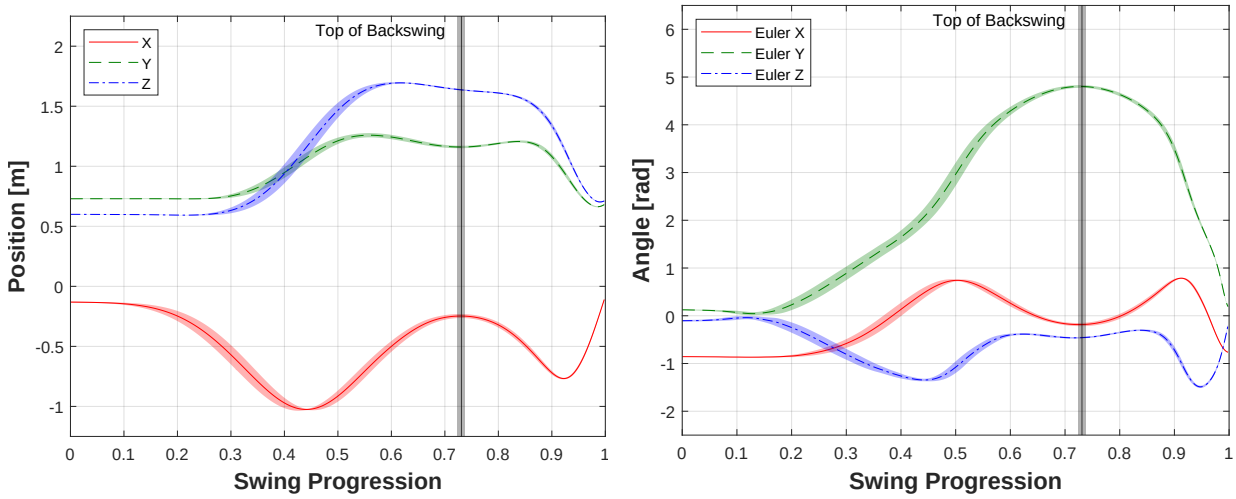

(a) grip position

(b) grip angles (YXZ Euler)

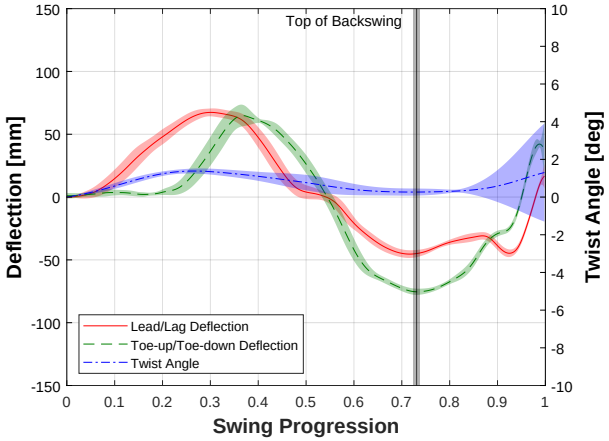

(c) clubhead deflections

Figure B.9: Golfer 9 mean club kinematics: Driver A1

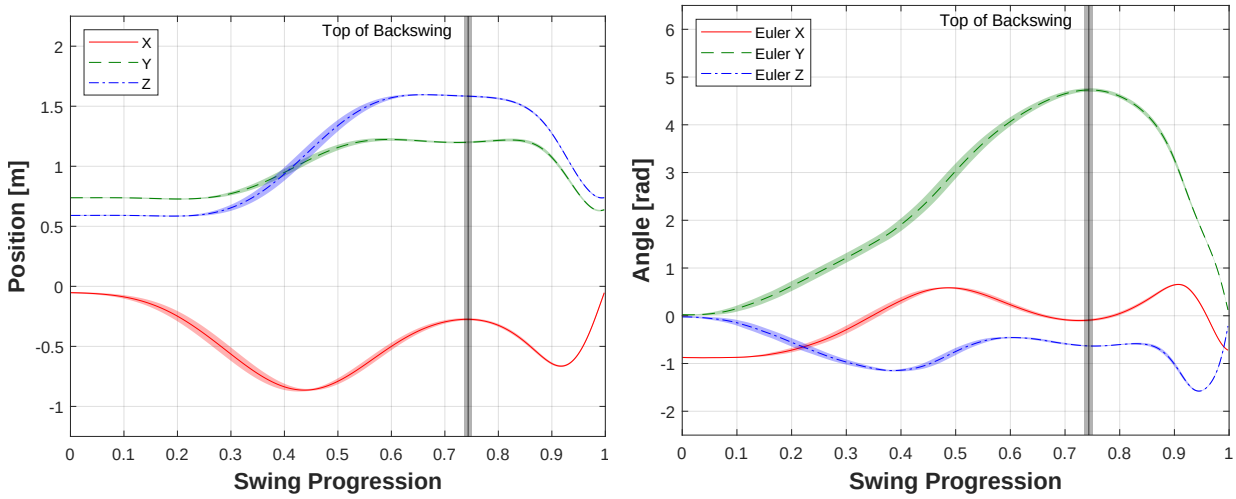

(a) grip position

(b) grip angles (YXZ Euler)

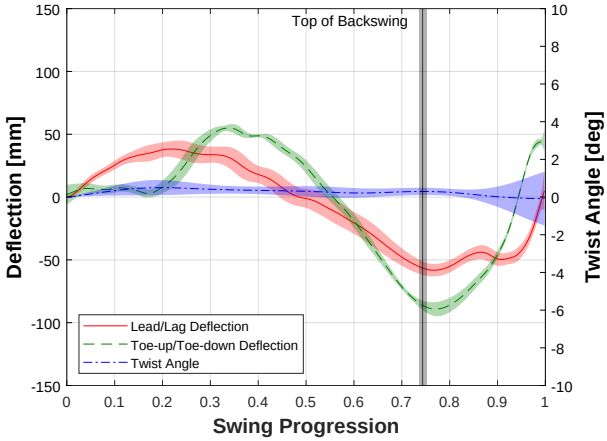

(c) clubhead deflections

Figure B.10: Golfer 10 mean club kinematics: Driver A1

Appendix C

Motion Capture Experiment Mean Club Kinematics: Driver A2

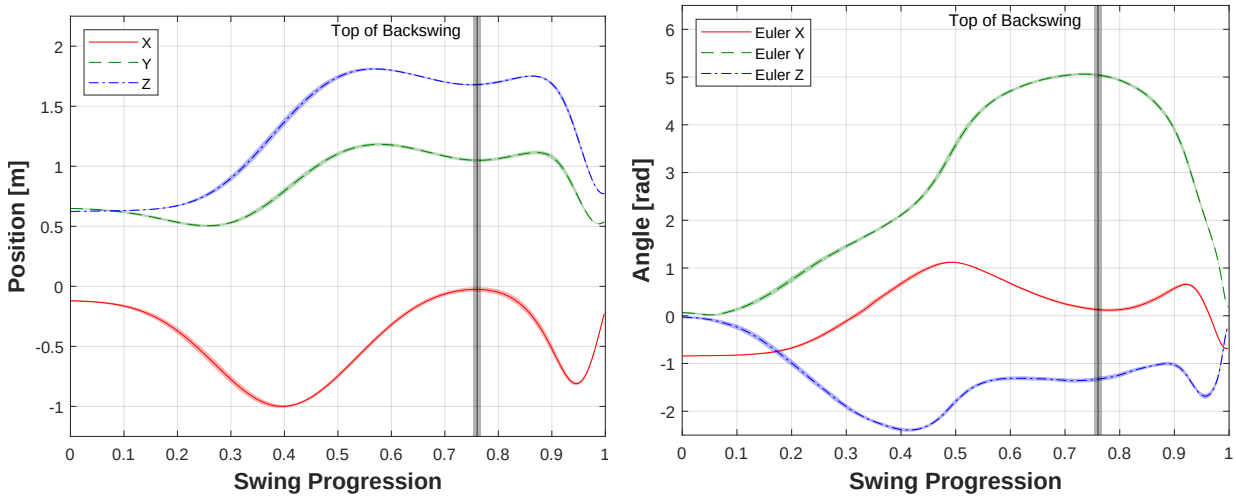

(a) grip position

(b) grip angles (YXZ Euler)

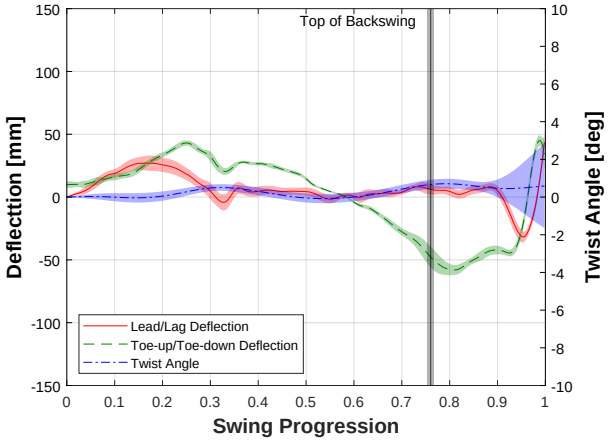

(c) clubhead deflections

Figure C.1: Golfer 1 mean club kinematics: Driver A2

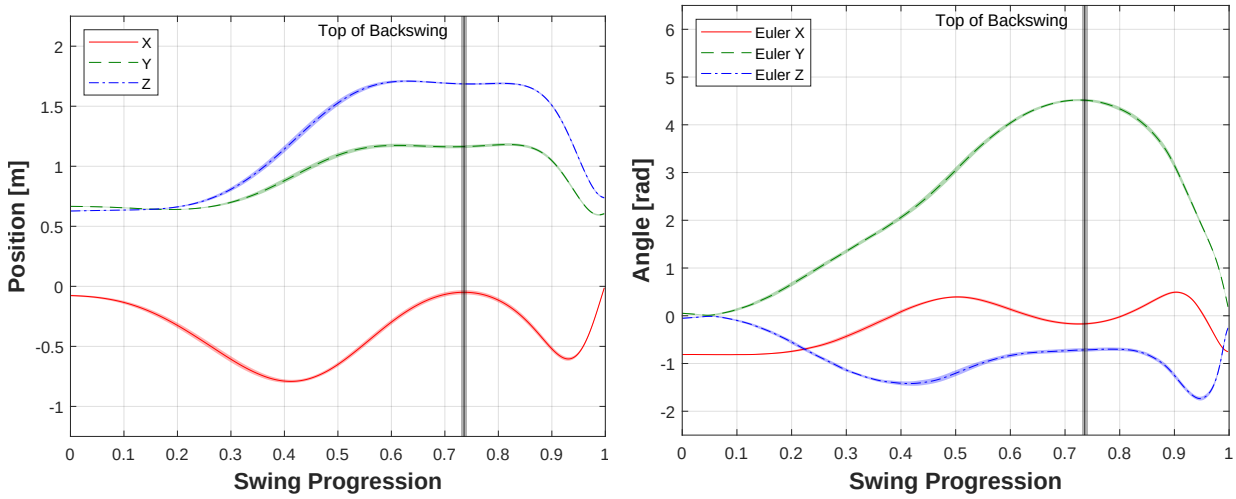

(a) grip position

(b) grip angles (YXZ Euler)

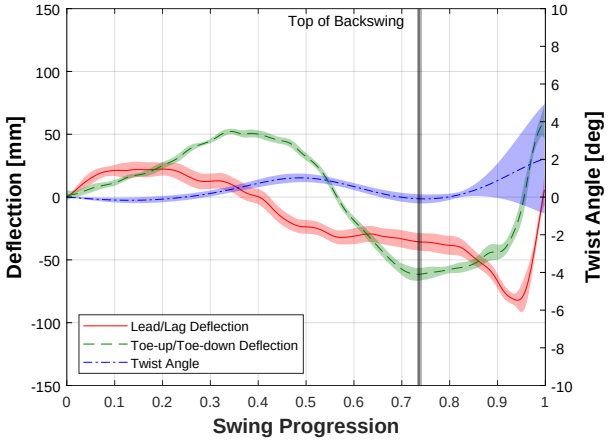

(c) clubhead deflections

Figure C.2: Golfer 2 mean club kinematics: Driver A2

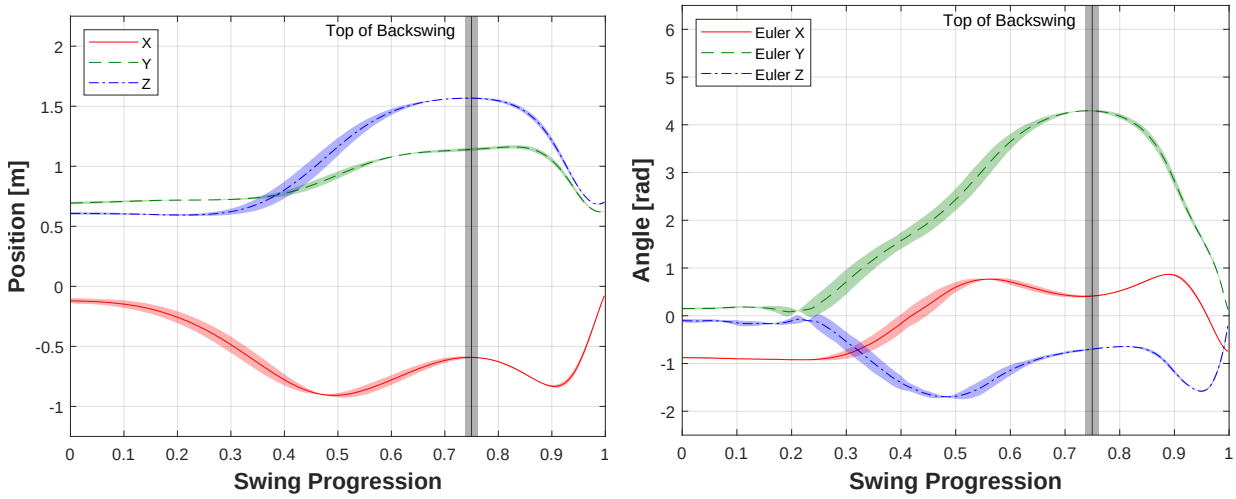

(a) grip position

(b) grip angles (YXZ Euler)

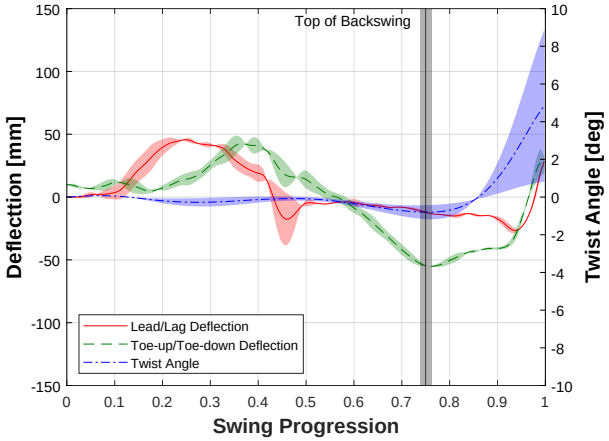

(c) clubhead deflections

Figure C.3: Golfer 3 mean club kinematics: Driver A2

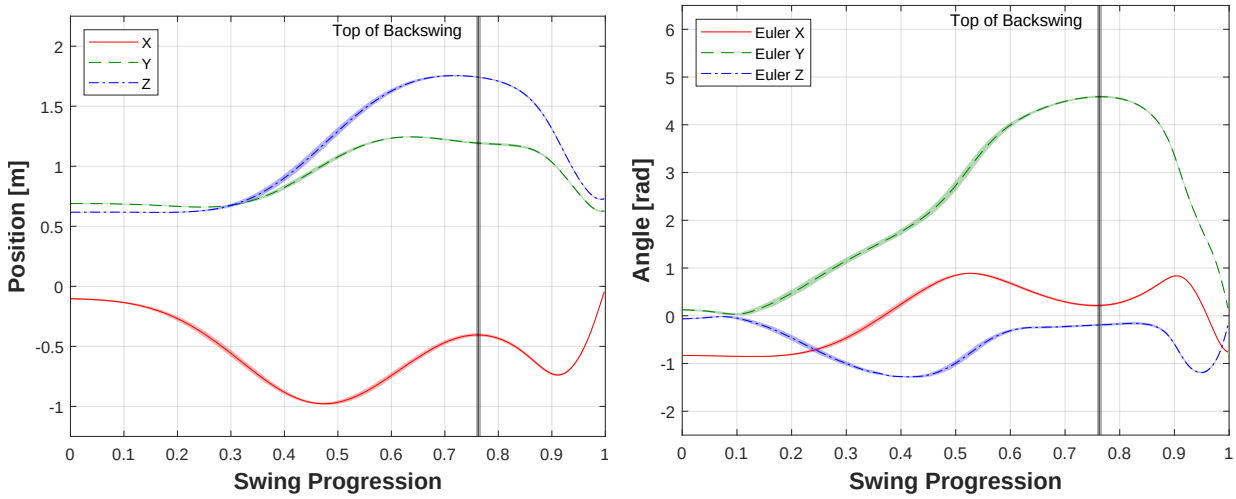

(a) grip position

(b) grip angles (YXZ Euler)

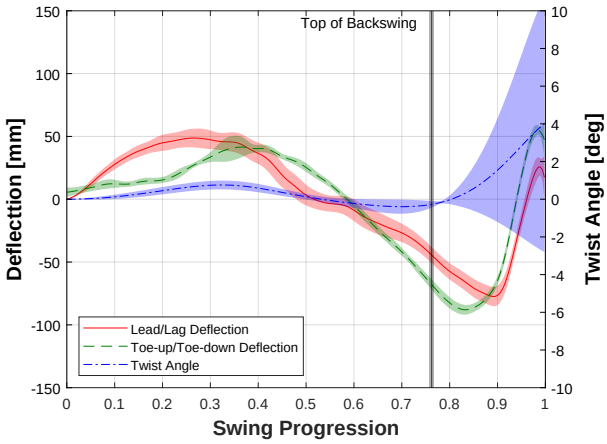

(c) clubhead deflections

Figure C.4: Golfer 4 mean club kinematics: Driver A2

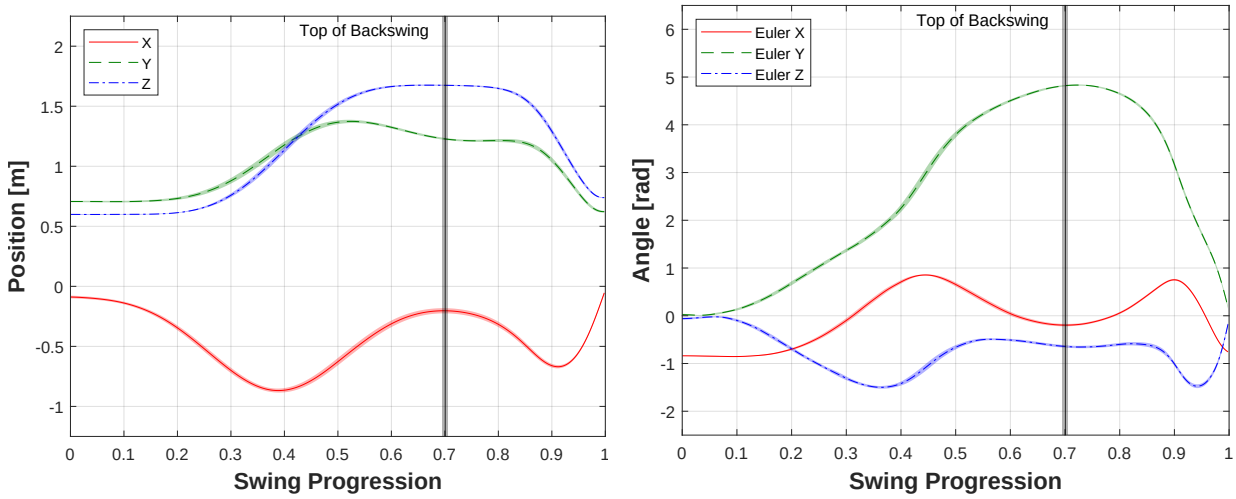

(a) grip position

(b) grip angles (YXZ Euler)

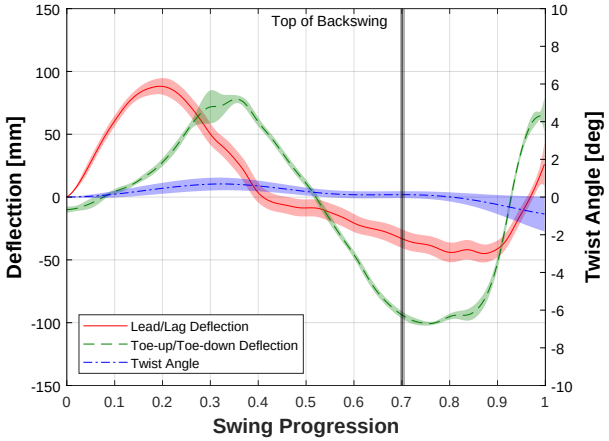

(c) clubhead deflections

Figure C.5: Golfer 5 mean club kinematics: Driver A2

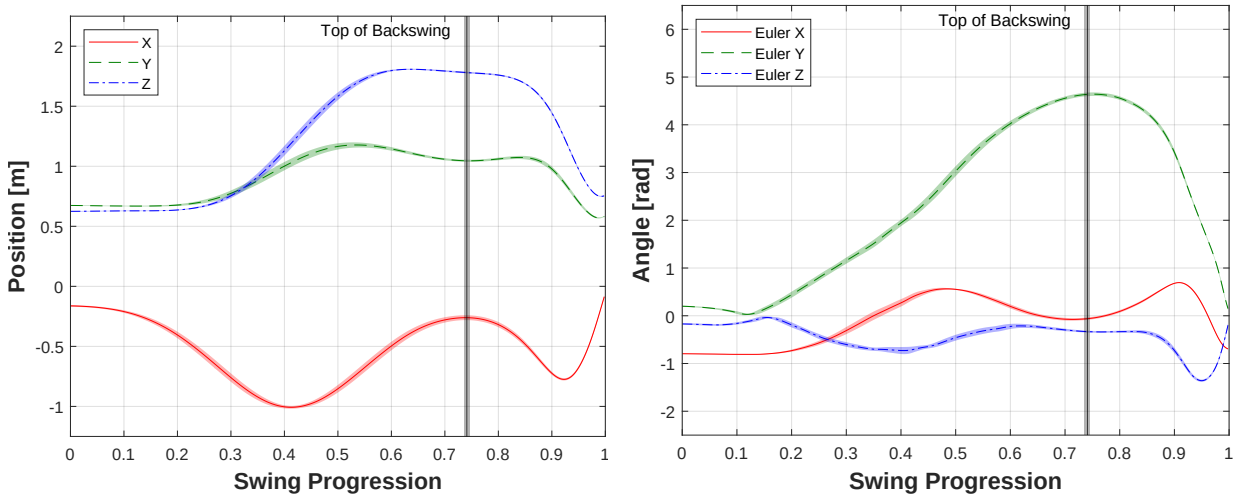

(a) grip position

(b) grip angles (YXZ Euler)

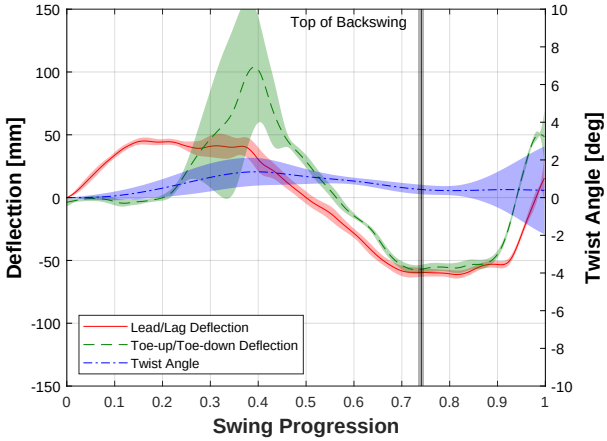

(c) clubhead deflections

Figure C.6: Golfer 6 mean club kinematics: Driver A2

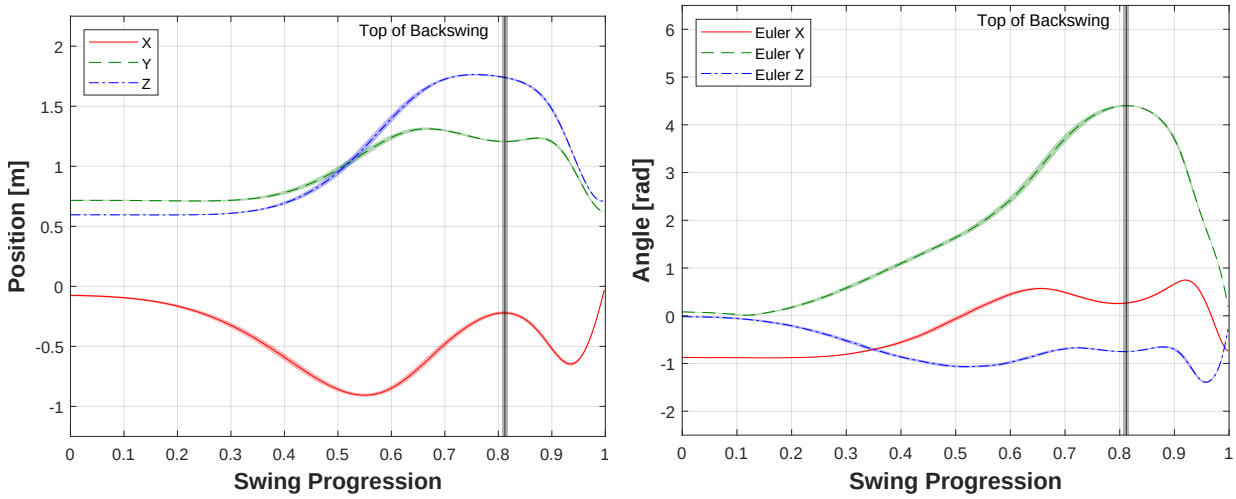

(a) grip position

(b) grip angles (YXZ Euler)

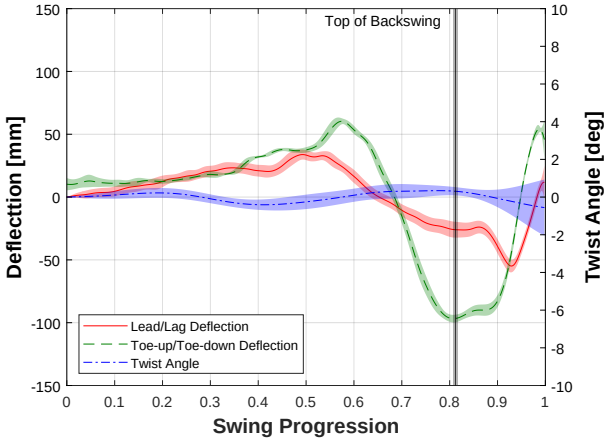

(c) clubhead deflections

Figure C.7: Golfer 7 mean club kinematics: Driver A2

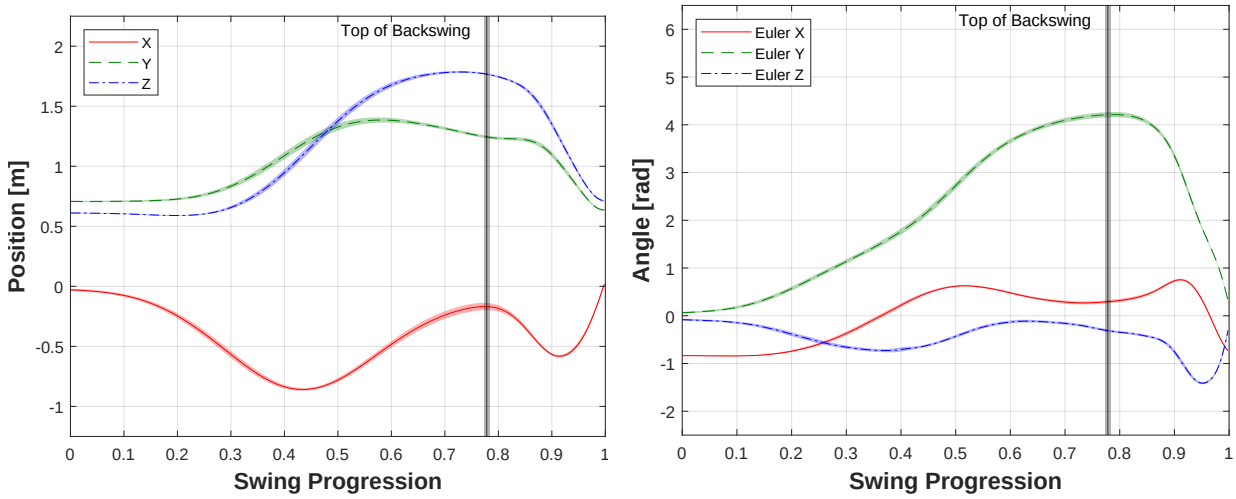

(a) grip position

(b) grip angles (YXZ Euler)

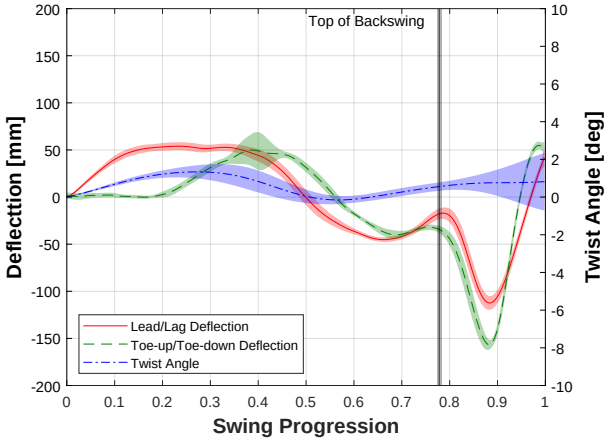

(c) clubhead deflections

Figure C.8: Golfer 8 mean club kinematics: Driver A2

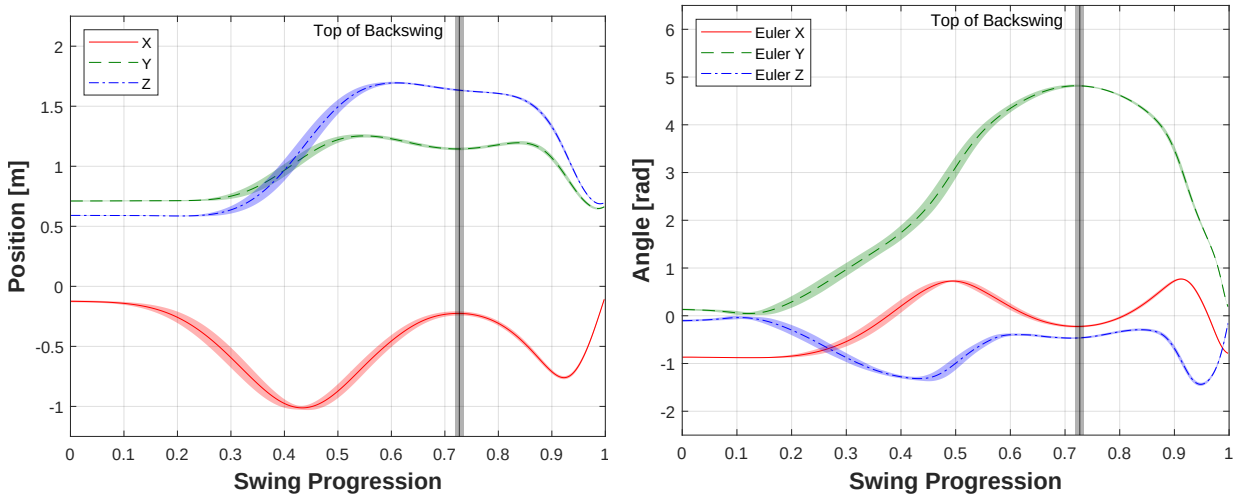

(a) grip position

(b) grip angles (YXZ Euler)

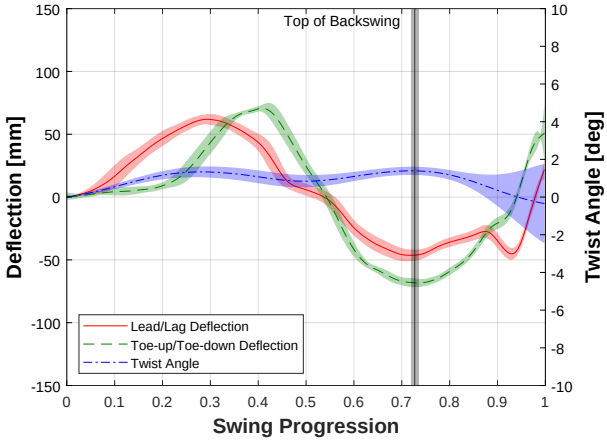

(c) clubhead deflections

Figure C.9: Golfer 9 mean club kinematics: Driver A2

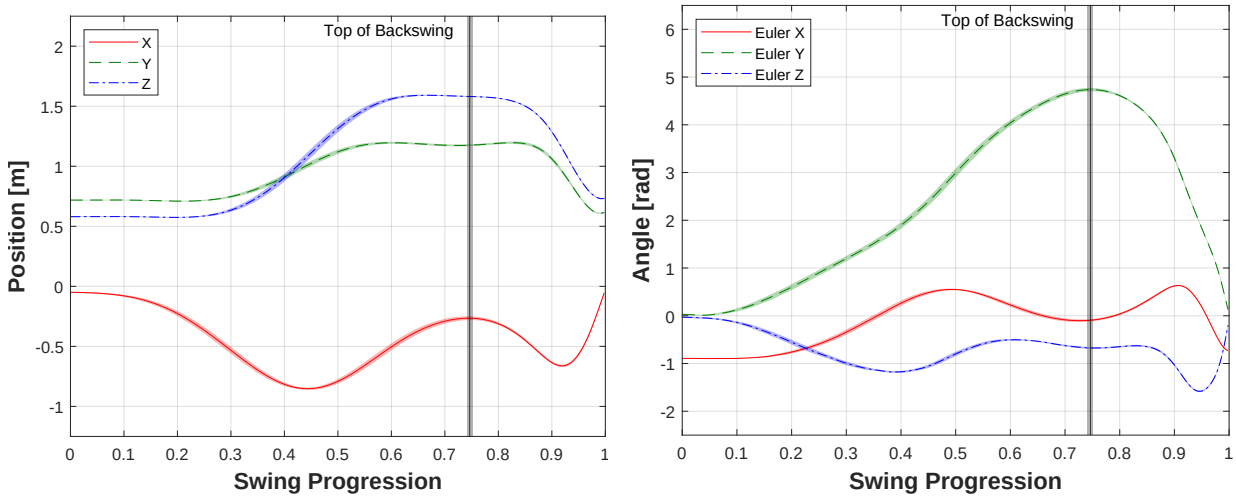

(a) grip position

(b) grip angles (YXZ Euler)

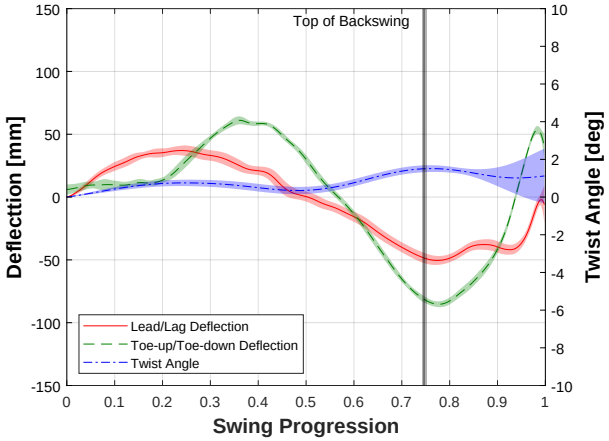

(c) clubhead deflections

Figure C.10: Golfer 10 mean club kinematics: Driver A2

Appendix D

Motion Capture Experiment Mean Club Kinematics: Driver B1

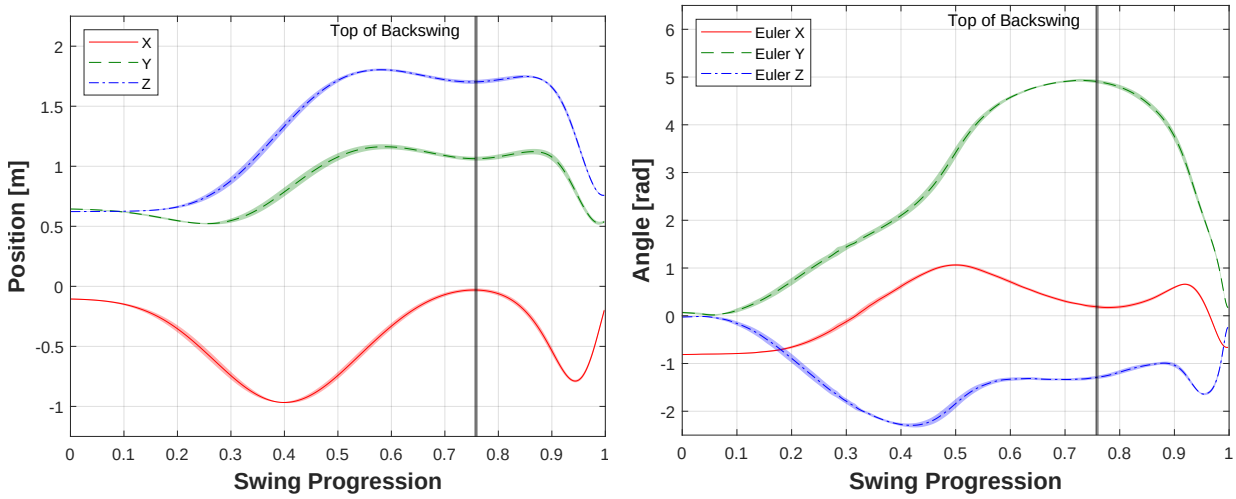

(a) grip position

(b) grip angles (YXZ Euler)

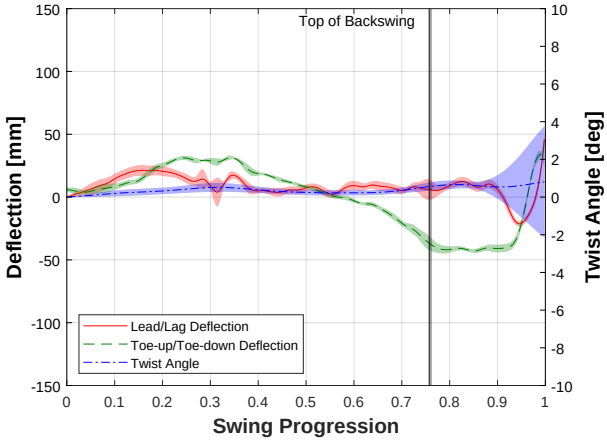

(c) clubhead deflections

Figure D.1: Golfer 1 mean club kinematics: Driver B1

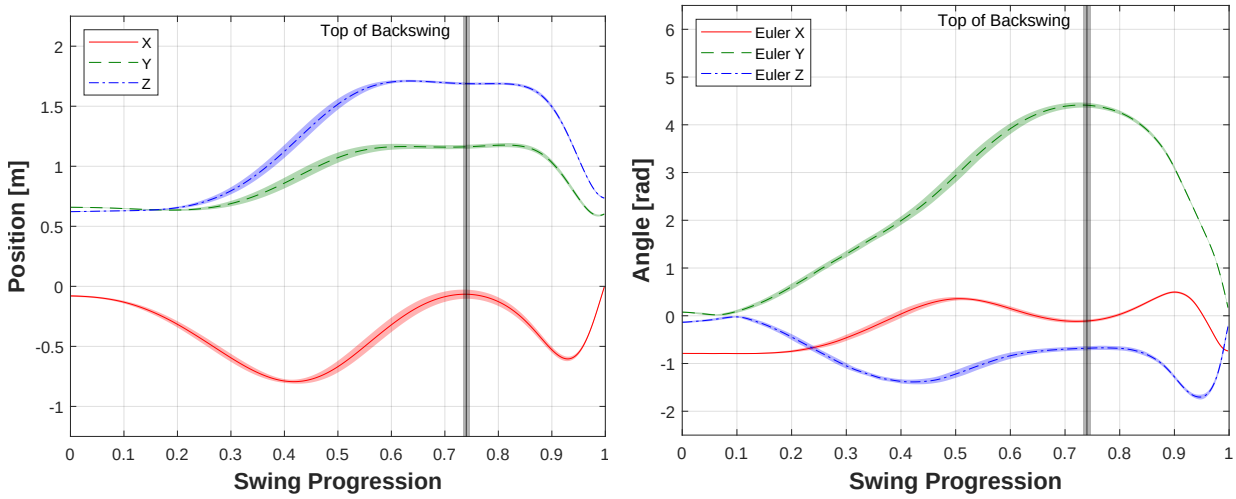

(a) grip position

(b) grip angles (YXZ Euler)

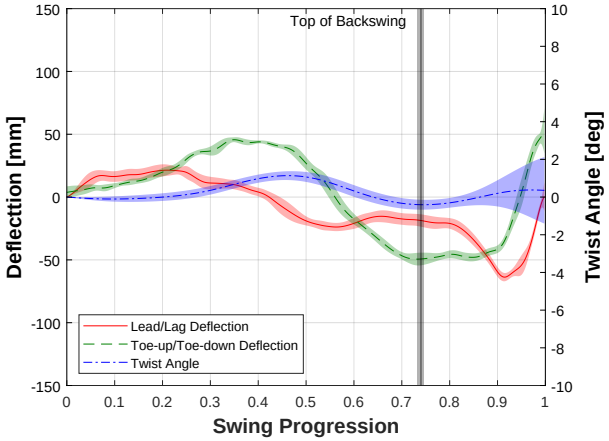

(c) clubhead deflections

Figure D.2: Golfer 2 mean club kinematics: Driver B1

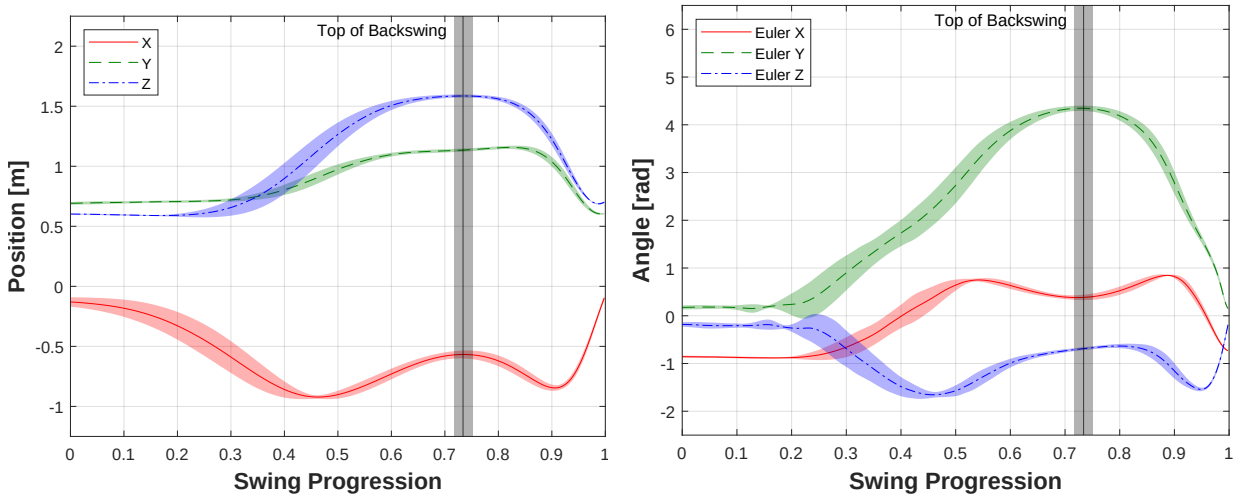

(a) grip position

(b) grip angles (YXZ Euler)

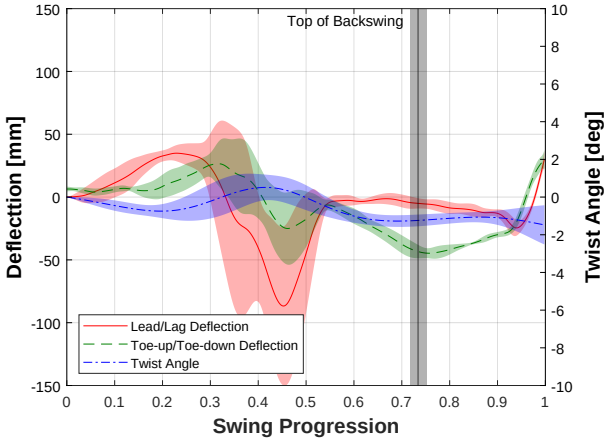

(c) clubhead deflections

Figure D.3: Golfer 3 mean club kinematics: Driver B1

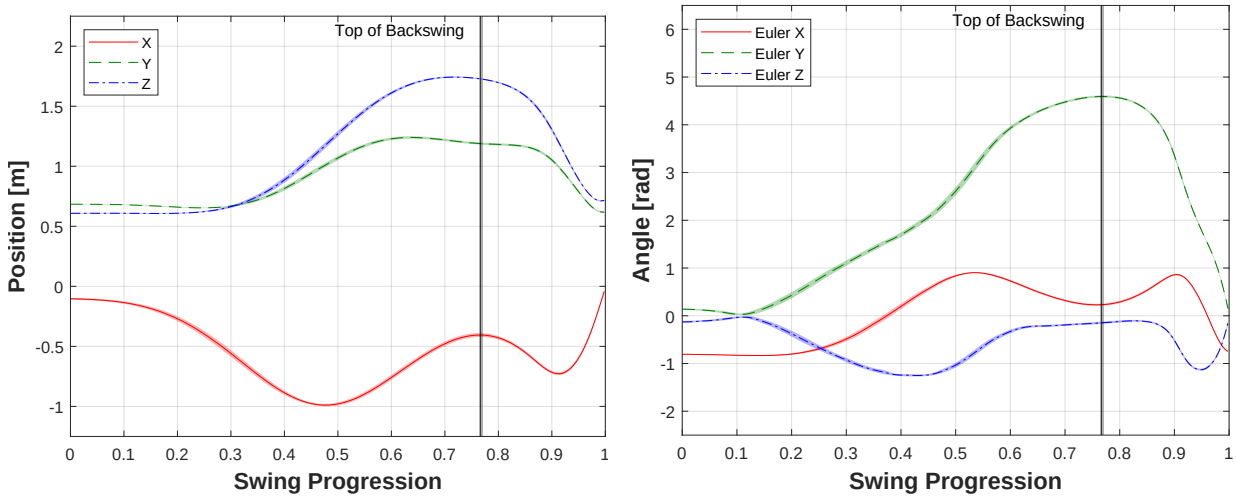

(a) grip position

(b) grip angles (YXZ Euler)

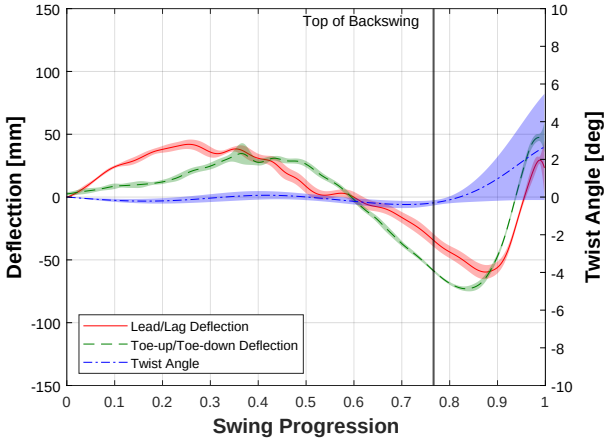

(c) clubhead deflections

Figure D.4: Golfer 4 mean club kinematics: Driver B1

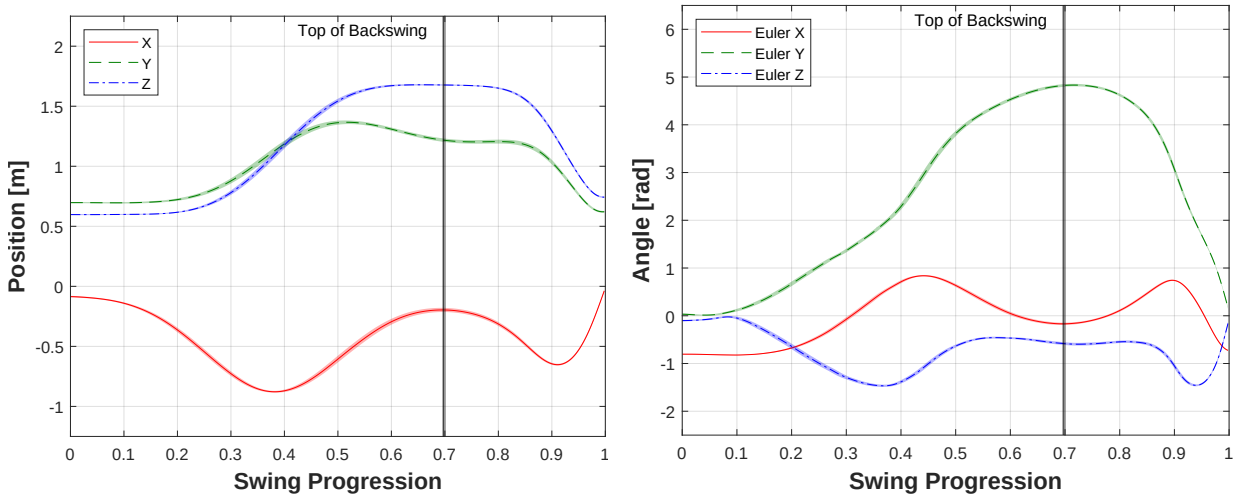

(a) grip position

(b) grip angles (YXZ Euler)

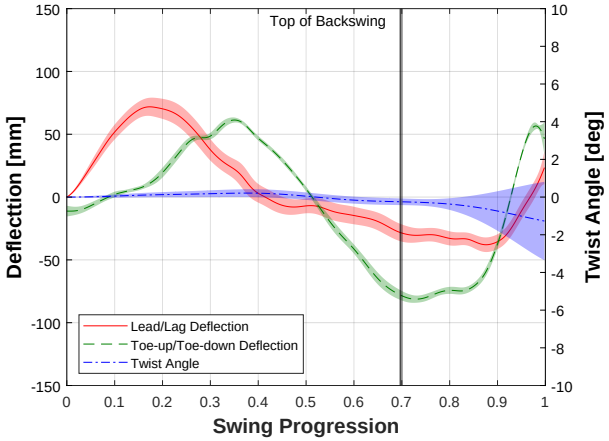

(c) clubhead deflections

Figure D.5: Golfer 5 mean club kinematics: Driver B1

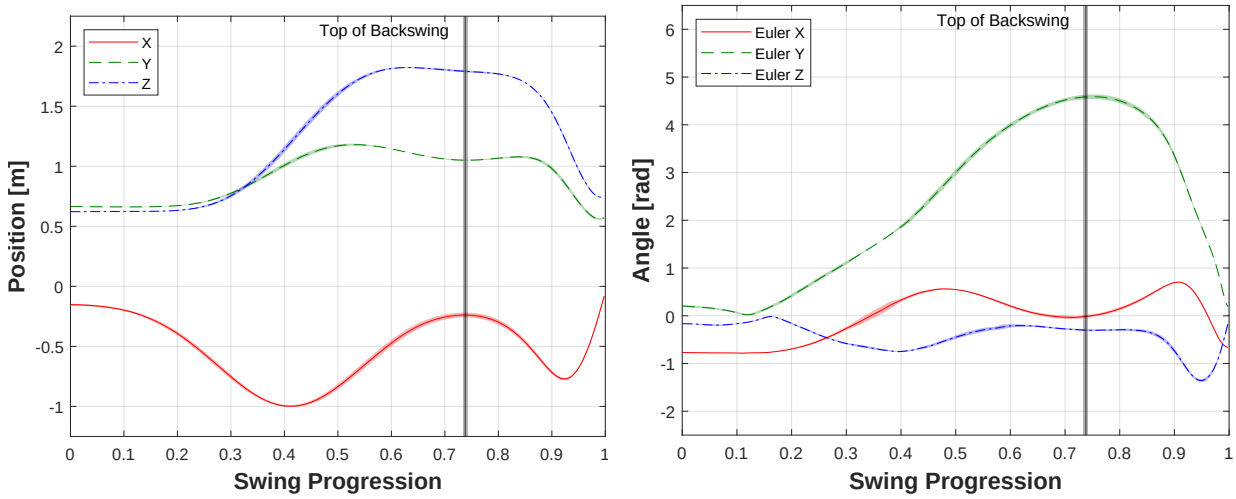

(a) grip position

(b) grip angles (YXZ Euler)

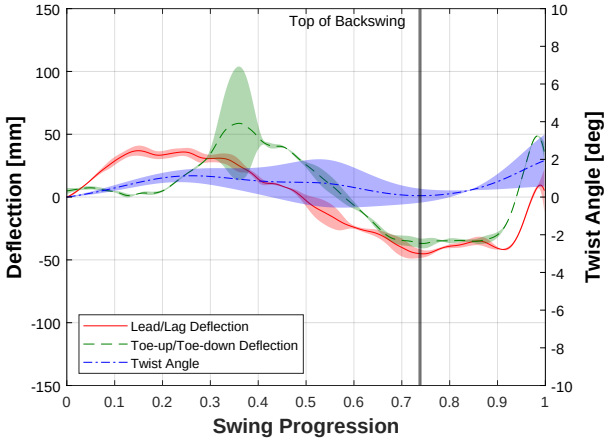

(c) clubhead deflections

Figure D.6: Golfer 6 mean club kinematics: Driver B1

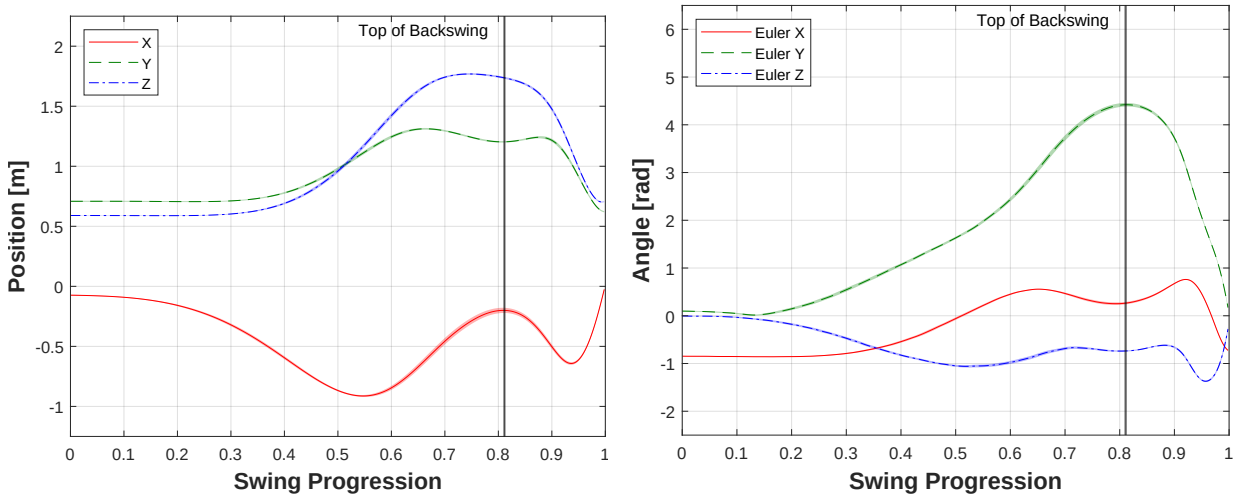

(a) grip position

(b) grip angles (YXZ Euler)

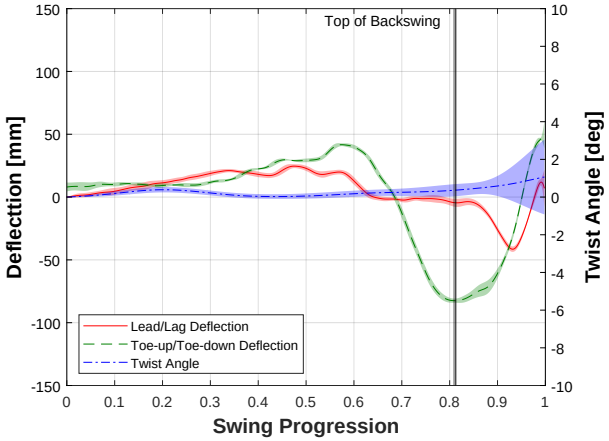

(c) clubhead deflections

Figure D.7: Golfer 7 mean club kinematics: Driver B1

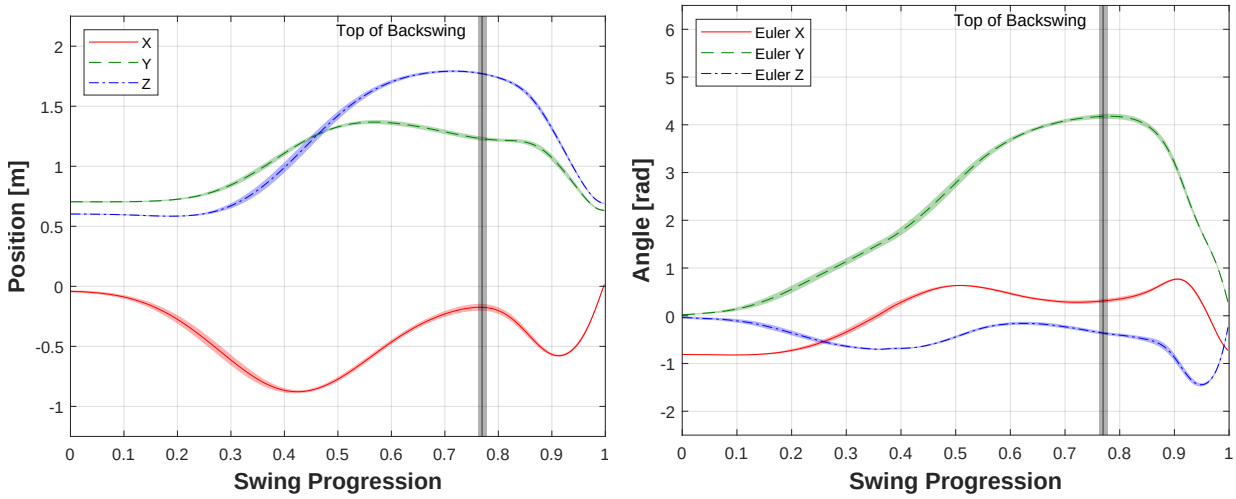

(a) grip position

(b) grip angles (YXZ Euler)

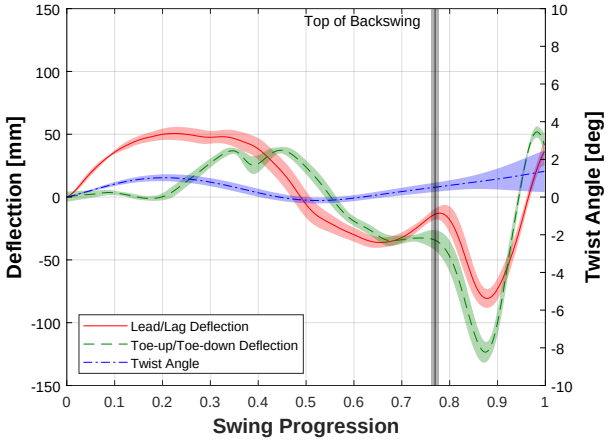

(c) clubhead deflections

Figure D.8: Golfer 8 mean club kinematics: Driver B1

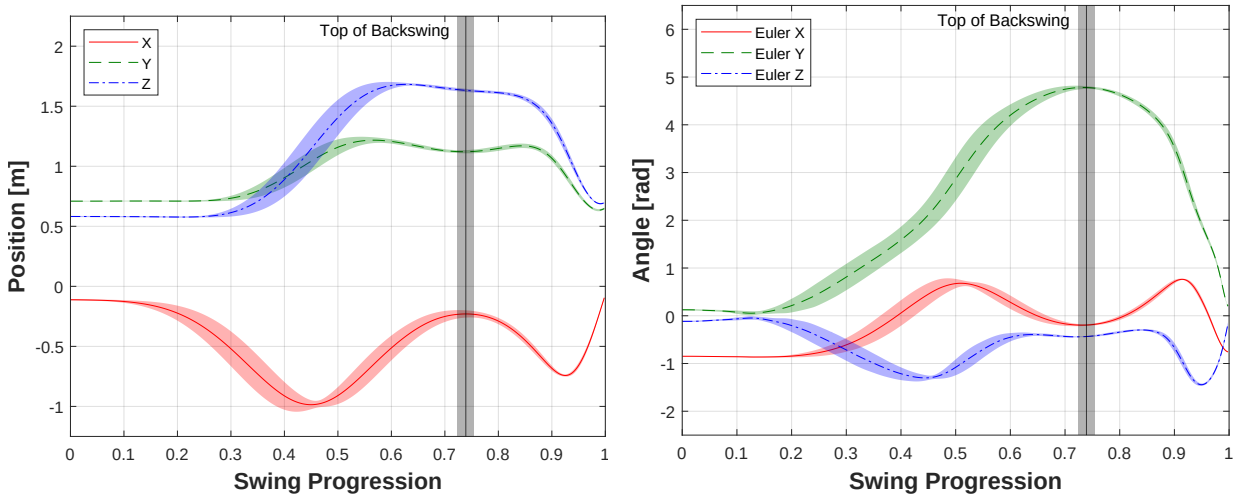

(a) grip position

(b) grip angles (YXZ Euler)

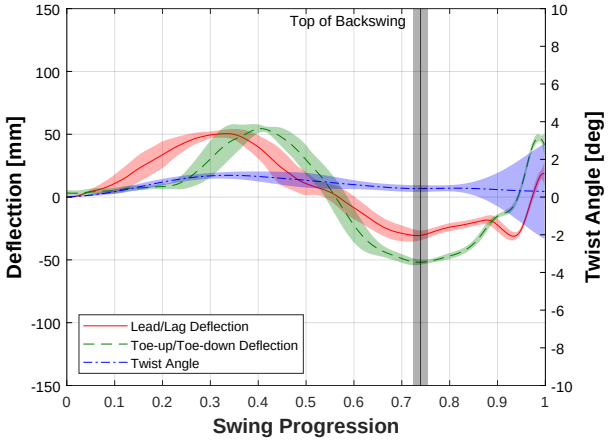

(c) clubhead deflections

Figure D.9: Golfer 9 mean club kinematics: Driver B1

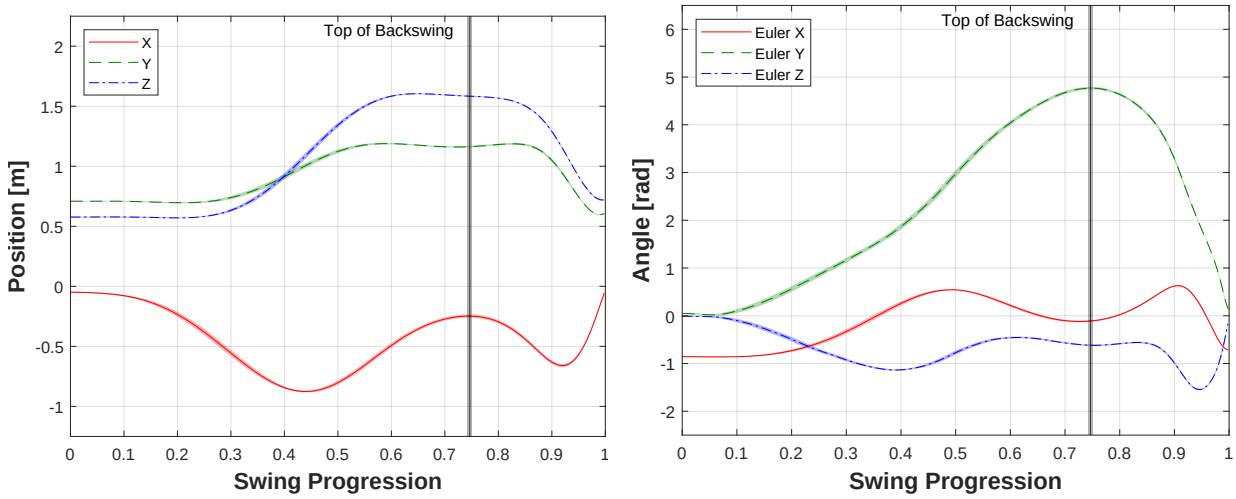

(a) grip position

(b) grip angles (YXZ Euler)

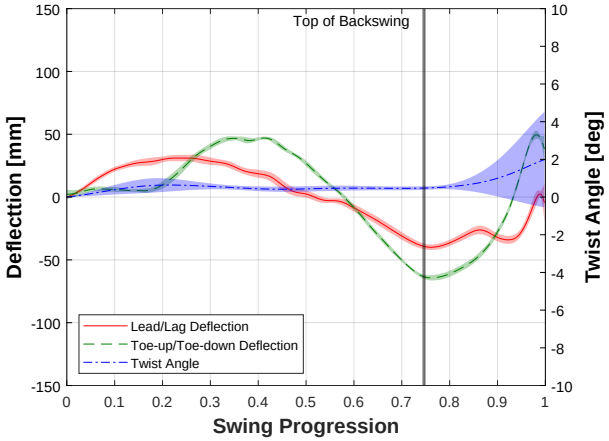

(c) clubhead deflections

Figure D.10: Golfer 10 mean club kinematics: Driver B1

Appendix E

Motion Capture Experiment Mean Biomechanics Compared to Model Optimal Swing: Driver B1.

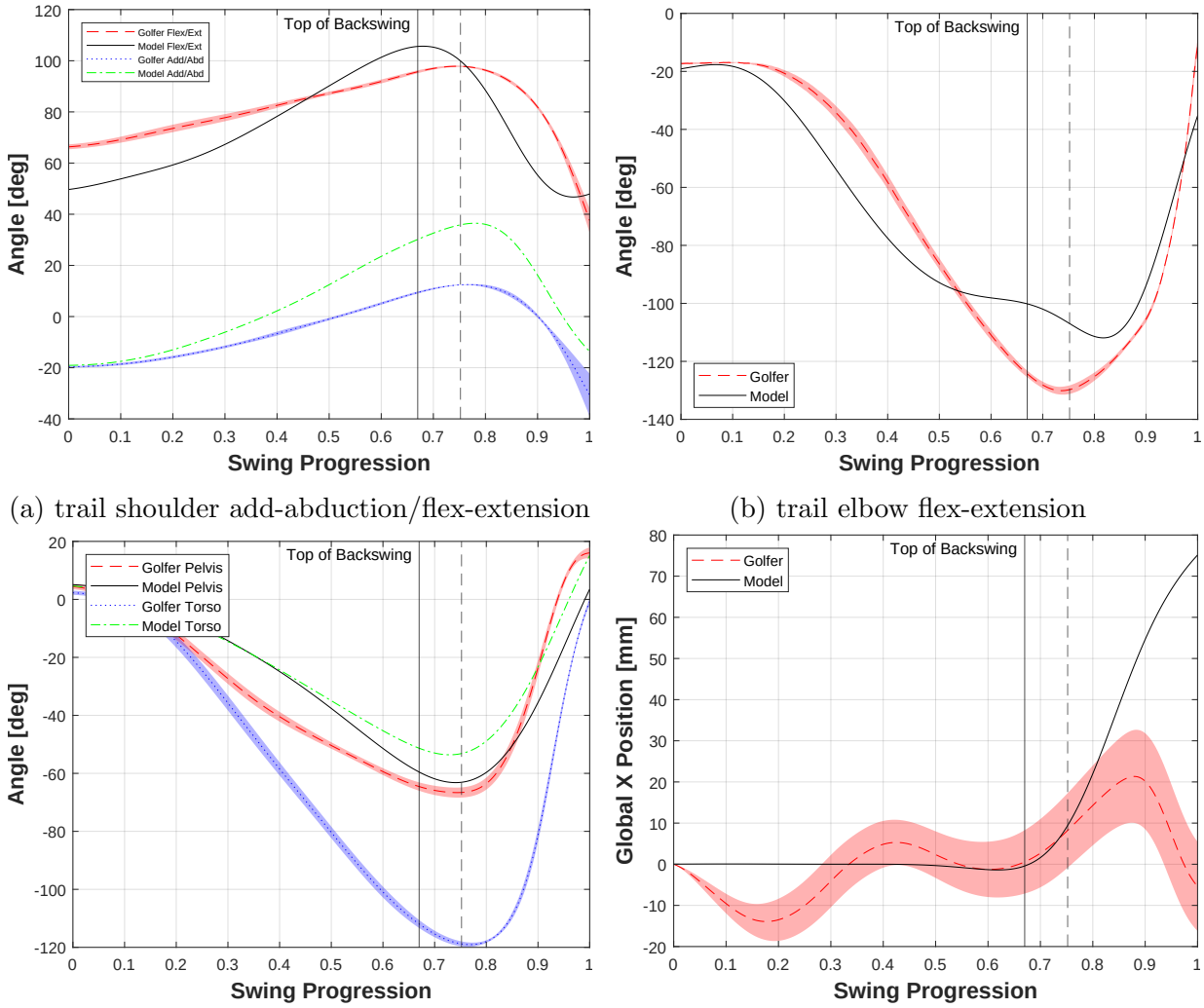

(a) trail shoulder add-abduction/flex-extension

(b) trail elbow flex-extension

(c) torso/pelvis rotation angle

(d) pelvis translation

Figure E.1: Golfer 1 mean biomechanics compared to model optimal swing: Driver B1.

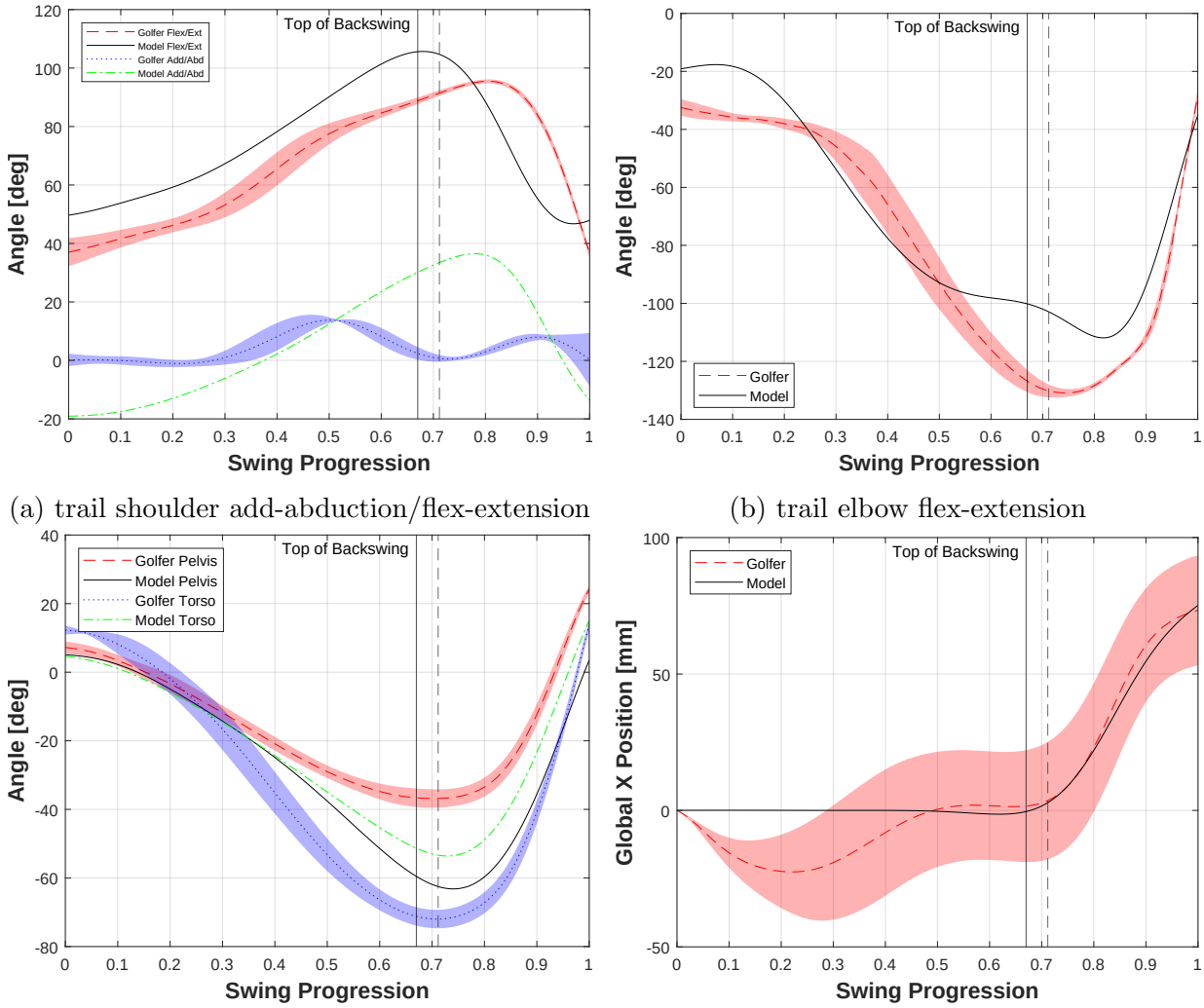

(a) trail shoulder add-abduction/flex-extension

(b) trail elbow flex-extension

(c) torso/pelvis rotation angle

(d) pelvis translation

Figure E.2: Golfer 3 mean biomechanics compared to model optimal swing: Driver B1.

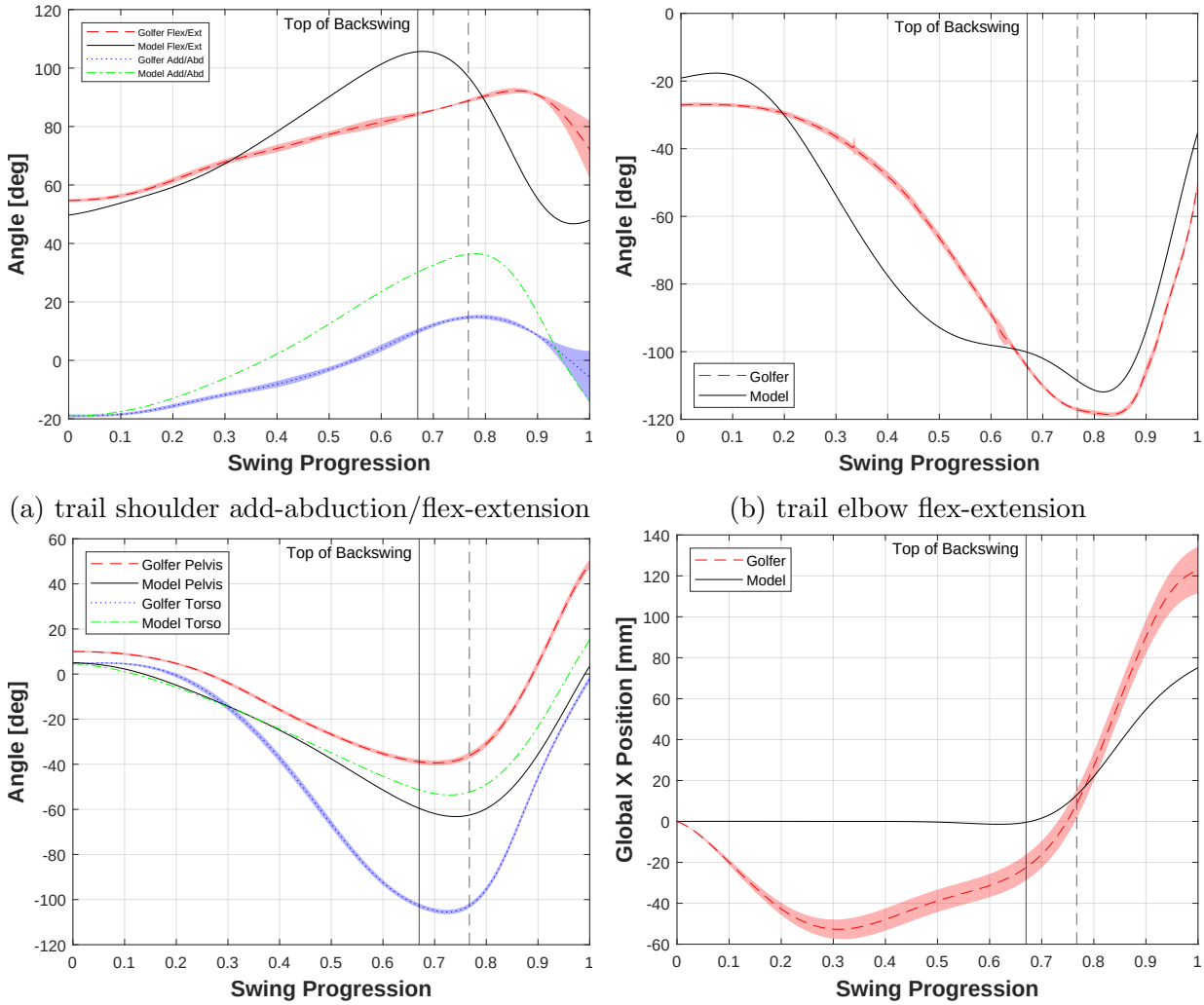

(a) trail shoulder add-abduction/flex-extension

(b) trail elbow flex-extension

(c) torso/pelvis rotation angle

(d) pelvis translation

Figure E.3: Golfer 4 mean biomechanics compared to model optimal swing: Driver B1.

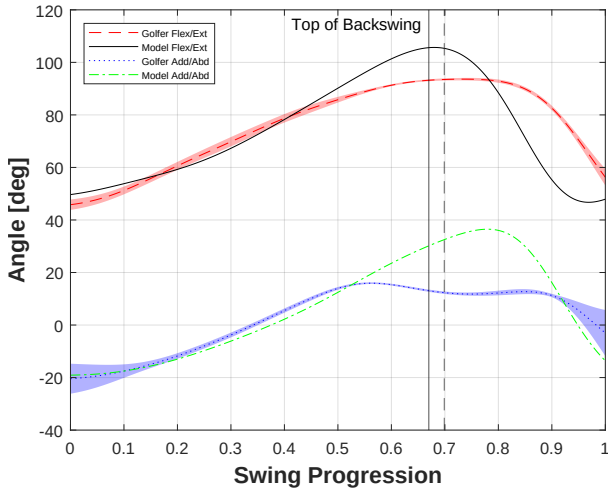

(a) trail shoulder add-abduction/flex-extension

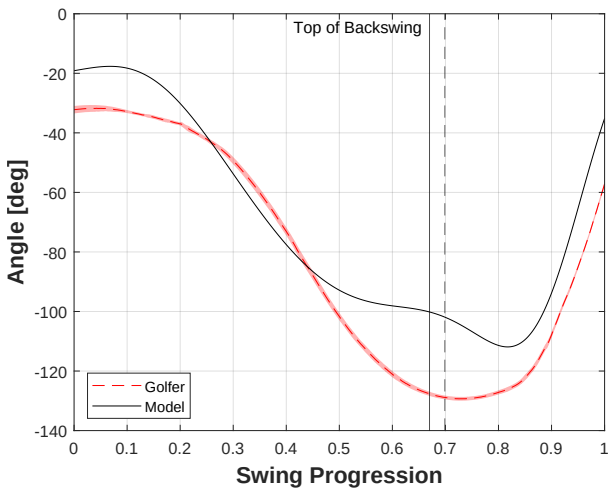

(b) trail elbow flex-extension

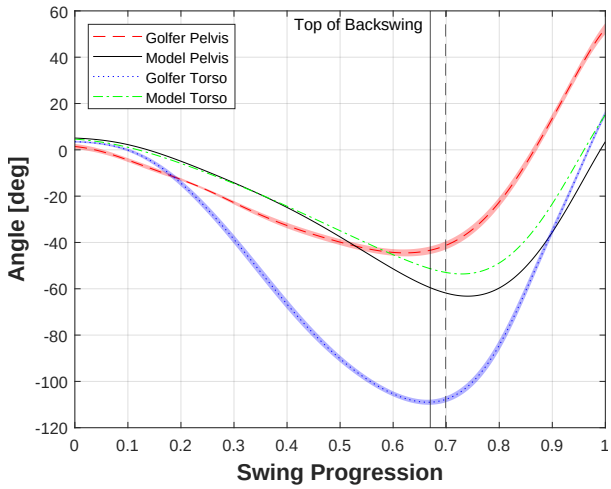

(c) torso/pelvis rotation angle

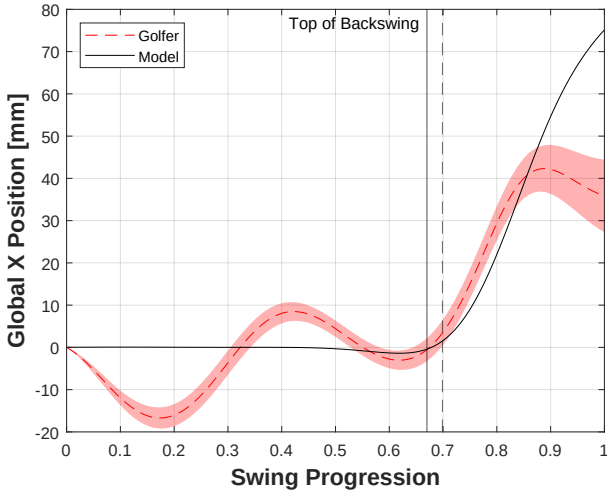

(d) pelvis translation

Figure E.4: Golfer 5 mean biomechanics compared to model optimal swing: Driver B1.

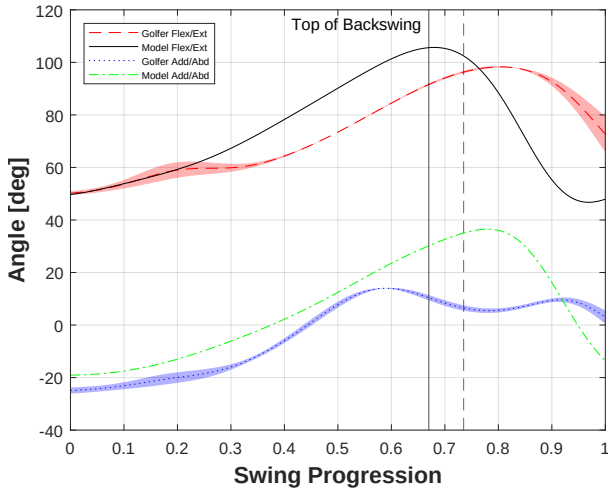

(a) trail shoulder add-abduction/flex-extension

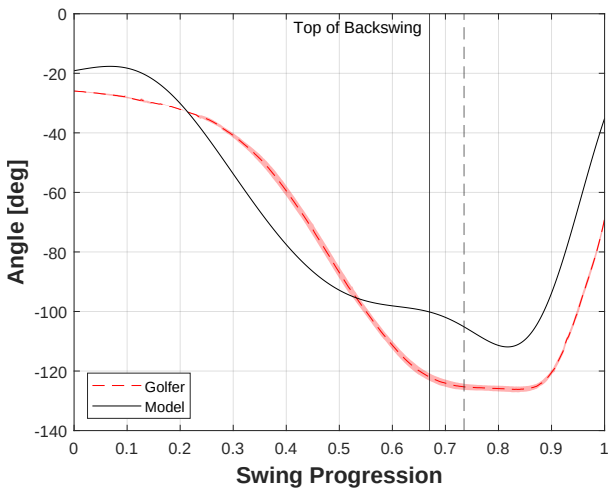

(b) trail elbow flex-extension

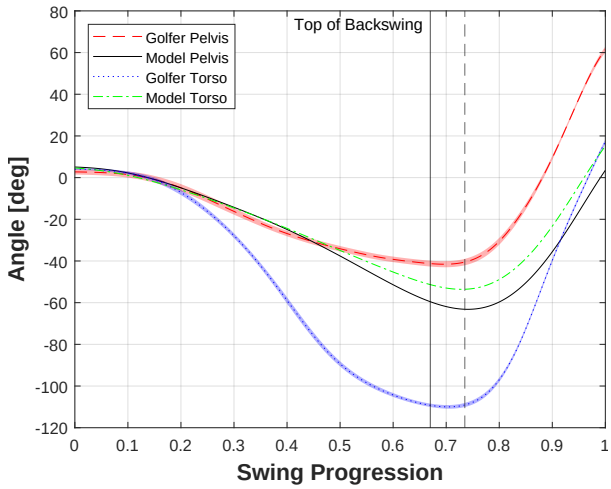

(c) torso/pelvis rotation angle

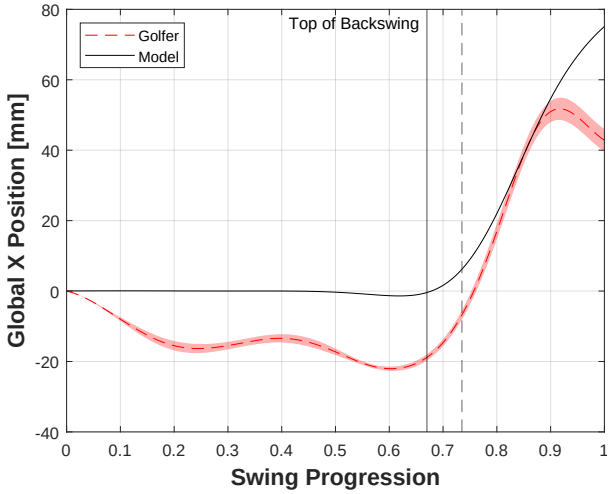

(d) pelvis translation

Figure E.5: Golfer 6 mean biomechanics compared to model optimal swing: Driver B1.

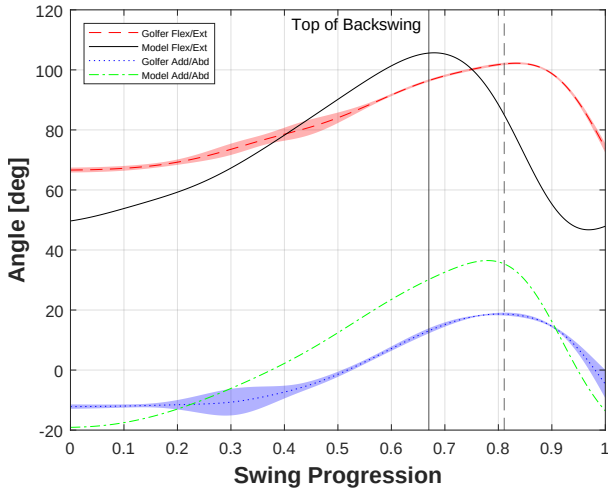

(a) trail shoulder add-abduction/flex-extension

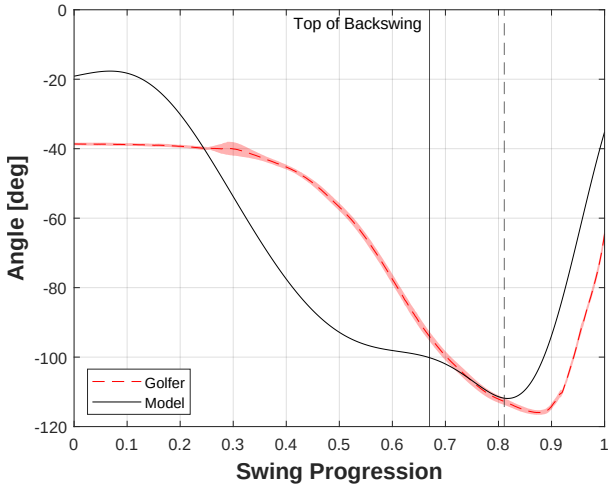

(b) trail elbow flex-extension

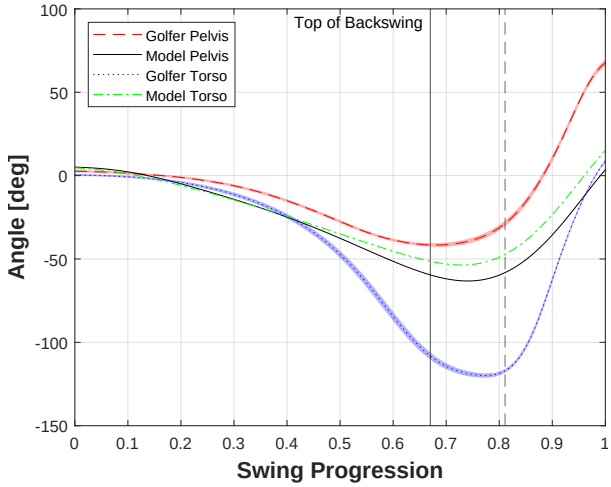

(c) torso/pelvis rotation angle

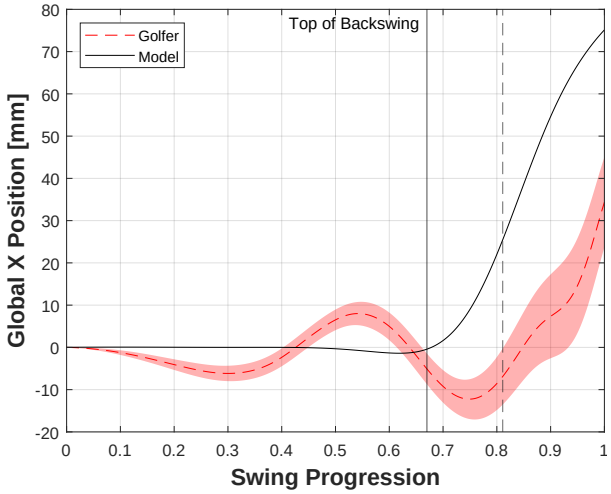

(d) pelvis translation

Figure E.6: Golfer 7 mean biomechanics compared to model optimal swing: Driver B1.

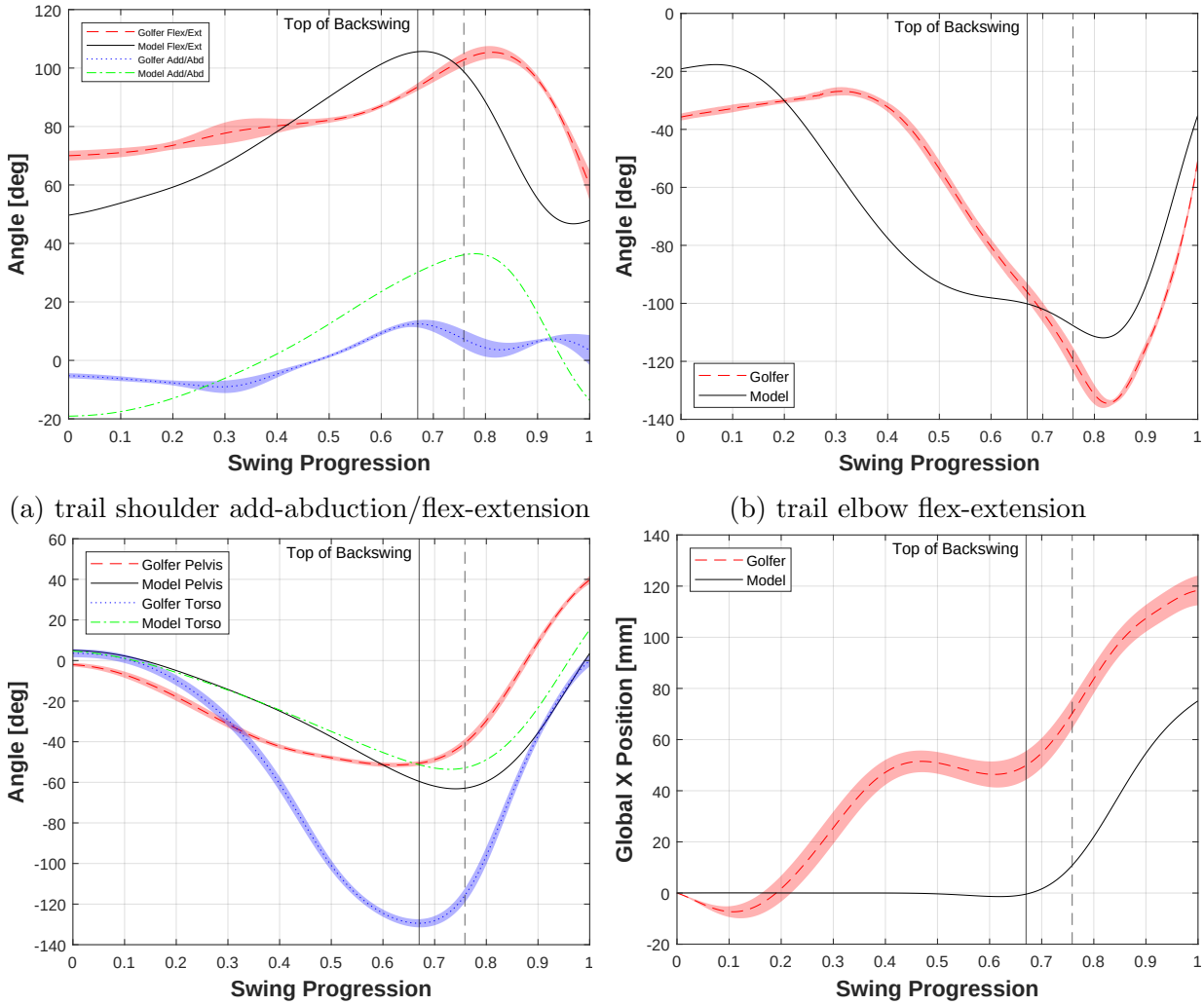

(a) trail shoulder add-abduction/flex-extension

(b) trail elbow flex-extension

(c) torso/pelvis rotation angle

(d) pelvis translation

Figure E.7: Golfer 8 mean biomechanics compared to model optimal swing: Driver B1.

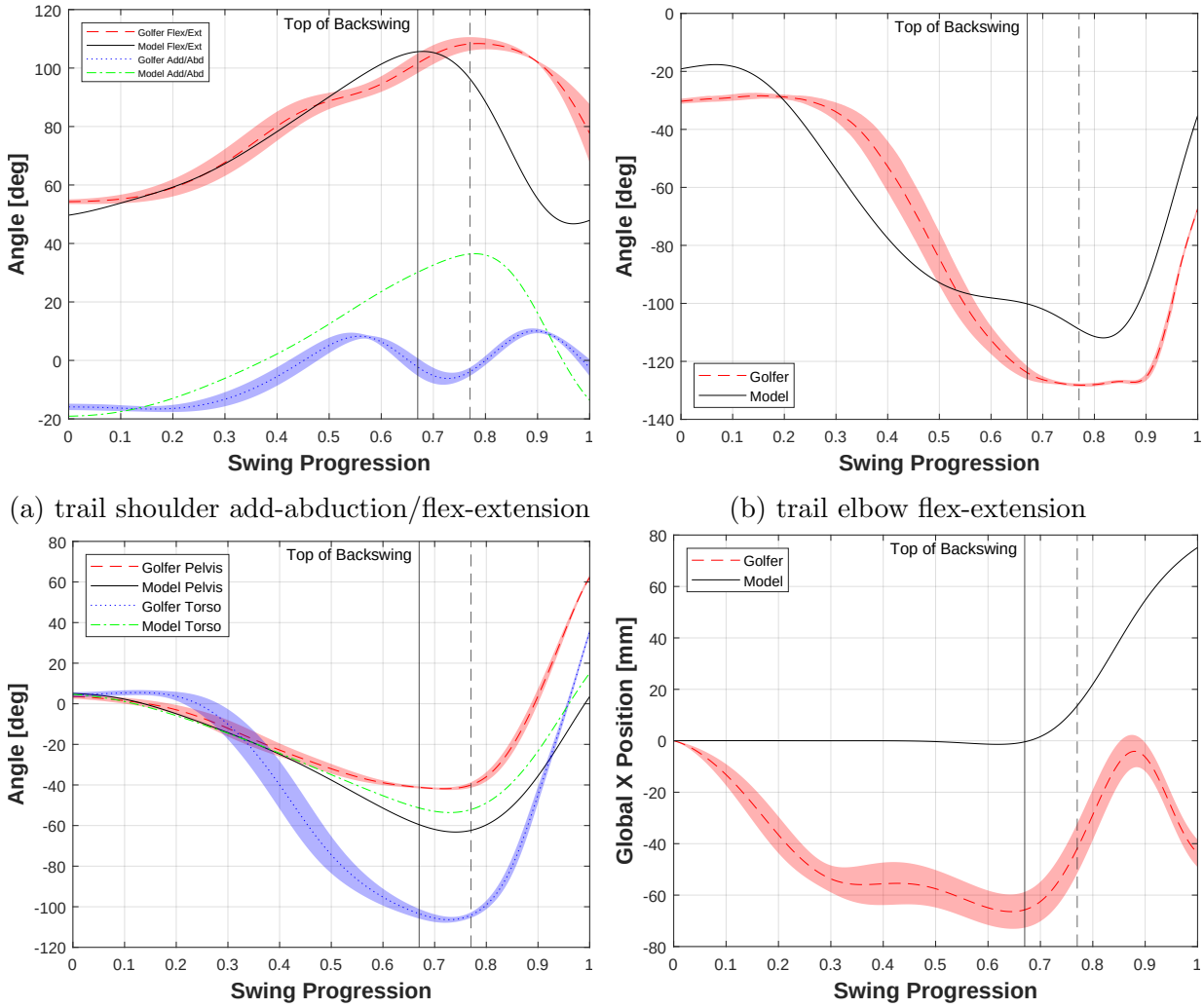

(a) trail shoulder add-abduction/flex-extension

(b) trail elbow flex-extension

(c) torso/pelvis rotation angle

(d) pelvis translation

Figure E.8: Golfer 9 mean biomechanics compared to model optimal swing: Driver B1.

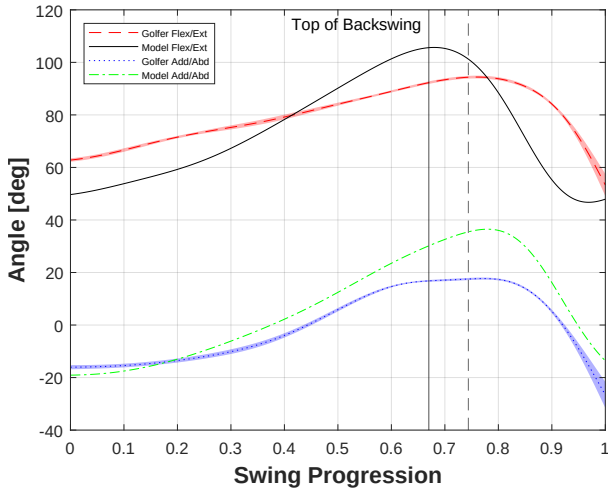

(a) trail shoulder add-abduction/flex-extension

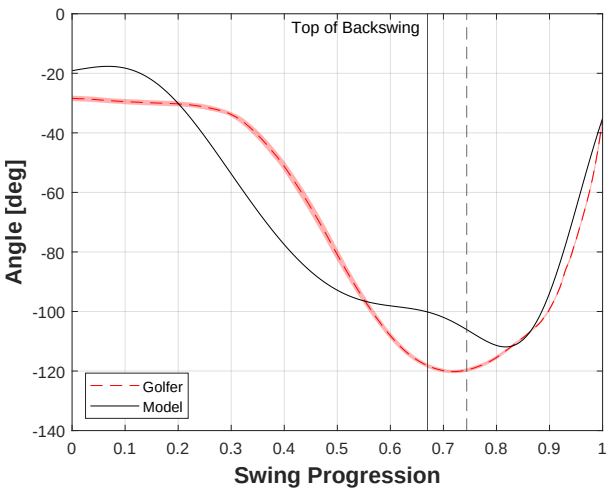

(b) trail elbow flex-extension

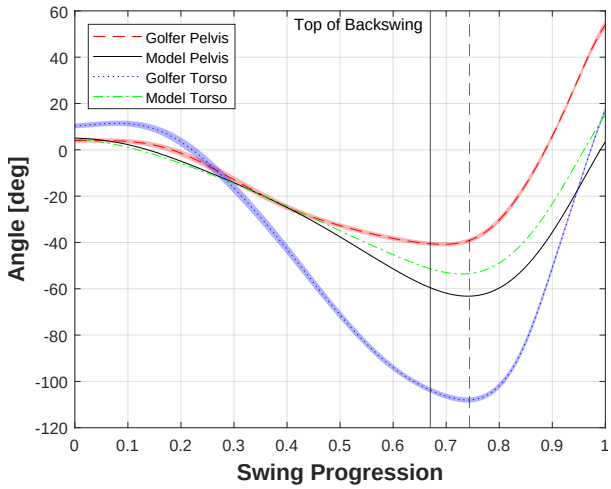

(c) torso/pelvis rotation angle

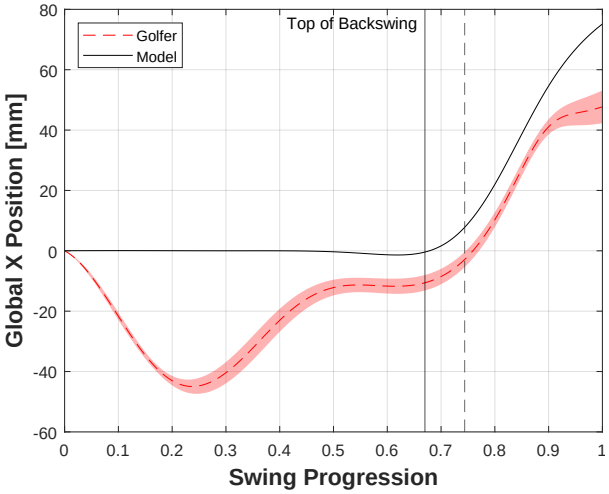

(d) pelvis translation

Figure E.9: Golfer 10 mean biomechanics compared to model optimal swing: Driver B1.